

# UC Irvine

## UC Irvine Electronic Theses and Dissertations

### Title

Development of an Orthogonal Cofactor System

### Permalink

<https://escholarship.org/uc/item/3z83j881>

### Author

Black, William

### Publication Date

2020

### Copyright Information

This work is made available under the terms of a Creative Commons Attribution License, available at <https://creativecommons.org/licenses/by/4.0/>

Peer reviewed|Thesis/dissertation

UNIVERSITY OF CALIFORNIA,  
IRVINE

Development of an Orthogonal Redox Cofactor System

DISSERTATION

submitted in partial satisfaction of the requirements  
for the degree of

DOCTOR OF PHILOSOPHY

in Chemical and Biomolecular Engineering

by

William Bentley Sowizral Black

Dissertation Committee:  
Assistant Professor Han Li, Chair  
Professor Nancy A. Da Silva  
Professor Sheryl Tsai

2020

Chapter 2 © 2019, Springer Nature  
Chapter 3 © 2020, American Chemical Society  
Chapter 4 © 2020, Springer Nature  
All other materials © 2020, William Bentley Sowizral Black

## **DEDICATION**

To

my mother and father

for their endless inspiration, guidance, love, and support

# TABLE OF CONTENTS

<b>LIST OF FIGURES.....</b>	<b>V</b>
<b>LIST OF TABLES.....</b>	<b>VI</b>
<b>ACKNOWLEDGEMENTS.....</b>	<b>VII</b>
<b>VITA.....</b>	<b>IX</b>
<b>ABSTRACT OF THE DISSERTATION.....</b>	<b>XII</b>
<b>CHAPTER 1: INTERFACING NONCANONICAL REDOX COFACTORS WITH <i>IN VITRO</i> AND <i>IN VIVO</i> BIOTRANSFORMATION.....</b>	<b>1</b>
1.1 INTRODUCTION.....	2
1.2 CLASSES OF NONCANONICAL REDOX COFACTORS.....	3
1.3 UTILIZATION OF mNADs BY ENZYMES.....	6
1.4 <i>IN VITRO</i> mNAD SYSTEMS WITH PURIFIED PROTEINS.....	6
1.4.1 Systems with reduced cofactor supplementation.....	6
1.4.2 Cofactor regeneration.....	7
1.5 INTERFACING mNADs WITH COMPLEX CELLULAR SYSTEMS FOR ORTHOGONAL ELECTRON DELIVERY.....	14
1.6 MOTIVATION.....	16
1.7 OBJECTIVES.....	17
1.8 REFERENCES.....	17
<b>CHAPTER 2: ENGINEERING A NICOTINAMIDE MONONUCLEOTIDE REDOX COFACTOR SYSTEM FOR BIOCATALYSIS.....</b>	<b>22</b>
2.1 INTRODUCTION.....	23
2.2 METHODS.....	25
2.2.1 Plasmids and strains.....	25
2.2.2 Protein expression and purification.....	27
2.2.3 GDH enzymatic assays and kinetics study.....	28
2.2.4 Coupled enzymatic biotransformation.....	29
2.2.5 NMN <sup>+</sup> -dependent whole-cell biotransformation.....	30
2.2.6 GC-FID analytical methods.....	31
2.2.7 GDH Total Turnover Number (TTN) Determination.....	32
2.2.8 Quantification of intracellular NMN <sup>+</sup> and NAD <sup>+</sup> levels.....	33
2.3 RESULTS.....	34
2.3.1 Engineering Bs GDH to utilize NMN <sup>+</sup> .....	34
2.3.2 <i>In vitro</i> NMN(H) cycling supports efficient biocatalysis.....	37
2.3.3 <i>In vitro</i> NMN(H) cycling supports diverse chemistries.....	41
2.3.4 <i>In vivo</i> NMN(H) accumulation.....	41
2.3.5 NMN(H) enables specific electron delivery in <i>E. coli</i> .....	43
2.4 CONCLUSION.....	45
2.5 REFERENCES.....	46
<b>CHAPTER 3: ALDEHYDE PRODUCTION IN CRUDE LYSATE- AND WHOLE CELL-BASED BIOTRANSFORMATION USING A NONCANONICAL REDOX COFACTOR SYSTEM.....</b>	<b>51</b>
3.1 INTRODUCTION.....	52
3.2 METHODS.....	54
3.2.1 Plasmids and Strains.....	54
3.2.2 Crude Lysate Biotransformations.....	55
3.2.3 Determination of Molar Concentrations of Recombinant Protein in Crude Lysates.....	56
3.2.4 Resting Whole-Cell Biotransformation.....	57

3.2.5 GC-FID Analysis .....	58
3.2.6 Determination of Relative Plasmid Expression Levels .....	59
3.3 RESULTS .....	60
3.3.1 Citronellal production in crude lysate-based biotransformation.....	60
3.3.3 Optimizing the crude lysate-based biotransformation .....	63
3.3.4 Citronellal production in <i>E. coli</i> whole cells .....	69
3.4 CONCLUSIONS.....	71
3.5 REFERENCES .....	72
<b>CHAPTER 4: METABOLIC ENGINEERING OF <i>ESCHERICHIA COLI</i> FOR OPTIMIZED BIOSYNTHESIS OF NICOTINAMIDE MONONUCLEOTIDE, A NONCANONICAL REDOX COFACTOR .....</b>	<b>74</b>
4.1 INTRODUCTION .....	75
4.2 MATERIALS AND METHODS .....	77
4.2.1 Plasmid and Strain Construction.....	77
4.2.2 Growth-based Screening Platform.....	79
4.2.3 Intracellular NMN <sup>+</sup> Generation and Quantification.....	80
4.2.4 Cell growth with high concentrations of NMN <sup>+</sup> .....	81
4.3 RESULTS .....	82
4.3.1 Identification of NMN <sup>+</sup> Biosynthetic Routes.....	82
4.3.2 Evaluating the NMN <sup>+</sup> biosynthetic pathways <i>in vivo</i> .....	84
4.3.3 Bioprospecting NadV homologs and optimizing NMN <sup>+</sup> biosynthesis .....	87
4.3.4 Investigating the physiological response to NMN <sup>+</sup> accumulation.....	91
4.4 DISCUSSION .....	93
4.5 CONCLUSIONS.....	96
4.6 REFERENCES .....	96
<b>CHAPTER 5: CONSTRUCTION OF A NONCANONICAL REDOX COFACTOR SYSTEM IN <i>SACCHAROMYCES CEREVISIAE</i> .....</b>	<b>100</b>
5.1 INTRODUCTION .....	101
5.2 METHODS .....	102
5.2.1 Plasmid and Strain Construction.....	102
5.2.2 Resting Cell Biotransformations.....	105
5.2.3 GC-FID Analytical Method .....	106
5.2.4 Intracellular NMN <sup>+</sup> Generation .....	106
5.3 RESULTS AND DISCUSSION .....	107
5.3.1 System and Strain Construction .....	107
5.3.2 Resting Whole Cell Biotransformation in <i>S. cerevisiae</i> .....	108
5.3.3 Intracellular NMN <sup>+</sup> Generation in <i>S. cerevisiae</i> .....	110
5.4 CONCLUSIONS.....	114
5.5 REFERENCES .....	114

## LIST OF FIGURES

Figure 1: Noncanonical redox cofactors (mNADs) in their reduced form.....	3
Figure 2: GDH Tripe efficiently recycles NMN <sup>+</sup> in <i>in vitro</i> biotransformation.....	38
Figure 3: <i>In vivo</i> NMN <sup>+</sup> cycling supports <i>E. coli</i> growth .....	42
Figure 4: Bs GDH Ortho selectively provides reducing power for levodione production in <i>E. coli</i> whole cells .....	43
Figure 5: Product levels in whole-cell ketoisophorone (KIP) conversion with co-expression of XenA, LVR, and ADH .....	45
Figure 6: System design and reaction scheme for citronellal production .....	61
Figure 7: NMN <sup>+</sup> -dependent orthogonal redox cofactor system enables citronellal accumulation .....	62
Figure 8: Optimizing crude lysate conditions for citronellal production in Buffer A .....	64
Figure 9: Crude lysate-based biotransformation in potassium phosphate buffer.....	66
Figure 10 Time-course of citral biotransformation and optimization in Phosphate Buffer.....	68
Figure 11: Orthogonal cofactor system enables specific aldehyde accumulation in <i>E. coli</i> whole cells.....	70
Figure 12: Establishing NMN <sup>+</sup> Biosynthetic Routes in <i>Escherichia coli</i> .....	82
Figure 13: Identification of efficient NMN <sup>+</sup> production pathways <i>in vivo</i> using a growth-based screening platform .....	85
Figure 14: <i>Francisella tularensis</i> NadE*-based Growth Restoration is Not Nicotinamide Feeding Dependent .....	87
Figure 15: Pathway combination and strain modification improved NMN <sup>+</sup> production .....	89
Figure 16: <i>Francisella tularensis</i> NadE* Expression Alleviates <i>R. solanacearum</i> NadV Growth Challenge.....	90
Figure 17: Intracellular NAD <sup>+</sup> Decreases in NMN <sup>+</sup> Accumulating Strains .....	91
Figure 18 NMN <sup>+</sup> accumulation affects cell physiology possibly via NadR.....	93
Figure 19: Citral Biotransformation with resting <i>S. cerevisiae</i> cells .....	109
Figure 20: Establishing NMN <sup>+</sup> biosynthetic routes in <i>S. cerevisiae</i> .....	111
Figure 21: Intracellular NMN <sup>+</sup> levels increase with heterologous pathway introduction ..	113

## LIST OF TABLES

<b>Table 1: In vitro Noncanonical Redox Cofactor Cycling Systems</b> .....	8
<b>Table 2: Apparent Kinetic Parameters for Engineered Enzymes with Oxidized mNADs</b> ...	12
<b>Table 3: In vivo Noncanonical Redox Cofactor Systems</b> .....	16
<b>Table 4: Strains and Plasmids Used in Chapter 2</b> .....	25
<b>Table 5: Accession Numbers for Proteins Used in Chapter 2</b> .....	27
<b>Table 6: Mass Spectrometry Parameters for Intracellular Cofactor Concentration Analysis</b> .....	34
<b>Table 7: Full Steady-State Kinetics Parameters</b> .....	36
<b>Table 8: Conversion of a range of substrates using NMN<sup>+</sup> as the cycling cofactor</b> .....	40
<b>Table 9: Strain and Plasmids Used in Chapter 3</b> .....	54
<b>Table 10: Accession Numbers for Proteins Used in Chapter 3</b> .....	54
<b>Table 11: Strains and Plasmids Used in Chapter 4</b> .....	79
<b>Table 12: Strains and Plasmids Used in Chapter 5</b> .....	102



## ACKNOWLEDGEMENTS

First, I want to express my immense gratitude to Professor Han Li for her mentorship and support. For the last five years she has enabled me to reach higher, grow strong, and think like a true scientist. The opportunity to be a professor's first student has been a truly special experience. I want to thank Professor Nancy Da Silva and Professor Sheryl Tsai for their guidance through both my thesis work and as teachers.

When the lab first started, the lab had nothing. No chemicals, no glassware, no instruments. The generosity of Professor Da Silva and Professor Szu-Wen Wang to gift us a space to work, reagents, and equipment to run experiments in the initial months and years of starting the lab was paramount to being able to complete this work. I also want to thank Dr. Felix Grun and Dr. Ben Katz for their help with my GC and LC work, great conversation, and for fixing the instruments I broke more times than I would like to admit at the Mass Spectrometry Facility.

I want to thank our collaborators at UC Irvine, UC Davis, and UCLA, Professor Justin Siegel, Professor Ray Luo, Professor James Liao, Dr. Wei Shun Mak, and Youtian Cui, for their hard work and dedication.

I want to thank the entire Li Lab for their friendship, hard work, and collaboration. Linyue Zhang, Edward King, Sarah Maxel, Derek Aspacio, and Kelly Richardson have all had a significant role in my journey. Our rotation students Danielle Bever and Andrew Rowley also greatly contributed to this body of work. I've also had the pleasure of mentoring some incredible undergraduate students, Alex Babayi, Kosuke Seki, Bonnie Fong, Alicia Sanchez Martinez, Kelly

Richardson, Austin Si, and Samer Saleh. Working with them and watching them grow has been incredible rewarding.

I don't believe graduate school would have been as rich of an experience without my friends. Traveling, learning, and experiencing life with them has been some of my most treasured memories.

Finally, I want to thank my family. My family has always been my greatest support. They inspired my love for science, and they taught me the joy of investigating the world around me. They are my constant inspiration. This journey would not have been possible without them.

## VITA

### EDUCATION

- 2020 Ph.D., Chemical and Biomolecular Engineering, University of California Irvine
- 2016 M. S., Chemical and Biochemical Engineering, University of California Irvine
- 2015 B. S., Chemical Engineering, Iowa State University

### PUBLICATIONS

Richardson, K. R. \*, **Black, W. B.\***, and Li, H. “Aldehyde Production in Crude Lysate- and Whole Cell-Based Biotransformation Using a Noncanonical Redox Cofactor System,” *ACS Catalysis*, 10, 8898-8903. 2020. (\* indicates equal contributors)

**Black, W. B.**, Aspacio, D., Bever, D., King, E., Zhang, L., and Li, H. “Metabolic Engineering of *Escherichia coli* for Optimized Biosynthesis of Nicotinamide Mononucleotide, a Noncanonical Redox Cofactor,” *Microbial Cell Factories*, 19, No. 150. 2020.

**Black, W. B.\***, Zhang, L. \*, Mak, W. S. \*, Maxel, S., Cui, Y., King, E., Fong, B., Sanchez Martinez, A., Siegel J. B., and Li, H. “Engineering a Nicotinamide Mononucleotide Redox Cofactor System for Biocatalysis,” *Nature Chemical Biology*, 16, 87-94. 2020. (\* indicates equal contributors)

**Black, W. B.**, King, E., Wang, Y., Jenic, A., Rowley, A. T., Seki, K., Luo, R., and Li, H. “Engineering a Coenzyme A Detour to Expand the Product Scope and Enhance the Selectivity of the Ehrlich Pathway,” *ACS Synthetic Biology*, vol. 7, no. 12, 2018.

**Black W. B.**, Zhang, L., Kamoku, C., Liao, J. C., and Li, H. “Rearrangement of Coenzyme A-Acylated Carbon Chain Enables Synthesis of Isobutanol via a Novel Pathway in *Ralstonia eutropha*,” *ACS Synthetic Biology*, vol. 7, no. 3, 2018.

Tan, Z., **Black, W.**, Yoon, J. M., Shanks, J. V., and Jarboe, L. R. “Improving *Escherichia coli* Membrane Integrity and Fatty Acid Production by Expression Tuning of FadL and OmpF,” *Microbial Cell Factories*, vol. 16, no. 38, 2017.

### ORAL PRESENTATIONS

**Black, W. B.**, Zhang, L., Mak, W. S., Maxel, S., Cui, Y., King, E., Fong, B., Sanchez Martinez, A., Siegel J. B., and Li, H. “Engineering a Nicotinamide Mononucleotide Redox Cofactor System for Biocatalysis,” *University of California Irvine Chemical and Biomolecular Engineering Seminar*, Irvine, CA, November 9, 2019.

**Black, W. B.**, Mak, W. S., Zhang, L., Maxel, S., Fong, B., Siegel, J. B., Li, H. “Computational Protein Design Enables Efficient Regeneration of a Biomimetic Cofactor to Support Diverse Redox Chemistries,” *American Institute of Chemical Engineers Annual Meeting*, Pittsburgh, PA, October 29, 2018.

**Black, W. B.**, Zhang, C., Liao, J. C., and Li, H. “Synthesis of Isobutanol and n-Butanol Using Engineered Coenzyme A-Dependent Pathways in *Ralstonia eutropha* H16,” *American Institute of Chemical Engineers Annual Meeting*, Minneapolis, MN, October 31, 2017.

**Black, W. B.** and Li, H. “Expanding the Biological Toolbox Through Free-Radical Enzyme Engineering,” *Directed Evolution and Synthetic Biology Seminar*, Irvine, CA, February 10, 2017.

**Black, W. B.**, Tan, Z., Jarboe, L. “Increasing *Escherichia coli* Membrane Robustness to Long-Chain Fatty Acids,” *Symposium on Undergraduate Research*, Ames, IA, April 14, 2015.

## POSTER PRESENTATIONS

**Black, W. B.\***, Zhang, L.\* , Mak, W. S.\* , Maxel, S., Cui, Y., King, E., Fong, B., Sanchez Martinez, A., Siegel J. B., and Li, H. “Engineering a Nicotinamide Mononucleotide Redox Cofactor System for Biocatalysis,” *University of California Irvine Chemical and Biomolecular Engineering Department Graduate Student Visitation*, Irvine, CA, March 6, 2020. (\* **Indicates equal contributors**)

**Black, W. B.\***, Zhang, L.\* , Mak, W. S.\* , Maxel, S., Cui, Y., King, E., Fong, B., Sanchez Martinez, A., Siegel J. B., and Li, H. “Engineering a Nicotinamide Mononucleotide Redox Cofactor System for Biocatalysis,” *Synthetic and Chemical Biology Club*, Irvine, CA, September 27, 2019. (\* **Indicates equal contributors**)

**Black, W. B.** and Li, H. “Towards a Universal and Orthogonal Redox Cofactor in Living Cells,” *University of California Irvine Chemical and Biochemical Engineering and Materials Science and Engineering Department Graduate Student Visitation*, Irvine, CA, March 8, 2019.

**Black, W. B.** and Li, H. “Engineering a Novel 3-Methyl-1-Butanol Biosynthetic Pathway in *Escherichia coli*,” *University of California Irvine Chemical and Biochemical Engineering and Materials Science and Engineering Department Graduate Student Visitation*, Irvine, CA, March 15, 2018.

**Black, W. B.** and Li, H. “Engineering a Novel 3-Methyl-1-Butanol Biosynthetic Pathway in *Escherichia coli*,” *American Institute of Chemical Engineers Annual Meeting*, Minneapolis, MN, October 31, 2017.

**Black, W. B.** and Li, H. “Synthetic Biology for Renewable Fuels and Chemicals,” *University of California Irvine Chemical and Biochemical Engineering and Materials Science and Engineering Department Graduate Student Visitation*, Irvine, CA, January 13, 2017.

**Black, W. B.** and Li, H. “Synthetic Biology for Renewable Fuels and Chemicals,” *University of California Irvine Chemical and Biochemical Engineering and Materials Science and Engineering Department Graduate Student Visitation*, Irvine, CA, February 12, 2016.

## ABSTRACT OF THE DISSERTATION

Development of an Orthogonal Cofactor System

by

William Bentley Sowizral Black

Doctor of Philosophy in Chemical and Biomolecular Engineering

University of California Irvine, 2020

Assistant Professor Han Li, Chair

Biological production of chemicals often requires the use of cellular cofactors, such as nicotinamide adenine dinucleotide phosphate (NADP<sup>+</sup>), but these cofactors are expensive to use *in vitro* and difficult to control *in vivo*. Recently, the use of noncanonical redox cofactors, or cofactor mimics, has emerged as a less expensive alternative to native cofactors in enzymatic biotransformation. While these noncanonical cofactors have shown promising results with reductive biotransformation, regeneration of spent cofactor and integration of these cofactors in biological systems has been met with limited success. In this work, we demonstrate the development and application of a noncanonical redox cofactor system based on nicotinamide mononucleotide (NMN<sup>+</sup>).

First, using a computationally designed glucose dehydrogenase with high cofactor specificity towards NMN<sup>+</sup>, we construct an NMN<sup>+</sup>-cycling system to support diverse redox chemistries *in vitro* with a high total turnover number (~39,000) and temporal stability. Then we

introduced this system into *Escherichia coli* whole cells, demonstrating the ability of this system to channel reducing power specifically *in vivo* from glucose to levodione, a pharmaceutical intermediate.

Subsequently, we applied the NMN(H)-cycling system for the production of the terpenoid aldehyde citronellal in crude lysate- and whole cell-based biotransformation. By specifically delivering reducing power to a recombinant enoate reductase, but not to endogenous ADHs, we convert citral to citronellal with minimal byproduct formation (97–100% product purity in crude lysate-based biotransformation). Using knowledge gained from rapidly prototyping the crude-lysate system expression ratios, we translated the system into whole cells, achieving a product purity of 83%. Remarkably, this was achieved without the need to disrupt any of the endogenous alcohol dehydrogenases.

Ultimately, the ability to perform crude lysate- and whole cell-based biotransformation without the need to supplement NMN<sup>+</sup> and to generate NMN<sup>+</sup> renewably for purified protein-based biotransformation is desired. We next engineered *E. coli* cells to biosynthesize NMN<sup>+</sup>. First, we developed a growth-based screening platform to identify effective NMN<sup>+</sup> biosynthetic pathways in *E. coli*. Second, we explored various pathway combinations and host gene disruption to achieve an intracellular level of ~ 1.5 mM NMN<sup>+</sup>, a 130-fold increase over the cell's basal level, in the best strain, which features a previously uncharacterized nicotinamide phosphoribosyltransferase (NadV) from *Ralstonia solanacearum*. Last, we revealed mechanisms through which NMN<sup>+</sup> accumulation impacts *E. coli* cell fitness, which sheds light on future work aiming to improve the production of this noncanonical redox cofactor.

Finally, we expanded the breadth of our orthogonal NMN(H)-cycling system by integrating it with *Saccharomyces cerevisiae*. Using the aforementioned production of citronellal as a model

system, we demonstrated that our orthogonal redox cofactor system translates well across organisms, producing 28 mg/L of citronellal while the activity of endogenous alcohol dehydrogenases in the cellular background remained low. Furthermore, we engineered *S. cerevisiae* cells to accumulate 188  $\mu\text{M}$  of  $\text{NMN}^+$  by integrating the  $\text{NMN}^+$  synthetase,  $\text{NadE}^*$ , and phosphoribosyltransferase,  $\text{NadV}$ , from *Francisella tularensis*. Due to the cell wall of *S. cerevisiae* being resistant to the free diffusion of  $\text{NMN}^+$  into the cell, pairing the  $\text{NMN}^+$  accumulating strain with the  $\text{NMN}(\text{H})$ -cycling system may enable the first example of an *in vivo* noncanonical redox cofactor system which does not require the supplementation of cofactor into the reaction system.



# Chapter 1

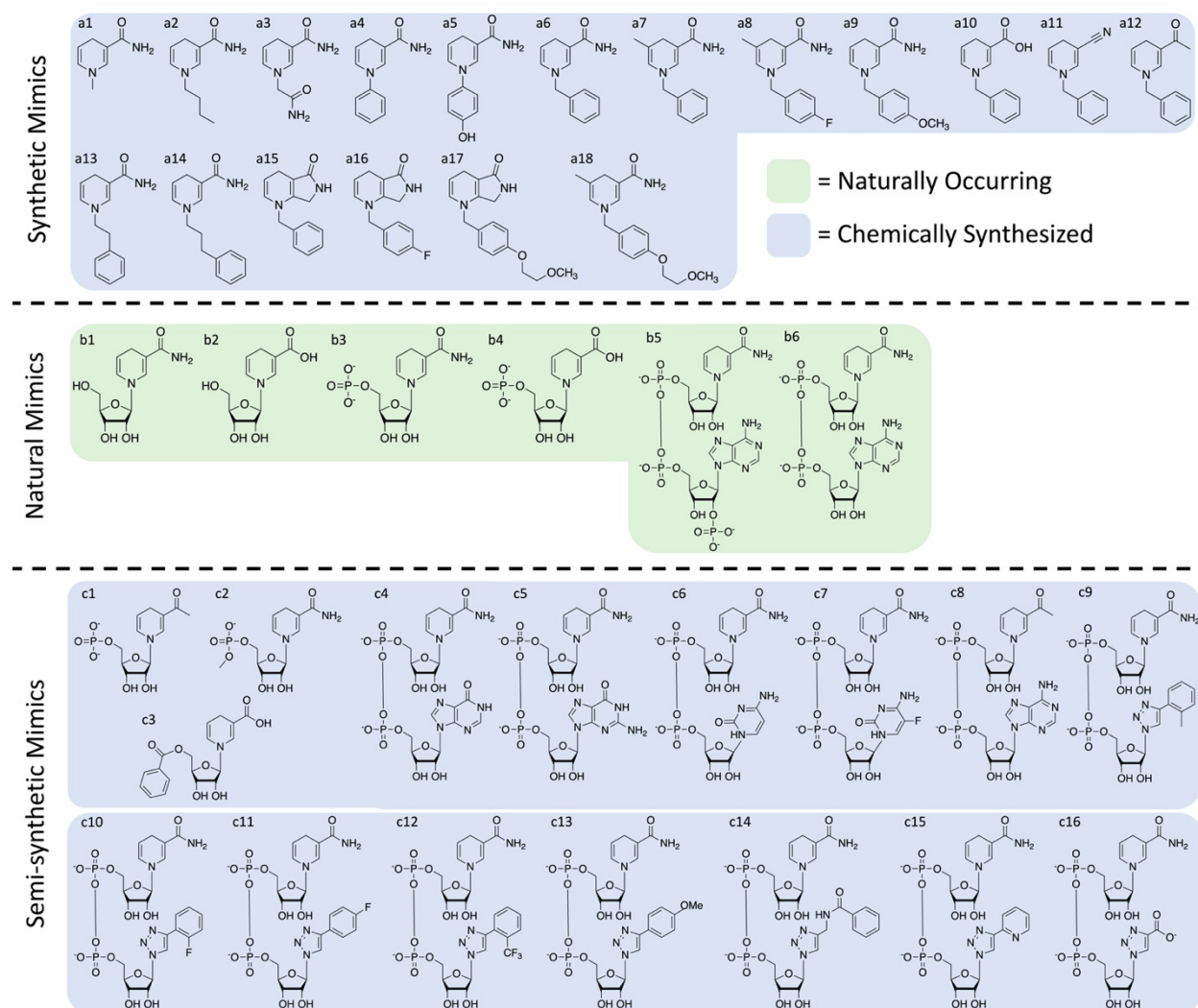
## Interfacing Noncanonical Redox Cofactors with *in vitro* and *in vivo* biotransformation

## 1.1 Introduction

Reductive biotransformation is a valuable tool in the production of many chemicals in *in vitro* and *in vivo* biotransformation. To perform these reactions, oxidoreductase enzymes recruit the reduced redox cofactors nicotinamide adenine dinucleotide, NADH, and nicotinamide adenine dinucleotide phosphate, NADPH, to act as reducing agents for the supply of electrons for enzymatic reduction. However, these enzymes typically require a stoichiometric equivalent of reduced NAD(P)H, which quickly increases the cost of *in vitro* reductive biotransformation as processes increase in scale<sup>1,2</sup>. To minimize these costs, the substitution of NAD(P)H for noncanonical redox cofactors, which are regularly smaller, simpler, and cheaper mimics of NAD(P)H, mNADs, has been proposed<sup>3-5</sup>. Surveying of mNADs for activity with oxidoreductases has found high levels of activity between mNADs and flavin-containing enzymes, flavoenzymes, especially ene reductases<sup>6,7</sup> and nitroreductase<sup>8,9</sup>. However, expanding the search for efficient mNAD/enzyme pairs outside of flavoenzymes has yielded fewer positive results<sup>10,11</sup>. To further minimize the cost of mNAD supply *in vitro*, *in situ* cofactor regenerating systems have been employed to recycle mNADs, enabling a significant reduction in mNAD supplementation requirements<sup>9,12-15</sup>. Recently, protein engineering efforts have produced a variety of mNAD reducing enzymes, and in some cases, these engineered enzymes demonstrate the specific reduction of the mNAD of interest, with very low activity towards native NAD(P)<sup>+</sup><sup>9,15-17</sup>. The ability to specifically, or orthogonally, reduce mNADs opened the door for mNAD reducing systems to be utilized with *in vivo* and crude lysate-based biotransformation<sup>9,18-20</sup>. This review will focus on interfacing mNADs with biological systems, with focus on system design, cofactor cycling advances, and mNAD biotransformation in systems with high cellular background.

## 1.2 Classes of Noncanonical Redox Cofactors

Exploration and synthesis of mNADs has largely focused around cofactors which are inexpensive to produce, structurally distinct from NAD(P)<sup>+</sup>, and interface well with oxidoreductase enzymes. To these aims, a variety of mimics containing different electron withdrawing groups and “handles” for the enzyme to bind the cofactor have been developed (Figure 1). mNADs can be generally grouped into three classes: natural, semi-synthetic, and fully synthetic.



**Figure 1: Noncanonical redox cofactors (mNADs) in their reduced form.** mNADs can be grouped into three classes: synthetic mimics, natural mimics, and semi-synthetic mimics. a1) 1-methylnicotinamide, a2) 1-butyl-1,4-dihyronicotinamide, a3) 1-carbamoylmethyl-1,4-

dihydronicotinamide, a4) 1-phenyl-1,4-dihydronicotinamide a5) 1-(4-hydroxyphenyl)-1,4-dihydronicotinamide, a6) 1-benzyl-1,4-dihydronicotinamide, a7) 1-benzyl-3-carbamoyl-5-methyl-1,4-dihydropyridine, a8) 1-(4-fluorobenzyl)-5-methyl-1,4-dihydropyridine-3-carboxamide, a9) N-4-methoxybenzyl-1,4-dihydro-nicotinamide, a10) 1-benzyl-1,4-dihydronicotinic acid, a11) 1-benzyl-3-cyano-1,4-dihydropyridine, a12) 1-benzyl-3-acetyl-1,4-dihydropyridine, a13) 1-phenethyl-1,4-dihydropyridine-3-carboxamide, a14) 1-(3-phenylpropyl)-1,4-dihydropyridine-3-carboxamide, a15) 1-benzyl-1,4,6,7-tetrahydro-5H-pyrrolo[3,4-b]pyridin-5-one, a16) 1-(4-fluorobenzyl)-1,4,6,7-tetrahydro-5H-pyrrolo[3,4-b]pyridin-5-one, a17) 1-(4-(2-methoxyethoxy)benzyl)-1,4,6,7-tetrahydro-5H-pyrrolo[3,4-b]pyridin-5-one, a18) 1-(4-(2-methoxyethoxy)benzyl)-5-methyl-1,4-dihydropyridine-3-carboxamide. b1) nicotinamide riboside, b2) nicotinic acid riboside, b3) nicotinamide mononucleotide, b4) nicotinic acid mononucleotide, b5) nicotinamide adenine dinucleotide phosphate, b6) nicotinamide adenine dinucleotide. c1) 3-acetylpyridine-ribose, c2)  $\beta$ -nicotinamide-5'-ribose methyl phosphate, c3) nicotinic acid 5'-O-benzoyl riboside, c4) nicotinamide hypoxanthine dinucleotide, c5) nicotinamide guanine dinucleotide, c6) nicotinamide cytosine dinucleotide, c7) nicotinamide flucytosine dinucleotide, c8) 3-acetylpyridine-adenine dinucleotide, c9) nicotinamide 4-(2-methylphenyl)-[1,2,3]-triazole dinucleotide, c10) nicotinamide 4-(2-fluorophenyl)-[1,2,3]-triazole dinucleotide, c11) nicotinamide 4-(4-fluorophenyl)-[1,2,3]-triazole dinucleotide, c12) nicotinamide 4-(2-trifluoromethylphenyl)-[1,2,3]-triazole dinucleotide, c13) nicotinamide 4-(4-methoxyphenyl)-[1,2,3]-triazole dinucleotide, c14) nicotinamide 4-(N-benzyl-ethyl)-[1,2,3]-triazole dinucleotide, c15) nicotinamide 4-(2-pyridinyl)-[1,2,3]-triazole dinucleotide, c16) nicotinamide 4-naphthyl-[1,2,3]-triazole dinucleotide.

Fully-synthetic mNADs like 1-benzylnicotinamide, BNA<sup>+</sup> <sup>3,6,21,22</sup>, and 3-carbamoyl-1-phenethylpyridin-1-ium, P2NA<sup>+</sup> <sup>23,24</sup>, have high structural deviation from NAD(P)<sup>+</sup>. They regularly only retain the catalytic nicotinamide moiety of NAD(P)<sup>+</sup>, and they are functionalized with various “handle” prosthetic groups ranging from -CH<sub>3</sub> (e. g. 1-methylnicotinamide, MNA<sup>+</sup> <sup>8,24,25</sup> to long carbon chains with a terminal benzyl group (e. g. 3-carbamoyl-1-(3-phenylpropyl)pyridin-1-ium, P3NA<sup>+</sup> <sup>23,24</sup>. In some examples, the amide electron withdrawing group of the nicotinamide moiety is exchanged for a carboxyl, keto, or nitrile group<sup>3,6,14</sup>. Due to their small size and relative ease of synthesis<sup>5</sup>, they have been touted as inexpensive alternatives to NAD(P)<sup>+</sup> for *in vitro* applications<sup>1,2,5</sup>.

Semi-synthetic cofactors are structurally very similar to native NAD(P)<sup>+</sup>. However, they feature slight alterations in structure to differentiate them from NAD(P)<sup>+</sup>, most frequently modifying the adenine on the adenosine moiety<sup>15,26,27</sup> (Figure 1). For example, nicotinamide

cytosine dinucleotide, NCD<sup>+</sup>, contains as cytosine in place of the adenine on NAD<sup>+</sup> <sup>15,17,20</sup>. These semi-synthetic cofactors can offer high similarity to NAD(P)<sup>+</sup>, which may enable higher probability of finding enzymes and engineering enzymes to have high levels of activity with the mNAD.

Natural mimics are mNADs which are naturally produced by the cell. Natively, these compounds serve as intermediates in the *de novo* synthesis or salvage of NAD<sup>+</sup> <sup>28,29</sup>, and they are typically smaller, truncated versions of the native cofactors. Recently, nicotinamide mononucleotide, NMN<sup>+</sup>, has been shown to be produced intracellularly in *E. coli* at levels at or higher than typical levels of NAD(P)<sup>+</sup> <sup>28,30</sup>. Marinescu and coworkers utilized a nicotinamide phosphoribosyltransferase (NadV) to produce 23.57 mM of intracellular NMN<sup>+</sup> from nicotinamide fed into the growth medium<sup>30</sup>. Natural mimics serve as attractive candidates for biotransformation because they can be produced renewably, and intracellular production in a host organism may enable *in vivo* biotransformation without the need for exogenous cofactor supply.

When selecting a mNAD for biotransformation, the type of system in which the mNAD will be integrated into is important to consider. In an *in vitro* system with purified proteins, simple synthetic cofactors may significantly reduce cost of cofactor supply to a large-scale system. However, in systems which contain significant cellular background, like *in vivo* or crude lysate-based systems, cofactors which offer improved insulation or orthogonality from the cellular background may reduce native cofactor crosstalk with the engineered system. In addition to system design, breadth of application should be considered. While synthetic cofactors with simpler structures may reduce supply costs, semi-synthetic and natural cofactors may offer a better trade-off in cost/activity since these cofactors are structurally most similar to the native cofactors.

### 1.3 Utilization of mNADs by enzymes

Ultimately, broad utilization of mNAD cofactor systems relies on having a diverse toolkit of enzymes which can receive these mimics efficiently. To date, the majority of enzymes which have demonstrated appreciable activity with mNADs have used the reduced forms of the mimics to perform reactions. Nitroreductases<sup>8,31</sup>, alcohol dehydrogenases<sup>13,32</sup>, dehydrogenases, monooxygenases<sup>9,12,33-35</sup>, azoreductases<sup>36</sup>, NADH oxidases<sup>24,25</sup>, and enoate reductases<sup>3,6,7,14,37,38</sup> have all demonstrated activity with mNADs at varying levels. In particular, the Old Yellow Enzyme family has demonstrated high activity with a wide array of mNADs and substrates, as summarized by Scholtissek and coworkers<sup>39</sup>. Protein engineering serves as a valuable tool to further broaden the scope of enzymes capable of utilizing mNADs for reductive biotransformation. For example, the cytochrome P450 BM-3 from *Bacillus megaterium*, which has exhibited no activity towards mNADs under the conditions tested, was demonstrated by Ryan et al. to have high levels of activity with BNAH and  $\beta$ -nicotinamide-5'-ribose methyl phosphate, NMNCH, when mutations R966D-W1046S were applied<sup>12</sup>. Furthermore, biomimetics have been shown to enable indirect enzymatic reduction by reducing flavins in solution, which can be subsequently bound by an enzyme for reductive biotransformation<sup>35</sup>.

### 1.4 *In vitro* mNAD systems with purified proteins

#### 1.4.1 Systems with reduced cofactor supplementation

The simplest form of an mNAD biotransformation system is an *in vitro* system using purified protein, reduced mNAD, and substrate spiked into buffer. This system represents the vast majority of mNAD systems investigated to date. Since concentrations and supply of buffers, enzymes, cofactor, and substrates are all user defined, highly specific biotransformation at high

catalytic rate can be achieved. In addition, since native cofactors are not present, enzymes can be selected or engineered for mNAD activity, rather than for orthogonality. For example, Guarneri et al. utilized the synthetic mNAD 1-(2-carbamoylmethyl)-1,4-dihydronicotinamide, AmNAH, with the *para*-hydroxybenzoate hydrolase, PHBH, from *Pseudomonas fluorescens* to catalyze the hydroxylation of 5 mM 4-hydroxybenzoate to 3,4-dihydroxybenzoate with 100% conversion in 30 minutes, nearing the activity demonstrated with the native cofactors<sup>34</sup>.

#### 1.4.2 Cofactor regeneration

While the cost of *in vitro* biotransformation can be decreased by substituting the supply of NAD(P)H for mNADHs, the cost of equimolar mNADH supply may limit economic viability at larger scales. To further reduce the cost of cofactor supply *in vitro*, *in situ* cofactor regeneration using organometallic catalysts<sup>6,12,13,21</sup>, artificial metalloenzymes<sup>14</sup>, and engineered enzymes<sup>15,18,19,23,28</sup> has been employed to significantly reduce the amount and cost of cofactor needed to be supplied (Table 1). However, these recycling methods need to be able to function for extended time periods to be viable. The efficiency of these recycling methods can be modeled by the Total Turnover Number (TTN), which represents the moles of product generated per mole of catalyst supplied before the catalyst becomes inactive.

**Table 1: *In vitro* Noncanonical Redox Cofactor Cycling Systems**

Cofactor Reducing Component	Cofactor <sup>a</sup>	Cofactor Oxidizing Enzyme	Buffer	Substrate	Yield	TTN	Ref
Rh-complex <sup>b</sup>	BNA <sup>+</sup>	BM3 P450* ( <i>Bacillus megaterium</i> )	20 mM potassium phosphate, pH 7.4	60 μM p-nitrophenoxydecanoic acid	n.r.	312	[12]
Rh-complex <sup>b</sup>	BNA <sup>+</sup>	Horse Liver Alcohol Dehydrogenase	100 mM potassium phosphate, pH 7	83.58 μM 1-phenyl-3-butanone <sup>c</sup>	90%	n.r.	[21]
Rh-complex <sup>b</sup>	BNA <sup>+</sup>	P450 CAM ( <i>Pseudomonas putida</i> )	20 mM potassium phosphate, pH 7.4	1 mM camphor	n.r.	38	[12]
Rh-complex <sup>c</sup>	BNA <sup>+</sup>	Enoate Reductase ( <i>Thermus scotoductus</i> )	50 mM MOPS buffer, pH 7.0	10 mM ketoisophorone	66%	n.r.	[6]
Rh-complex <sup>b</sup>	NMNC <sup>+</sup>	Horse Liver Alcohol Dehydrogenase	100 mM potassium phosphate, pH 7	83.58 μM 1-phenyl-3-butanone <sup>c</sup>	90%	n.r.	[21]
Ir Metalloenzyme <sup>d</sup>	BAP <sup>+</sup>	Enoate Reductase ( <i>Thermus scotoductus</i> )	600 mM MOPS, pH 7.0	30mM <i>N</i> -ethyl-2-methylmaleimide <sup>c</sup>	99%	2000	[14]
Ir Metalloenzyme <sup>d</sup>	BCNP <sup>+</sup>	Enoate Reductase ( <i>Thermus scotoductus</i> )	50 mM MOPS buffer, pH 7.0	10mM <i>N</i> -ethyl-2-methylmaleimide	12%	n.r.	[14]
Ir Metalloenzyme <sup>d</sup>	BCOA <sup>+</sup>	Enoate Reductase ( <i>Thermus scotoductus</i> )	600 mM MOPS, pH 7.0	10mM <i>N</i> -ethyl-2-methylmaleimide	18%	n.r.	[14]
Ir Metalloenzyme <sup>d</sup>	BNA <sup>+</sup>	Enoate Reductase ( <i>Thermus scotoductus</i> )	600 mM MOPS, pH 7.0	10mM <i>N</i> -ethyl-2-methylmaleimide	37%	n.r.	[14]
Ir Metalloenzyme <sup>d</sup>	MNA <sup>+</sup>	Enoate Reductase ( <i>Thermus scotoductus</i> )	600 mM MOPS, pH 7.0	10mM <i>N</i> -ethyl-2-methylmaleimide	12%	n.r.	[14]
Horse Liver Alcohol Dehydrogenase	BNA <sup>+</sup>	Hemoglobin ( <i>Bovine erythrocytes</i> )	50 mM phosphate buffer, pH 8	10 mM H <sub>2</sub> O <sub>2</sub>	~60%	n.r.	[22]
Horse Liver Alcohol Dehydrogenase	BNA <sup>+</sup>	Horseradish Peroxidase ( <i>Armoracia rusticana</i> )	50 mM phosphate buffer, pH 7	10 mM H <sub>2</sub> O <sub>2</sub>	~75%	n.r.	[22]
Horse Liver Alcohol Dehydrogenase	BNA <sup>+</sup>	Myoglobin ( <i>Equus caballus</i> )	50 mM Phosphate buffer, pH 8	10mM H <sub>2</sub> O <sub>2</sub>	93%	n.r.	[22]
Malic Enzyme* ( <i>Escherichia coli</i> )	NCD <sup>+</sup>	Formate Dehydrogenase* ( <i>Pseudomonas</i> sp.)	50 mM HEPES, pH 7.5	10 mM formate, 50 mM pyruvate	53.5%	n.r.	[20]
Phosphite dehydrogenase* ( <i>Ralstonia</i> sp.)	NCD <sup>+</sup>	Malic Enzyme* ( <i>Escherichia coli</i> )	50 mM HEPES, pH 7.5	5 mM phosphite, 50 mM malate	n.r.	n.r.	[18]



Malic Enzyme* ( <i>Escherichia coli</i> )	NFCD <sup>+</sup>	Lactate Dehydrogenase* ( <i>Lactobacillus helveticus</i> )	50 mM HEPES, pH 7.5	5 mM Malate	~99%	n.r.	[15]
Lactate Dehydrogenase* ( <i>Lactobacillus helveticus</i> )	NFCD <sup>+</sup>	Malic Enzyme* ( <i>Escherichia coli</i> )	50 mM HEPES, pH 7.5	5 mM Malate	~99%	n.r.	[15]
<i>Glucose Dehydrogenase*</i> ( <i>Bacillus subtilis</i> )	NMN <sup>+</sup>	<i>BM3 P450*</i> ( <i>Bacillus megaterium</i> )	<i>200 mM potassium phosphate,</i> <i>pH 7.5</i>	<i>50 μM cytochrome c</i>	<i>&gt;99%</i>	<i>n.r.</i>	<i>[9]</i>
<i>Glucose Dehydrogenase*</i> ( <i>Bacillus subtilis</i> )	NMN <sup>+</sup>	<i>Nitroreductase</i> ( <i>Escherichia coli</i> )	<i>200 mM potassium phosphate,</i> <i>pH 7.5</i>	<i>2 mM nitrofurazone</i>	<i>92%</i>	<i>n.r.</i>	<i>[9]</i>
<i>Glucose Dehydrogenase*</i> ( <i>Bacillus subtilis</i> )	NMN <sup>+</sup>	<i>Old Yellow Enzyme 3</i> ( <i>Saccharomyces cerevisiae</i> )	<i>200 mM potassium phosphate,</i> <i>pH 7.5</i>	<i>5 mM 4-phenyl-3-butyn-2-one</i>	<i>&gt;99%</i>	<i>n.r.</i>	<i>[9]</i>
6-phosphogluconate dehydrogenase* ( <i>Thermotoga maritima</i> )	NMN <sup>+</sup>	Enoate Reductase ( <i>Thermus scotoductus</i> )	100 mM HEPES, pH 7.5	10 mM 2-methyl-2-cyclohexen-1-one	98%	n.r.	[26]
<i>Glucose Dehydrogenase*</i> ( <i>Bacillus subtilis</i> )	NMN <sup>+</sup>	<i>Enoate Reductase</i> ( <i>Pseudomonas putida</i> )	<i>200 mM potassium phosphate,</i> <i>pH 7.5</i>	<i>3.28 mM citral</i>	<i>58%</i>	<i>n.r.</i>	<i>[19]</i>
<i>Glucose Dehydrogenase*</i> ( <i>Bacillus subtilis</i> )	NMN <sup>+</sup>	<i>Enoate Reductase</i> ( <i>Pseudomonas putida</i> )	<i>200 mM potassium phosphate,</i> <i>pH 7.5</i>	<i>33 mM ketoisophorone<sup>e</sup></i>	<i>&gt;99%<sup>f</sup></i>	<i>39000</i>	<i>[9]</i>
Glucose Dehydrogenase* ( <i>Sulfolobus solfataricus</i> )	P2NA <sup>+</sup>	Enoate Reductase ( <i>Thermus scotoductus</i> )	100 mM Tris-HCl, pH 8	10 mM 2-methylbut-2-enal	100%	1183	[23]

Entries in italics (not including species names) represents work from this thesis

\* = engineered enzyme

n.r. = not reported

<sup>a</sup> Names of cofactors: NFCD<sup>+</sup>, nicotinamide flucytosine dinucleotide; NCD<sup>+</sup>, nicotinamide cytosine dinucleotide; BNA<sup>+</sup>, 1-benzylnicotinamide; P2NA<sup>+</sup>, 3-carbamoyl-1-phenethylpyridin-1-ium; NMN<sup>+</sup>, nicotinamide mononucleotide; NMNC<sup>+</sup>, β-nicotinamide-5'-ribose methyl phosphate; BAP<sup>+</sup>, 1-benzyl-3-acetylpyridinium; BCNP<sup>+</sup>, 1-benzyl-3-cyanopyridinium; BCOA<sup>+</sup>, 1-benzyl-3-carboxypyridinium; MNA<sup>+</sup>, 1-methylnicotinamide.

<sup>b</sup> [Cp\*Rh(bpy)(H<sub>2</sub>O)](OTf)<sub>2</sub>

<sup>c</sup> [Cp\*Rh(bpy)(H<sub>2</sub>O)](Cl)<sub>2</sub>

<sup>d</sup> IrC-S112K

<sup>e</sup> additional substrates tested

<sup>f</sup> Conversion experiments differed in conditions to TTN experiments. Thus, yield values are higher than was demonstrated in the TTN experiments.

Rhodium-based catalysts have been used to reduce mNADs to from cofactor cycling systems with cytochrome P450s<sup>12,13</sup>, horse liver alcohol dehydrogenase<sup>13,21</sup>, and enoate reductases<sup>6</sup> (Table 1). Ryan et al. constructed an mNAD cycling system around BNA<sup>+</sup> using a [Cp\*Rh(bpy)(H<sub>2</sub>O)](Otf)<sub>2</sub> complex with an engineered cytochrome P450 from *Bacillus megaterium*. Using the reduction of *p*-nitrophenoxydecanoic acid as a model system, a total turnover number (TTN) of 312 was achieved<sup>12</sup> (Table 1). In addition, these metal catalysts can serve as mediators for indirect photochemical reduction of mNADs<sup>40</sup>. However, in some cases, Rh-complex cycling has been shown to cause mutual inactivation of both the catalyst and the enzyme, resulting in decreased system activity and TTN<sup>41</sup>.

To combat the mutual inactivation between catalyst and enzyme, the docking of catalysts into protein scaffolds to “shield” the catalyst and enzyme from each other has been proposed<sup>14,42</sup>. Okamoto et al. demonstrated the use of a biotinylated iridium-pianostool cofactor docked into a streptavidin enzyme scaffold to reduce the mNADs BNA<sup>+</sup>, MNA<sup>+</sup>, 1-benzyl-3-acetylpyridinium (BAP<sup>+</sup>), 1-benzyl-3-carboxypyridinium (BCOA<sup>+</sup>), and 1-benzyl-3-cyanopyridinium (BCNP<sup>+</sup>)<sup>14</sup> (Table 1). They subsequently paired their artificial metalloenzyme, with the enoate reductase from *Thermus scotoductus*, *TsOYE*, to reduce the activated C=C double bond in *N*-ethyl-2-methylmaleimide. Using BAP<sup>+</sup> as the cofactor, a TTN of 1980 was achieved<sup>14</sup> (Table 1). Consistent with the Rh-complex-based cofactor cycling<sup>41</sup>, when the Ir-complex was not docking into the enzyme scaffold, catalyst activity was repressed in the presence of *TsOYE*<sup>14</sup>.

In Nature, enzymes are used to regenerate reduced cofactor in the cellular environment, especially through the central metabolism. However, wild type enzymes regularly exhibit low activities towards the oxidation of mNADs<sup>9,10,23</sup>. Recently, protein engineering has produced a variety of candidate enzymes for mNAD reduction (Table 1), including enzymes which consume

cheap sacrificial feed stocks like formate<sup>20</sup>, phosphite<sup>16,18</sup>, and glucose<sup>9,23</sup>. In addition, a few examples of intra-pathway enzymes which can be used to couple cofactor reduction and oxidation with pathway flux or *de novo* production, have also been engineered<sup>15,17,26</sup>.

**Table 2: Apparent Kinetic Parameters for Engineered Enzymes with Oxidized mNADs**

Enzyme	Mutations	Cofactor <sup>a</sup>	K <sub>M</sub> (mM)	k <sub>cat</sub> (s <sup>-1</sup> )	k <sub>cat</sub> /K <sub>M</sub> (mM <sup>-1</sup> s <sup>-1</sup> )	mNAD Preference (k <sub>cat</sub> /K <sub>M</sub> ratio)		Ref.
						mNAD/NAD <sup>+</sup>	mNAD/NADP <sup>+</sup>	
<i>Escherichia coli</i> Malic Enzyme	L310R/Q401C	NAD <sup>+</sup>	10.4	3.8	0.36			[15]
		NADP <sup>+</sup>	n.r.	n.r.	n.r.			
		NFCD <sup>+</sup>	1.70	162.4	96.7	269	n.r.	
		NCD <sup>+</sup>	1.02	158.2	154.6	427	n.r.	
<i>Pseudomonas</i> sp. 101 Formate Dehydrogenase	V198I/C256I/P 260S/E261P/S 381N/S383F	NAD <sup>+</sup>	7.97	0.07	0.00878			[20]
		NADP <sup>+</sup>	n.r.	n.r.	n.r.			
		NCD <sup>+</sup>	0.12382	0.18	1.45	165	n.r.	
<i>Sulfolobus</i> <i>solfataricus</i> Glucose Dehydrogenase	I192T/V306I	NAD <sup>+</sup>	0.17	0.95	5.65			[23]
		NADP <sup>+</sup>	n.r.	n.r.	n.r.			
		BNA <sup>+</sup>	5.49	0.00900	0.00164	2.90×10 <sup>-4</sup>	n.r.	
		P2NA <sup>+</sup>	8.16	0.04217	0.00517	0.0009	n.r.	
		P3NA <sup>+</sup>	4.1	0.0070	0.00170	3.01×10 <sup>-4</sup>	n.r.	
<i>Bacillus subtilis</i> Glucose Dehydrogenase	<i>Y39Q/A93K/I1 95R</i>	NAD <sup>+</sup>	3.7	0.41	0.11			[9]
		NADP <sup>+</sup>	0.61	4.4	7.5			
		NMN <sup>+</sup>	6.4	3.1	0.51	4.6	0.068	
	<i>S17E/Y39Q/A9 3K/I195R</i>	NAD <sup>+</sup>	6.5	0.025	0.0038			
		NADP <sup>+</sup>	2.0	0.022	0.011			
		NMN <sup>+</sup>	5.9	1.2	0.21	55.3	19.1	
<i>Lactobacillus</i> <i>helveticus</i> Lactate Dehydrogenase	V152R/I177K/ N213E	NAD <sup>+</sup>	1.60	0.08	0.049			[17]
		NADP <sup>+</sup>	n.r.	n.r.	n.r.			
		NCD <sup>+</sup>	1.38	2.95	2.1	44.1	n.r.	
	V152R/I177K/ N213I	NAD <sup>+</sup>	1.05	0.08	0.074			
		NADP <sup>+</sup>	n.r.	n.r.	n.r.			
		NCD <sup>+</sup>	0.6600	2.02	3.1	41.4	n.r.	
<i>Thermotoga</i> <i>maritima</i> 6-phosphogluconate dehydrogenase	Mut6-1 <sup>b</sup>	NAD <sup>+</sup>	n.r.	n.r.	n.r.			[26]
		NADP <sup>+</sup>	0.19	28.9	148.6			
		NMN <sup>+</sup>	13.5	27.4	2.04	n.r.	0.014	
<i>Ralstonia</i> sp. 4506 Phosphite Dehydrogenase	I151R/P176R/ M207A	NAD <sup>+</sup>	4.7	0.21	0.045			[16]
		NADP <sup>+</sup>	n.r.	n.r.	n.r.			
		NCD <sup>+</sup>	0.0991	0.20	2.04	44.9	n.r.	
	I151R/P176E/ M207A	NAD <sup>+</sup>	11.7	0.40	0.034			
		NADP <sup>+</sup>	n.r.	n.r.	n.r.			
		NCD <sup>+</sup>	0.2815	0.35	1.24	36.5	n.r.	
<i>Pyrococcus furiosus</i> Alcohol Dehydrogenase	K249G/H255R	NAD <sup>+</sup>	0.46	3	6.5			[10]
		NADP <sup>+</sup>	n.r.	n.r.	n.r.			
		NMN <sup>+</sup>	2.6	0.027	0.0104	0.0016	n.r.	

Entries in italics (not including organism names) represents work in this thesis

<sup>a</sup> Names of cofactors: NAD<sup>+</sup>, nicotinamide adenine dinucleotide; NADP<sup>+</sup>, nicotinamide adenine dinucleotide phosphate; NFCD<sup>+</sup>, nicotinamide flucytosine dinucleotide; NCD<sup>+</sup>, nicotinamide cytosine dinucleotide; BNA<sup>+</sup>, 1-benzylnicotinamide; P2NA<sup>+</sup>, 3-carbamoyl-1-phenethylpyridin-1-ium; P3NA<sup>+</sup>, 3-carbamoyl-1-(3-phenylpropyl)pyridin-1-ium; NMN<sup>+</sup>, nicotinamide mononucleotide.

<sup>b</sup>Mut6-1: A11G/K27R/R33I/T34I/F60Y/D82L/T83L/Q86L/K118N/I120F/D251E/D294V/F326S/F329Y/Y383C/N387S/V390G/A447V

On a systems level, enzymatic mNAD regeneration can be approached from two directions, high activity reduction for *in vitro* applications and specific, or orthogonal, mNAD reduction for *in vivo* and crude lysate-based systems. In a purified enzyme system, enzymes can be engineered for high activity with the mNAD without the need to limit native cofactor activity. However, in applications with high cellular background, orthogonal cofactor reduction is required to maintain an insulated system. For example, Huang et al. engineered a 6-phosphogluconate dehydrogenase, 6PGDH, to reduce NMN<sup>+</sup> <sup>26</sup>. This 6PGDH mutant exhibited a  $k_{cat}$  of 27.4 s<sup>-1</sup> with NMN<sup>+</sup> (Table 2), ~1.74 higher than the  $k_{cat}$  of the wild type enzyme with its native cofactor NADP<sup>+</sup> <sup>26</sup>. However, since the 6PGDH mutant still exhibited high levels of activity with the native NADP<sup>+</sup> and a high  $K_M$  for NMN<sup>+</sup> of 13.5 mM (Table 2) <sup>26</sup>, this enzyme is a strong candidate for use in *in vitro* biotransformation, but not for specific reduction *in vivo*. When paired with the ene reductase from *Thermus scotodutus* for the reduction of 2-methyl-2-cyclohexen-1-one to methylcyclohexanone, the system demonstrated nearly identical activity with NMN<sup>+</sup> as the wild type enzyme and NADP<sup>+</sup>, 10 mM of methylcyclohexanone in 2 hours <sup>26</sup>. Since the amount of cofactor supplied to *in vitro* systems is user defined, the high  $K_M$  of the 6PGDH mutant was overcome by supplementing 20 mM of NMN<sup>+</sup>, enabling the full utilization of the mutant's high turnover number <sup>26</sup>.

For *in vivo* applications, Liu et al. engineered a phosphite dehydrogenase, Pdh\*, to reduce NCD<sup>+</sup> <sup>16</sup>. This mutant had a low  $K_M$ , 0.282 mM, for NCD<sup>+</sup>, and a comparable  $k_{cat}$  to the wild type enzyme with NAD<sup>+</sup> (Table 2) <sup>16</sup>. Importantly, the  $K_M$  of Pdh\* with NAD<sup>+</sup> (Table 2) was high, well above expected intracellular NAD<sup>+</sup> levels, so in a cellular environment, this enzyme would likely selectively reduce NCD<sup>+</sup> over NAD<sup>+</sup> <sup>16</sup>. However, kinetic parameters with this mutant were not reported with NADP<sup>+</sup>, so the ability for the enzyme to function orthogonally to both native cofactors *in vivo* is not clear. Similar orthogonal cofactor regeneration systems have been

demonstrated with other enzymes using  $\text{NCD}^+$  and  $\text{NFCD}^+$ , however,  $\text{NADP}^+$  activity was not investigated (Table 2) <sup>15,20</sup>. The ideal orthogonal mNAD regenerating enzyme retains a high  $k_{\text{cat}}$  and low  $K_{\text{M}}$  for the target cofactor, but it exhibits a high  $K_{\text{M}}$  (above intracellular levels of native cofactors) and a low  $k_{\text{cat}}$  for both  $\text{NAD}^+$  and  $\text{NADP}^+$ .

### **1.5 Interfacing mNADs with complex cellular systems for orthogonal electron delivery**

In contrast to purified protein-based systems, integration of mNADs into cellular systems requires careful component selection to ensure the cellular background does not interfere with the mNAD system and vice versa. When working with an *in vivo*, whole cell system, a mechanism is needed to accumulate intracellular mNAD. Once the mNAD is present in the cell, mNAD degradation needs to be minimized. Next, the mNAD needs to be readily accepted by the enzyme(s) of interest, but not readily consumed by the cell's native enzymes. Finally, an efficient, orthogonal method for cofactor regeneration needs to be integrated.

Prior to this thesis, only one system had been demonstrated with the ability to drive *in vivo* biotransformation using mNADs, employing engineered enzymes to specifically reduce their respective mNADs (Table 3). Zhao and coworkers have developed a noncanonical redox cofactor system around the semi-synthetic mNAD  $\text{NCD}^+$  in *E. coli* through a series of papers. In this system, they utilized the nucleotide transporter, Ndt, from *Arabis thaliana* to transport exogenously supplied  $\text{NCD}^+$  into the cells<sup>18,20</sup>. Since  $\text{NCD}(\text{H})$  is structurally similar to  $\text{NAD}(\text{H})$ , the native NAD degradation enzyme, UshA, is active upon it<sup>43</sup>. Subsequent disruption of this enzyme decreases extracellular  $\text{NCD}^+$  degradation and subsequently aided in increased  $\text{NCD}^+$  uptake. However, intracellular  $\text{NCD}^+$  degradation still persisted in the  $\Delta\text{ushA}$  strain, especially in the presence of glucose<sup>44</sup>. The primary readout used for this system is the *de novo* production of malate from glucose. This has been achieved by coupling a malic enzyme from *E. coli*, which has

been engineered for NCD<sup>+</sup> preference<sup>15</sup>, with an engineered formate dehydrogenase, FDH\*<sup>20</sup>, or engineered phosphite dehydrogenase, Pdh\*<sup>18</sup>. When Pdh\* was used as the NCD regenerating system, 3.91 mM of malate was produced (Table 3)<sup>18</sup>. When FDH\* was coupled with malic enzyme, FDH\* was used to reduce NCD<sup>+</sup> and as a mechanism for CO<sub>2</sub> generation within the cell, generating ~2.5 mM of malate (Table 3)<sup>20</sup>. However, when NCD was not supplied, malate production was still present at a lower level (Table 3), indicating NAD(H)-dependent activity in the system was still present with the engineered enzymes<sup>18,20</sup>.

*in vivo* mNAD systems are relatively under-explored compared to their *in vitro* counterparts. Further investigation into methods of cofactor reduction which are whole-cell compatible and engineering of reductases for orthogonal mNAD utilization are critical to the success of this growing field. Additionally, tuning of these whole cells systems is important since they are not regulated by the host's system. Therefore, rapid prototyping tools like crude lysate-based screening can serve as a valuable tool to understand the relationship of system balance, cofactor supply needs, and large pathway development, especially since users have direct access to the cellular components<sup>19,45</sup>.

**Table 3: *In vivo* Noncanonical Redox Cofactor Systems**

Cofactor	Organism	Enzymes		Buffer	Substrates	Product Formation	Non-specific Product Formation <sup>c</sup>	Ref.
		Oxidizing <sup>a</sup>	Reducing <sup>b</sup>					
NCD <sup>+</sup>	<i>E. coli</i>	Malic Enzyme*	Phosphite dehydrogenase*	MOPS medium, 10 mM NaHCO <sub>3</sub>	2.5 mM phosphite, 100 mM glucose	3.91 mM malate	2.82 mM malate	[18]
NCD <sup>+</sup>	<i>E. coli</i>	Malic Enzyme*	Formate Dehydrogenase*	40 mM MOPS, pH 6.5	5 mM formate, 100 mM glucose	~2.5 mM malate	~0.25 mM malate	[20]
NMN <sup>+</sup>	<i>E. coli</i>	<i>Enoate Reductase</i>	<i>Glucose Dehydrogenase*</i>	<i>100 mM potassium phosphate, pH 7.5</i>	<i>33 mM ketoisophorone, 200 mM glucose</i>	<i>6.48 mM levodione</i>	<i>0.87 mM levodione<sup>d</sup></i>	<i>[9]</i>
NMN <sup>+</sup>	<i>E. coli</i>	<i>Enoate Reductase</i>	<i>Glucose Dehydrogenase*</i>	<i>100 mM potassium phosphate, pH 7.4</i>	<i>3.28 mM citral, 200 mM glucose</i>	<i>0.21 mM citronellal</i>	<i>0 mM citronellal</i>	<i>[19]</i>

\* indicates engineered enzyme

Entries in italics (not including organism names) represents work from this thesis

<sup>a</sup>Enzyme functions in the cofactor oxidizing direction

<sup>b</sup>Enzyme functions in the cofactor reducing direction

<sup>c</sup>Non-specific product formation is defined as when no mNAD was supplied, unless otherwise stated

<sup>d</sup>Cofactor reducing enzyme was not supplied

## 1.6 Motivation

To date, the majority of work with mNADs has focused on the activity of synthetic cofactors in purified protein-based systems, especially with enoate reductases. Additionally, many of the mNADs studied to date use similar “handles”, namely benzyl groups, for the enzymes to grip and position the cofactor in the active site. Expanded investigation of diverse cofactor “handles”, especially within the minimally-investigated natural mNAD group, may produce additional highly active mNAD candidates. Crucially, mNAD regeneration systems have been met with limited success, especially for the specific reduction of the mNAD over NAD<sup>+</sup> and NADP<sup>+</sup>, which is key for applications with high cellular background like crude lysate- and whole cell-based biotransformation. The successful construction of a highly active and orthogonal mNAD system has potential to be applied universally as an inexpensive, *in vitro* biotransformation system and as a highly-tunable, insulated redox system in engineered microorganisms.



## 1.7 Objectives

The goal of this thesis was to construct, optimize, and apply an orthogonal redox cofactor system centered around the noncanonical redox cofactor nicotinamide mononucleotide, NMN<sup>+</sup>, for both *in vitro* and *in vivo* biotransformation. The specific aims were as follows. First, build an *in vitro* system using purified proteins to enzymatically cycle NMN(H) with high activity, temporal stability, and broad application with different enzymes and substrates classes. Second, translate the NMN(H)-cycling system into *E. coli* whole cells to construct an orthogonal, third redox cofactor system capable of delivering specific reducing power in the cell. Third, develop a crude lysate-based biotransformation system to rapidly prototype, optimize, and tune the activity and orthogonality of NMN(H)-cycling system in high cellular background. Ideally, information learned in optimization of the crude lysate system translates well into whole cell design, and it can therefore be used as a facile tool for pathway design and optimization in the future. Fourth, use metabolic engineering to enable NMN<sup>+</sup> accumulation and production in *E. coli* cells. Finally, translate the NMN(H)-cycling system into *Saccharomyces cerevisiae* to enable the specific delivery of reducing power by a noncanonical redox cofactor in both prokaryotic and eukaryotic systems.

The following chapters will discuss these objectives.

## 1.8 References

- [1] Guarneri, A.; van Berkel, W. J.; Paul, C. E. Alternative Coenzymes for Biocatalysis. *Curr. Opin. Biotechnol.* **2019**, *60*, 63–71.
- [2] You, C.; Percival Zhang, Y.-H. Biomanufacturing by *in Vitro* Biosystems Containing Complex Enzyme Mixtures. *Process Biochem.* **2017**, *52*, 106–114.
- [3] Paul, C. E.; Gargiulo, S.; Opperman, D. J.; Lavandera, I.; Gotor-Fernández, V.; Gotor, V.; Taglieber, A.; Arends, I. W. C. E.; Hollmann, F. Mimicking Nature: Synthetic Nicotinamide Cofactors for C=C Bioreduction Using Enoate Reductases. *Org. Lett.* **2013**, *15*, 180–183.

- [4] Zachos, I.; Nowak, C.; Sieber, V. Biomimetic Cofactors and Methods for Their Recycling. *Curr. Opin. Chem. Biol.* **2019**, *49*, 59–66.
- [5] Paul, C. E.; Arends, I. W. C. E.; Hollmann, F. Is Simpler Better? Synthetic Nicotinamide Cofactor Analogues for Redox Chemistry. *ACS Catal.* **2014**, *4*, 788–797.
- [6] Knaus, T.; Paul, C. E.; Levy, C. W.; de Vries, S.; Mutti, F. G.; Hollmann, F.; Scrutton, N. S. Better than Nature: Nicotinamide Biomimetics That Outperform Natural Coenzymes. *J. Am. Chem. Soc.* **2016**, *138*, 1033–1039.
- [7] Löw, S. A.; Löw, I. M.; Weissenborn, M. J.; Hauer, B. Enhanced Ene-Reductase Activity through Alteration of Artificial Nicotinamide Cofactor Substituents. *ChemCatChem* **2016**, *8*, 911–915.
- [8] Knox, R. J.; Friedlos, F.; Jarman, M.; Davies, L. C.; Goddard, P.; Anlezark, G. M.; Melton, R. G.; Sherwood, R. F. Virtual Cofactors for an Escherichia Coli Nitroreductase Enzyme: Relevance to Reductively Activated Prodrugs in Antibody Directed Enzyme Prodrug Therapy (ADEPT). *Biochem. Pharmacol.* **1995**, *49*, 1641–1647.
- [9] Black, W. B.; Zhang, L.; Mak, W. S.; Maxel, S.; Cui, Y.; King, E.; Fong, B.; Sanchez Martinez, A.; Siegel, J. B.; Li, H. Engineering a Nicotinamide Mononucleotide Redox Cofactor System for Biocatalysis. *Nat. Chem. Biol.* **2020**, *16*, 87–94.
- [10] Campbell, E.; Meredith, M.; D. Minter, S.; Banta, S. Enzymatic Biofuel Cells Utilizing a Biomimetic Cofactor. *Chem. Commun.* **2012**, *48*, 1898–1900.
- [11] Paul, C. E.; Hollmann, F. A Survey of Synthetic Nicotinamide Cofactors in Enzymatic Processes. *Appl. Microbiol. Biotechnol.* **2016**, *100*, 4773–4778.
- [12] Ryan, J. D.; Fish, R. H.; Clark, D. S. Engineering Cytochrome P450 Enzymes for Improved Activity towards Biomimetic 1,4-NADH Cofactors. *ChemBioChem* **2008**, *9*, 2579–2582.
- [13] Lo, H. C.; Ryan, J. D.; Kerr, J. B.; Clark, D. S.; Fish, R. H. Bioorganometallic Chemistry: Co-Factor Regeneration, Enzyme Recognition of Biomimetic 1,4-NADH Analogs, and Organic Synthesis; Tandem Catalyzed Regioselective Formation of N-Substituted-1,4-Dihydronicotinamide Derivatives with [Cp\*Rh(Bpy)H]<sup>+</sup>, Coupled to Chiral S-Alcohol Formation with HLADH, and Engineered Cytochrome P450s, for Selective C-H Oxidation Reactions. *J. Organomet. Chem.* **2017**, *839*, 38–52.
- [14] Okamoto, Y.; Köhler, V.; Paul, C. E.; Hollmann, F.; Ward, T. R. Efficient In Situ Regeneration of NADH Mimics by an Artificial Metalloenzyme. *ACS Catal.* **2016**, *6* (6), 3553–3557.

- [15] Ji, D.; Wang, L.; Hou, S.; Liu, W.; Wang, J.; Wang, Q.; Zhao, Z. K. Creation of Bioorthogonal Redox Systems Depending on Nicotinamide Flucytosine Dinucleotide. *J. Am. Chem. Soc.* **2011**, *133*, 20857–20862.
- [16] Liu, Y.; Feng, Y.; Wang, L.; Guo, X.; Liu, W.; Li, Q.; Wang, X.; Xue, S.; Zhao, Z. K. Structural Insights into Phosphite Dehydrogenase Variants Favoring a Non-Natural Redox Cofactor. *ACS Catal.* **2019**, *9*, 1883–1887.
- [17] Liu, Y.; Li, Q.; Wang, L.; Guo, X.; Wang, J.; Wang, Q.; Zhao, Z. K. Engineering D-Lactate Dehydrogenase to Favor an Non-Natural Cofactor Nicotinamide Cytosine Dinucleotide. *ChemBioChem* **2020**, *21*, 1972–1975.
- [18] Wang, L.; Ji, D.; Liu, Y.; Wang, Q.; Wang, X.; Zhou, Y. J.; Zhang, Y.; Liu, W.; Zhao, Z. K. Synthetic Cofactor-Linked Metabolic Circuits for Selective Energy Transfer. *ACS Catal.* **2017**, *7*, 1977–1983.
- [19] Richardson, K. N.; Black, W. B.; Li, H. Aldehyde Production in Crude Lysate- and Whole Cell-Based Biotransformation Using a Noncanonical Redox Cofactor System. *ACS Catal.* **2020**, *10*, 8898–8903.
- [20] Guo, X.; Liu, Y.; Wang, Q.; Wang, X.; Li, Q.; Liu, W.; Zhao, Z. K. Non-Natural Cofactor and Formate-Driven Reductive Carboxylation of Pyruvate. *Angew. Chem. Int. Ed.* **2020**, *59*, 3143–3146.
- [21] Lo, H. C.; Fish, R. H. Biomimetic NAD<sup>+</sup> Models for Tandem Cofactor Regeneration, Horse Liver Alcohol Dehydrogenase Recognition of 1,4-NADH Derivatives, and Chiral Synthesis. *Angew. Chem. Int. Ed.* **2002**, *41*, 478–481.
- [22] Jia, H.-Y.; Zong, M.-H.; Zheng, G.-W.; Li, N. Myoglobin-Catalyzed Efficient In Situ Regeneration of NAD(P)<sup>+</sup> and Their Synthetic Biomimetic for Dehydrogenase-Mediated Oxidations. *ACS Catal.* **2019**, *9*, 2196–2202.
- [23] Nowak, C.; Pick, A.; Lommes, P.; Sieber, V. Enzymatic Reduction of Nicotinamide Biomimetic Cofactors Using an Engineered Glucose Dehydrogenase: Providing a Regeneration System for Artificial Cofactors. *ACS Catal.* **2017**, *7*, 5202–5208.
- [24] Nowak, C.; Pick, A.; Csepei, L.-I.; Sieber, V. Characterization of Biomimetic Cofactors According to Stability, Redox Potentials, and Enzymatic Conversion by NADH Oxidase from *Lactobacillus Pentosus*. *ChemBioChem* **2017**, *18*, 1944–1949.
- [25] Nowak, C.; Beer, B. C.; Pick, A.; Roth, T.; Lommes, P.; Sieber, V. A Water-Forming NADH Oxidase from *Lactobacillus Pentosus* Suitable for the Regeneration of Synthetic Biomimetic Cofactors. *Front. Microbiol.* **2015**, *6*, 957.

- [26] Huang, R.; Chen, H.; Upp, D. M.; Lewis, J. C.; Zhang, Y.-H. P. J. A High-Throughput Method for Directed Evolution of NAD(P)<sup>+</sup>-Dependent Dehydrogenases for the Reduction of Biomimetic Nicotinamide Analogues. *ACS Catal.* **2019**, *9*, 11709–11719.
- [27] Hou, S.; Liu, W.; Ji, D.; Wang, Q.; Zhao, Z. K. Synthesis of 1,2,3-Triazole Moiety-Containing NAD Analogs and Their Potential as Redox Cofactors. *Tetrahedron Lett.* **2011**, *52*, 5855–5857.
- [28] Black, W. B.; Aspacio, D.; Bever, D.; King, E.; Zhang, L.; Li, H. Metabolic Engineering of Escherichia Coli for Optimized Biosynthesis of Nicotinamide Mononucleotide, a Noncanonical Redox Cofactor. *Microb. Cell Fact.* **2020**, *19*, 150.
- [29] Evans, C.; Bogan, K. L.; Song, P.; Burant, C. F.; Kennedy, R. T.; Brenner, C. NAD<sup>+</sup> Metabolite Levels as a Function of Vitamins and Calorie Restriction: Evidence for Different Mechanisms of Longevity. *BMC Chem. Biol.* **2010**, *10*, 2.
- [30] Marinescu, G. C.; Popescu, R.-G.; Stoian, G.; Dinischiotu, A.  $\beta$ -Nicotinamide Mononucleotide (NMN) Production in Escherichia Coli. *Sci. Rep.* **2018**, *8*, 12278.
- [31] Zhang, L.; Yuan, J.; Xu, Y.; Percival Zhang, Y.-H.; Qian, X. New Artificial Fluoro-Cofactor of Hydride Transfer with Novel Fluorescence Assay for Redox Biocatalysis. *Chem. Commun.* **2016**, *52*, 6471–6474.
- [32] Sicsic, S.; Durand, P.; Langrene, S.; le Goffic, F. A New Approach for Using Cofactor Dependent Enzymes: Example of Alcohol Dehydrogenase. *FEBS Letters* **1984**, *176*, 321–324.
- [33] Lutz, J.; Hollmann, F.; Ho, T. V.; Schnyder, A.; Fish, R. H.; Schmid, A. Bioorganometallic Chemistry: Biocatalytic Oxidation Reactions with Biomimetic NAD<sup>+</sup>/NADH Co-Factors and [Cp\*Rh(Bpy)H]<sup>+</sup> for Selective Organic Synthesis. *J. Organomet. Chem.* **2004**, *689*, 4783–4790.
- [34] Guarneri, A.; Westphal, A. H.; Leertouwer, J.; Lunsonga, J.; Franssen, M. C. R.; Opperman, D. J.; Hollmann, F.; van Berkel, W. J. H.; Paul, C. E. Flavoenzyme-Mediated Regioselective Aromatic Hydroxylation with Coenzyme Biomimetics. *ChemCatChem* **2020**, *12*, 1368–1375.
- [35] Eggerichs, D.; Mügge, C.; Mayweg, J.; Apfel, U.-P.; Tischler, D. Enantioselective Epoxidation by Flavoprotein Monooxygenases Supported by Organic Solvents. *Catalysts* **2020**, *10*, 568.
- [36] Qi, J.; Paul, C. E.; Hollmann, F.; Tischler, D. Changing the Electron Donor Improves Azoreductase Dye Degrading Activity at Neutral PH. *Enzyme Microb. Technol.* **2017**, *100*, 17–19.

- [37] Riedel, A.; Mehnert, M.; Paul, C. E.; Westphal, A. H.; van Berkel, W. J. H.; Tischler, D. Functional Characterization and Stability Improvement of a ‘Thermophilic-like’ Ene-Reductase from *Rhodococcus Opacus* 1CP. *Front. Microbiol.* **2015**, *6*, 1073.
- [38] Tischler, D.; Gädke, E.; Eggerichs, D.; Gomez Baraibar, A.; Mügge, C.; Scholtissek, A.; Paul, C. E. Asymmetric Reduction of (R)-Carvone through a Thermostable and Organic-Solvent-Tolerant Ene-Reductase. *ChemBioChem* **2020**, *21*, 1217–1225.
- [39] Scholtissek, A.; Tischler, D.; Westphal, A. H.; Van Berkel, W. J. H.; Paul, C. E. Old Yellow Enzyme-Catalysed Asymmetric Hydrogenation: Linking Family Roots with Improved Catalysis. *Catalysts* **2017**, *7*, 130.
- [40] Kim, J.; Lee, S. H.; Tieves, F.; Choi, D. S.; Hollmann, F.; Paul, C. E.; Park, C. B. Biocatalytic C=C Bond Reduction through Carbon Nanodot-Sensitized Regeneration of NADH Analogues. *Angew. Chem. Int. Ed.* **2018**, *57*, 13825–13828.
- [41] Poizat, M.; Arends, I. W. C. E.; Hollmann, F. On the Nature of Mutual Inactivation between [Cp\*Rh(Bpy)(H<sub>2</sub>O)]<sup>2+</sup> and Enzymes – Analysis and Potential Remedies. *J. Mol. Catal. B: Enzym.* **2010**, *63*, 149–156.
- [42] Köhler, V.; Wilson, Y. M.; Dürrenberger, M.; Ghislieri, D.; Churakova, E.; Quinto, T.; Knörr, L.; Häussinger, D.; Hollmann, F.; Turner, N. J.; Ward, T. R. Synthetic Cascades Are Enabled by Combining Biocatalysts with Artificial Metalloenzymes. *Nat. Chem.* **2013**, *5*, 93–99.
- [43] Wang, L.; Zhou, Y. J.; Ji, D.; Lin, X.; Liu, Y.; Zhang, Y.; Liu, W.; Zhao, Z. K. Identification of UshA as a Major Enzyme for NAD Degradation in *Escherichia Coli*. *Enzyme Microb. Technol.* **2014**, *58–59*, 75–79.
- [44] Wang, L.; Liu, B.; Liu, Y.; Sun, Y.; Liu, W.; Yu, D.; Zhao, Z. K. *Escherichia Coli* Strain Designed for Characterizing in Vivo Functions of Nicotinamide Adenine Dinucleotide Analogues. *Org. Lett.* **2019**, *21*, 3218–3222.
- [45] Karim, A. S.; Dudley, Q. M.; Juminaga, A.; Yuan, Y.; Crowe, S. A.; Heggestad, J. T.; Garg, S.; Abdalla, T.; Grubbe, W. S.; Rasor, B. J.; Coar, D. N.; Torculas, M.; Krein, M.; Liew, F. (Eric); Quattlebaum, A.; Jensen, R. O.; Stuart, J. A.; Simpson, S. D.; Köpke, M.; Jewett, M. C. In Vitro Prototyping and Rapid Optimization of Biosynthetic Enzymes for Cell Design. *Nat. Chem. Biol.* **2020**, *16*, 912–919.

## Chapter 2

### Engineering a nicotinamide mononucleotide redox cofactor system for biocatalysis

The text, data, and figures in this chapter are adapted from a previously published manuscript. **Black, W. B.\***, Zhang, L.\*, Mak, W. S.\*, Maxel, S.; Cui, Y., King, E.; Fong, B., Sanchez Martinez, A.; Siegel, J. B.; Li, H., “Engineering a Nicotinamide Mononucleotide Redox Cofactor System for Biocatalysis” *Nature Chemical Biology*, 16, 87-94, 2020.

\* indicates equal contribution

This chapter is based on work from a collaboration with many researchers. For the purpose of this thesis, sections in which W.B.B. did not contribute to were summarized briefly, or in some cases removed. Author contributions were as follows. H.L. and J.B.S. conceived the research. L.Z., **W.B.B.**, and E.K. performed mutant enzyme kinetics characterization. **W.B.B.**, L.Z., S.M., E.K., and B.F. performed the in vitro biotransformation. **W.B.B.**, S.M., B.F., and A.S.M. performed the whole-cell biotransformation. **W.B.B.** performed the intracellular NMN<sup>+</sup> and NAD<sup>+</sup> level analysis. S.M. performed the NMN<sup>+</sup>-dependent growth experiments. W.S.M. and Y.C. performed the computational modeling. All authors analyzed the data and wrote the manuscript.

## 2.1 Introduction

Biomanufacturing is the synthesis of chemicals from renewable resources by engineered microbes. Although numerous fuels, pharmaceuticals, and commodities have been biomanufactured, most of these processes failed to proceed beyond laboratory scale because the productivity, titer, and yield are still low<sup>1</sup>. This problem highlights the existence of a critical knowledge gap in our understanding of cell metabolism. This knowledge gap exists largely due to the extraordinary complexity of metabolic systems<sup>2,3</sup>.

To overcome the complexity problem, one solution is to insulate the much simpler, engineered pathways in an orthogonal metabolic system that operates in parallel to the hosts' complex native metabolism<sup>2,4</sup>. Catabolism and anabolism are the most universal orthogonal metabolic systems in nature. These two seemingly opposing processes coexist without interference largely because they each have a designated redox cofactor, nicotinamide adenine dinucleotide (NAD<sup>+</sup>) and nicotinamide adenine dinucleotide phosphate (NADP<sup>+</sup>), respectively. Therefore, it has been hypothesized that a third, orthogonal metabolic system could be established if one could introduce a noncanonical redox cofactor inside the cells<sup>5</sup>.

In addition to their applications *in vivo*, noncanonical redox cofactors have also been explored as alternatives to NADP<sup>+</sup> during *in vitro* biotransformation, where purified enzymes are used to manufacture chemicals. The majority of industrial biotransformation processes developed so far involve oxidoreductase enzymes<sup>6,7</sup>, which require redox cofactors. Analogs of NADP<sup>+</sup> with simpler structures are easier to synthesize and have faster mass transfer rates, which may greatly reduce the cost of *in vitro* biotransformation<sup>8,9,10</sup>.

However, with the exception of some flavoenzymes<sup>9,10</sup>, most natural enzymes have low activity with noncanonical redox cofactors. Moreover, shifting enzymes' cofactor preference

toward noncanonical redox cofactors remains a challenging task <sup>8,10-12</sup>. For example, *Sulfolobus solfataricus* glucose dehydrogenase (Ss GDH) has been engineered to use simpler NAD<sup>+</sup> analogs <sup>10</sup>. However, the catalytic efficiency of the engineered enzyme was still low ( $k_{\text{cat}}/K_{\text{m}} \approx 5.17 \times 10^{-3} \text{ mM}^{-1} \text{ s}^{-1}$ , for the cofactor 3-carbamoyl-1-phenethylpyridin-1-ium chloride, where  $k_{\text{cat}}$  is turnover number and  $K_{\text{m}}$  is the Michaelis constant for the cofactor). Furthermore, most engineered enzymes still retain substantial levels of activity with the natural redox cofactor NADP<sup>+</sup>, which lowers their orthogonality *in vivo*. For example, a metabolic circuit based on the synthetic cofactor nicotinamide cytosine dinucleotide (NCD<sup>+</sup>) has been constructed in *E. coli* <sup>5</sup>. However, the engineered phosphite dehydrogenase enzyme responsible for reducing NCD<sup>+</sup> only had a ~four-fold preference of NCD<sup>+</sup> over NAD<sup>+</sup>, which resulted in cross-talk between the metabolic circuit and the NAD<sup>+</sup>-dependent natural metabolism.

To overcome this challenge, we used a computationally designed glucose dehydrogenase from *Bacillus subtilis* which readily reduces NMN<sup>+</sup>, but not the native cofactors <sup>13</sup>. By coupling the engineered Bs GDH with various enzymes, we first demonstrated that NMN<sup>+</sup> can support diverse chemistries during *in vitro* biotransformation processes, which include the reduction of C=C double bonds, C≡C triple bonds, and nitro groups, as well as supply electrons to cytochrome P450. In particular, C=C double bonds were reduced with industrially relevant activity and robustness (total turnover number (TTN)  $\approx 39,000$ ) <sup>14</sup>. Then, we demonstrated in *E. coli* whole cells that NMN<sup>+</sup> can mediate orthogonal reducing power delivery from glucose to the production of a pharmaceutical intermediate, levodione, while keeping other NAD(P)H-dependent competing reactions inactive.



## 2.2 Methods

### 2.2.1 Plasmids and strains

All plasmids and strains used in this study are summarized in Table 4. The plasmids and strains were previously generated in the lab <sup>13</sup>. The accession numbers for proteins used in this study are summarized in Table 5.

**Table 4: Strains and Plasmids Used in Chapter 2**

<b>Strains</b>	<b>Description</b>	<b>Reference</b>
XL-1 Blue	Cloning strain	Stratagene
BL21 (DE3)	Protein expression strain	Invitrogen
BW25113	<i>E. coli</i> $\Delta(\text{araD-araB})567, \Delta\text{lacZ4787}>::\text{rrnB-3), } \lambda\text{-, rph-1, } \Delta(\text{rhaD-rhaB})568, \text{hsdR514}$	Keio Collection
JW2670-1	BW25113 $\Delta\text{pncC}::\text{kan}$	Keio Collection
MX101	BW25113 $\Delta\text{pncC } \Delta\text{nadR}::\text{kan}$	[42]
MX102	BW25113 $\Delta\text{pncC } \Delta\text{pgi } \Delta\text{zwf } \Delta\text{gntK}::\text{kan}$	[42]
MX103	BW25113 $\Delta\text{pncC } \Delta\text{pgi } \Delta\text{zwf } \Delta\text{nadR } \Delta\text{gnd}::\text{kan}$	[42]
<b>Plasmids</b>	<b>Description</b>	<b>Reference</b>
pEK101	$P_{LlacO1}::Bs \text{ gdh}, \text{ColE1 ori}, \text{Amp}^R$	[42]
pEK102	$P_{LlacO1}::Pp \text{ xenA}, \text{ColE1 ori}, \text{Amp}^R$	[42]
pLZ201	$P_{LlacO1}::Bs \text{ gdh N92A}, \text{ColE1 ori}, \text{Amp}^R$	[42]
pLZ202	$P_{LlacO1}::Bs \text{ gdh N92V}, \text{ColE1 ori}, \text{Amp}^R$	[42]
pLZ203	$P_{LlacO1}::Bs \text{ gdh G94S}, \text{ColE1 ori}, \text{Amp}^R$	[42]
pLZ204	$P_{LlacO1}::Bs \text{ gdh I195R}, \text{ColE1 ori}, \text{Amp}^R$	[42]
pLZ205	$P_{LlacO1}::Bs \text{ gdh I195S}, \text{ColE1 ori}, \text{Amp}^R$	[42]
pLZ206	$P_{LlacO1}::Bs \text{ gdh I195T}, \text{ColE1 ori}, \text{Amp}^R$	[42]
pLZ207	$P_{LlacO1}::Bs \text{ gdh S17Q-P194N}, \text{ColE1 ori}, \text{Amp}^R$	[42]
pLZ208	$P_{LlacO1}::Bs \text{ gdh M143S}, \text{ColE1 ori}, \text{Amp}^R$	[42]
pLZ209	$P_{LlacO1}::Bs \text{ gdh M143T}, \text{ColE1 ori}, \text{Amp}^R$	[42]
pLZ210	$P_{LlacO1}::Bs \text{ gdh I195R-A93K-Y39Q}, \text{ColE1 ori}, \text{Amp}^R$	[42]
pLZ211	$P_{LlacO1}::Bs \text{ gdh I195R-Y39Q}, \text{ColE1 ori}, \text{Amp}^R$	[42]

pLZ212	<i>P<sub>LlacO1</sub>::Bs gdh I195R-A93K, ColE1 ori, Amp<sup>R</sup></i>	[42]
pLZ213	<i>P<sub>LlacO1</sub>::Bs gdh A93K, ColE1 ori, Amp<sup>R</sup></i>	[42]
pLZ214	<i>P<sub>LlacO1</sub>::Bs gdh Y39Q, ColE1 ori, Amp<sup>R</sup></i>	[42]
pLZ215	<i>P<sub>LlacO1</sub>::Bs gdh A93K-Y39Q, ColE1 ori, Amp<sup>R</sup></i>	[42]
pLZ216	<i>P<sub>LlacO1</sub>::Bs gdh I195R-A93K-Y39Q-S17E, ColE1 ori, Amp<sup>R</sup></i>	[42]
pLZ217	<i>P<sub>BAD</sub>::Pp xenA, RSF ori, Spec<sup>R</sup></i>	[42]
pLZ218	<i>P<sub>BAD</sub>::Bs gdh I195R-A93K-Y39Q-S17E - Pp xenA, RSF ori, Spec<sup>R</sup></i>	[42]
pLZ219	<i>P<sub>BAD</sub>::Bs gdh - Pp xenA, RSF ori, Spec<sup>R</sup></i>	[42]
pLZ220	<i>P<sub>BAD</sub>::Bs gdh - Ca lvr, RSF ori, Spec<sup>R</sup></i>	[42]
pLZ221	<i>P<sub>BAD</sub>::Bs gdh I195R-A93K-Y39Q-S17E - Ca lvr, RSF ori, Spec<sup>R</sup></i>	[42]
pLZ222	<i>P<sub>BAD</sub>::Ca lvr, RSF ori, Spec<sup>R</sup></i>	[42]
pLZ223	<i>P<sub>BAD</sub>::Bs gdh - Rs adh, RSF ori, Spec<sup>R</sup></i>	[42]
pLZ224	<i>P<sub>BAD</sub>::Bs gdh I195R-A93K-Y39Q-S17E - Rs adh, RSF ori, Spec<sup>R</sup></i>	[42]
pLZ225	<i>P<sub>BAD</sub>::Rs adh, RSF ori, Spec<sup>R</sup></i>	[42]
pLZ226	<i>P<sub>LlacO1</sub>::Pp xenA - Ca lvr - Rs adh, ColE1 ori, Amp<sup>R</sup></i>	[42]
pSM101	<i>P<sub>LlacO1</sub>::Bm BM3, ColE1 ori, Amp<sup>R</sup></i>	[42]
pSM102	<i>P<sub>LlacO1</sub>::Bm BM3 W1046S, ColE1 ori, Amp<sup>R</sup></i>	[42]
pSM103	<i>P<sub>LlacO1</sub>::Ft nadEV - Zm glf - Re gntK, ColE1 ori, Amp<sup>R</sup></i>	[42]
pSM104	<i>P<sub>LlacO1</sub>::Zm glf, ColE1 ori, Amp<sup>R</sup></i>	[42]
pSM105	<i>P<sub>LlacO1</sub>::Empty, ColE1 ori, Amp<sup>R</sup></i>	[42]
pSM106	<i>P<sub>BAD</sub>::Bs gdh I195R-A93K-Y39Q-S17E, RSF ori, Spec<sup>R</sup></i>	[42]
pSM107	<i>P<sub>BAD</sub>::Bs gdh, RSF ori, Spec<sup>R</sup></i>	[42]
pSM108	<i>P<sub>BAD</sub>::Empty, RSF ori, Spec<sup>R</sup></i>	[42]
pSM109	<i>P<sub>LlacO1</sub>::Zm glf, p15A ori, Cm<sup>R</sup></i>	[42]
pSM110	<i>P<sub>LlacO1</sub>::Zm glf, ColE1 ori, Cm<sup>R</sup></i>	[42]
pWB201	<i>P<sub>LlacO1</sub>::Sc OYE3, ColE1 ori, Amp<sup>R</sup></i>	[42]
pWB202	<i>P<sub>LlacO1</sub>::Ec nfsB, ColE1 ori, Amp<sup>R</sup></i>	[42]
pWB203	<i>P<sub>LlacO1</sub>::Ft nadEV, ColE1 ori, Amp<sup>R</sup></i>	[42]

---

**Table 5: Accession Numbers for Proteins Used in Chapter 2**

Protein Name	Full Name	Protein ID
<i>Ec</i> PncC	NMN aminohydrolase	P0A6G3.1
<i>Ec</i> NadR	NMN adenylyltransferase	P27278.2
<i>Ec</i> Pgi	Glucose-6-phosphate isomerase	P0A6T1
<i>Ec</i> Zwf	NADP(+)-dependent glucose-6-phosphate dehydrogenase	NP_416366.1
<i>Ec</i> Gnd	6-phosphogluconate dehydrogenase	P00350
<i>Ec</i> GntK	D-gluconate kinase	P46859
<i>Ec</i> NfsB	Oxygen-insensitive NAD(P)H nitroreductase	WP_000351487.1
<i>Ft</i> NadE	NAD(+) synthase	WP_003015145.1
<i>Ft</i> NadV	Nicotinate phosphoribosyltransferase	WP_003018116.1
<i>Zm</i> Glf	UDP-galactopytanose	AVZ41684.1
<i>Sc</i> OYE3	Old Yellow Enzyme 3	NP_015154
<i>Re</i> GntK	Gluconate kinase	CAJ92320.1
<i>Bm</i> BM3	Bifunctional fatty acid monooxygenase	Addgene plasmid #85102
<i>Bs</i> Gdh	Glucose 1-dehydrogenase	WP_003246720.1
<i>Pp</i> XenA	NADH: flavin oxidoreductase/NADH oxidase	WP_016711963.1
<i>Ca</i> LVR	Levodione Reductase	Q9LBG2.1
<i>Rs</i> ADH	Alcohol dehydrogenase	ACB78191.1

### 2.2.2 Protein expression and purification

Proteins were purified as 6×His tag fusion at the N-terminus. *E. coli* BL21 (DE3) with plasmids were inoculated into LB medium with 200 mg L<sup>-1</sup> ampicillin. Cells were induced with 0.5 mM IPTG, and the proteins were expressed for 24 hours at 30°C while shaking at 250 rpm. BM3 cytochrome P450 was extracted with the BugBuster Plus Lysonase Kit (EMD Millipore) and purified using the HisPur Ni-NTA Superflow Purification System (Thermo Fisher) according to the manufacturer's instructions. Others proteins were purified using His-Spin Protein Miniprep kit (Zymo Research Corporation). The purified proteins were quantified by Bradford assay.

### 2.2.3 GDH enzymatic assays and kinetics study

The GDH activity was measured as described previously<sup>40</sup>. The reactions were started by adding the purified protein to the assay mixture containing 35 mM Tris-HCl buffer (pH 8.0), cofactors, and glucose. The absorbance variation at 340 nm was detected by a spectrophotometer at 25 °C. For specific activity, 3 mM NAD<sup>+</sup>, NADP<sup>+</sup>, or NMN<sup>+</sup> and 140 mM glucose were used. For apparent kinetics parameter determination, cofactor concentrations were varied with a constant 140 mM glucose. For full steady-state kinetics parameter determination, both cofactor and glucose concentrations were varied.

For apparent kinetic parameter analysis, the results were fitted to the standard Michaelis–Menten equation.

$$v_0 = \frac{E_t k_{cat} S}{K_M + S} \quad (1)$$

where  $v_0$  is the initial reaction rate,  $E_t$  is the total enzyme concentration,  $k_{cat}$  is turnover number,  $S$  is the concentration of cofactor,  $K_M$  is Michaelis constant for cofactor. In the case of Bs GDH wild type with NMN<sup>+</sup>, The reaction rate is linearly proportional to the cofactor concentration, and the enzyme could not be saturated with the cofactor concentrations tested. Therefore, the data was fitted to equation (2), which is a simplified form of equation (1) under  $K_M \gg S$ :

$$v_0 = \frac{E_t k_{cat}}{K_M} \cdot S \quad (2)$$

For full steady-state kinetic parameter analysis, the results were fitted to the following ordered bi-bi rate equation<sup>41</sup>:

$$v_0 = \frac{E_t k_{cat} AB}{k_{iA} K_B + K_B A + K_A B + AB} \quad (3)$$

Where  $v_0$  is the initial reaction rate,  $E_t$  is the total enzyme concentration,  $k_{cat}$  is turnover number, A and B are the concentrations of cofactor and glucose, respectively,  $K_A$  and  $K_B$  are Michaelis

constants for cofactor and substrate, respectively.  $k_{ia}$  is the dissociation constant for cofactor binding.

In the case of wild type Bs GDH with NMN<sup>+</sup>, and Bs GDH Ortho with NAD<sup>+</sup>, the data fitted poorly to equation (3) due to very large  $K_A$ . The reaction rate is linearly proportional to the cofactor concentration, and the enzyme could not be saturated with the cofactor concentrations tested. Therefore, equation (4) was used, which is a simplified form of equation (3) when  $K_A \gg A$ :

$$v_0 = \frac{E_t \left( \frac{k_{cat}}{K_A} \right)_{AB}}{\left( \frac{k_{ia}}{K_A} \right)_{K_B + B}} \quad (4)$$

Similarly, in the case of Bs GDH Triple with NAD<sup>+</sup>, the reaction rate is linearly proportional to the glucose concentration, and the enzyme could not be saturated with the glucose concentrations tested. Therefore, equation (5) was used, which is a simplified form of equation (3) when  $K_B \gg B$ :

$$v_0 = \frac{E_t \left( \frac{k_{cat}}{K_B} \right)_{AB}}{k_{ia} + A} \quad (5)$$

The microscopic reaction rates were calculated from the relationships <sup>41</sup>:

$$k_1 = \frac{k_{cat}}{K_A}, \quad k_2 = \frac{k_{cat}k_{ia}}{K_A}, \quad k_3 = \frac{k_{cat}}{K_B} \quad (6)$$

Where  $k_1$  is the on-rate of cofactor,  $k_2$  is the off-rate of cofactor,  $k_3$  is the on-rate of glucose.

#### 2.2.4 Coupled enzymatic biotransformation

All biotransformation reactions were performed in buffer A at 30°C for 24 hours. Buffer A, modified from a previous system <sup>15</sup>, contained 200 mM potassium phosphate buffer (pH 7.5), 1 M NaCl, 300 mM D-glucose, 6 mM NMN<sup>+</sup> (or NADP<sup>+</sup> as the positive control), and substrates. All assays were performed in triplicate, with no proteins or no cofactors added as negative controls.

The protein loading for GDH variants was kept at 0.33 mg mL<sup>-1</sup> or 11.7 μM. The various enzymes for biotransformation reactions were added at the concentration of 0.75 mg mL<sup>-1</sup>.

For XenA-Bs GDH coupled cycling assays, the substrates ketoisophorone, citral, or trans-2-hexen-1-al were added at 33 mM, 10 mM, or 50 mM, respectively. For the OYE3-GDH coupled cycling assays, the substrate 4-phenyl-3-buten-2-one<sup>16</sup> was added at 5 mM. At various time points over 24 hours, 100 μL samples were taken and extracted with 100 μL ethyl acetate. Conversion was determined *via* GC-FID with octanol as an internal standard (see below). For NfsB-Bs GDH coupled cycling assays, 2 mM nitrofurazone was used as the substrate<sup>17</sup>. Nitrofurazone conversion was measured spectroscopically at 400 nm and quantification was performed using a standard curve<sup>17</sup>. The initial levels added of the above-mentioned substrates were mainly determined by their solubility in the assay buffer. For P450 BM3-Bs GDH coupled cycling assays, 50 μM cytochrome *c* (C2506 Sigma) was used as the substrate. The reduction of cytochrome *c* was measured spectroscopically at 550 nm, and the quantification was performed using extinction coefficient  $\epsilon_{550}$  of 21.1 mM<sup>-1</sup> cm<sup>-1</sup><sup>18</sup>.

### 2.2.5 NMN<sup>+</sup>-dependent whole-cell biotransformation

One biotransformation plasmid expressing XenA, LVR, or ADH with a GDH (selected from pLZ217-pLZ225) and pSM104 containing the glucose transport facilitator were transformed into strain MX102 by electroporation. 4 mL seed cultures of 2xYT media with appropriate antibiotics, 0.1 mM IPTG, and 0.2 % (w/v) glucose were cultured at 30 °C while shaking at 250 rpm for 16 hours. 0.5 % (v/v) seed cultures were used to inoculate 150 mL of 2xYT media with appropriate antibiotics, A5 trace metals with cobalt, and 0.5 mM IPTG in a 250 mL baffled shake flask and cultured at 30 °C at 250 rpm. When an OD<sub>600</sub> ~ 0.4 was reached, protein expression was induced with 0.1 % (w/v) arabinose and cultured for an additional 8 hours at 30 °C while shaking

at 250 rpm. Cells were harvested by centrifugation for 15 minutes at 20 °C at 3750 rpm. The supernatant was discarded. Cells were washed 3 times with 50 mL of 100 mM potassium phosphate (pH 7.5), followed by being resuspended to an OD<sub>600</sub> of 100 in assay buffer consisting of 100 mM potassium phosphate buffer (pH 7.5), 200 mM D-glucose, 0.5 % arabinose, and 0.5 mM IPTG. 1 mL of resuspended cells were added to 20 mL of identical assay buffer in a 250 mL unbaffled, screw-cap shake flask. KIP was spiked into the flask to 5 g/L to initiate the reaction. Flask caps were secured tightly to prevent evaporative loss of substrate or products. Flasks were incubated at 30 °C while shaking at 250 rpm for 48 hours. After 48 hours, 1 mL of culture was pelleted, and the supernatant was used for analysis. 200 µL of supernatant was extracted with an equal volume of ethyl acetate containing 200 mg/L octanol as an internal standard, and the samples were analyzed by gas chromatography (See detailed method below). For samples expressing all three conversion enzymes (XenA, LVR, and ADH) on the same vector (pLZ226), the Bs GDH was expressed individually on a separate vector (pSM106, pSM107, or pSM108). The *Zm glf* gene was also expressed in this system (pSM110).

### **2.2.6 GC-FID analytical methods**

All gas chromatography (GC) was performed on an Agilent 6850 (Agilent Technologies) equipped with a flame ionization detector (FID). An Agilent DB-WAXetr capillary column (30 m x 0.56 mm x 1 µm) was used for separation. The inlet and detector were held at 250 °C and 260 °C, respectively. The GC was operated in constant pressure mode with a pressure of 3.66 psi. Helium was used as the carrier gas. Air and Hydrogen were supplied to the FID at 350 mL/min and 40 mL/min respectively. All gasses were purchased from Airgas (Radnor Township, PA). 5 µL of sample was injected with a split ratio of 2:1.

For analysis of citral and its reduction product citronellal, the oven was initially held at 150 °C for 10 minutes and then ramped at a rate of 45 °C/min to 240 °C. Citral and citronellal eluted at 9.32 and 4.50 minutes, respectively. Octanol was used as an internal standard.

For analysis of trans-2-hexen-1-al and its reduction product trans-2-hexan-1-al, the oven was initially held at 50 °C for 1 minute, the oven was ramped at 15 °C/min to 120 °C, then ramped at 20 °C/min to 230 °C, and held for 3 minutes. Trans-2-hexen-1-al and trans-2-hexan-1-al eluted at 6.41 minutes and 4.78 minutes, respectively. Octanol was used as an internal standard.

For analysis of 4-phenyl-3-butyne-2-one (containing C≡C triple bond) and its fully reduced product 4-phenyl-2-butanone, as well as the intermediate 4-phenyl-2-butene-2-one (containing C=C double bond), the oven was initially held at 200 °C for 1 minute, then ramped at 5 °C/min to 230 °C, and held for 1 minute. Octanol was used as an internal standard. *In vitro* ketoisophorone reduction to levodione was analyzed using the same method. Elution times are as follows: 4-phenyl-3-butyne-2-one (5.53 minutes), 4-phenyl-2-butene-2-one (6.76 minutes), 4-phenyl-2-butanone (4.55 minutes), ketoisophorone (3.65 minutes), levodione (4.08 minutes), and octanol (2.80 minutes).

For analysis of *in vivo* ketoisophorone biotransformation. The oven was held at 200 °C for 15 minutes. Elution times are as follows: Octanol (2.80 minutes), ketoisophorone (3.76 minutes), levodione (7.25 minutes), phorenol (8.35 minutes), and 4-hydroxyisophorone (12.90 minutes).

### **2.2.7 GDH Total Turnover Number (TTN) Determination**

Total turnover number (TTN) (Figure 2C) was determined by the number of moles of product formed divided by the moles of purified GDH added. The assays were performed in reaction buffer A, as shown above, at 30°C. 33 mM ketoisophorone was used as the substrate. The



reaction was started by spiking purified proteins (0.0132 mg mL<sup>-1</sup> or 0.47 μM for GDH, 0.75 mg mL<sup>-1</sup> for XenA). Samples were taken every 12 hours for 96 hours. The extraction and GC-FID analysis were performed using similar method mentioned above.

### 2.2.8 Quantification of intracellular NMN<sup>+</sup> and NAD<sup>+</sup> levels

A plasmid containing *Ft nadE* and *nadV* (pWB203) was transformed into *E. coli* strains BW25113, JW2670-1, and MX101 to examine their effects on NMN<sup>+</sup> generation. Overnight cultures were grown at 30 °C while shaking at 250 rpm in 2xYT media containing 0.1 mM IPTG, 0.2 % D-glucose, and appropriate antibiotics for 12 hours. To cultivate cells for nucleotide analysis, 10 mL of 2xYT media containing 0.5 mM IPTG, 1 mM nicotinamide, and appropriate antibiotics in a 50 mL conical tube was inoculated with 1 % v/v overnight culture. Tubes were incubated at 30 °C at 250 rpm for 4 hours.

Before harvesting cells, cell density was measured at 600 nm. 1 mL of culture was pelleted in a 1.5 mL microcentrifuge tube. Supernatant was removed by pipetting. The cell pellet was washed once with 1 mL of room temperature deionized water, repelleted, and the supernatant was removed by pipetting. Cells were lysed with 1 mL of 95 °C 1 % formic acid with 1 μM 1-methylnicotinamide as an internal standard. Cells were incubated at 95 °C for 2 minutes while intermittently vortexing to ensure complete lysis. Lysates were quenched in an ice water bath before pelleting cell debris. Supernatant was run on a UPLC-MS/MS system for analysis. Values from LC/MS/MS were correlated back to intracellular concentration using the number of cells per OD<sub>600</sub> of 1 in 1 mL of culture = 1x10<sup>9</sup> and the intracellular volume of an *E. coli* cell as 1×10<sup>-15</sup> L/cell<sup>19</sup>.

Liquid chromatography was performed on a Waters ACQUITY UPLC with a Waters ACQUITY UPLC CSH C18 column (1.7 μm x 2.1 mm x 50 mm). Mobile phases used in the

separation were (A) water with 2 % acetonitrile and 0.2 % acetic acid and (B) acetonitrile with 0.2 % acetic acid. The compounds were separated with a linear gradient from 10 % to 90 % buffer B over 1 minute, held at 90 % buffer B for 1 minute, then returned to 10 % buffer B and held at 10 % buffer B for 1 minute. Flow rate was held constant at 0.3 mL/min. 10  $\mu$ L of sample was injected for analysis.

MS/MS detection was performed by a Waters Micromass Quattro Premier XE Mass Spectrometer operating in positive ion, MRM mode. Capillary voltage was set to 3.3 kV. Desolvation gas flow rate was 800 L/hr at 300 °C. Cone gas flow rate was 50 L/hr. The source was maintained at 120 °C. Primary mass, fragment mass, cone voltages, and collision energies for each compound are listed in Table 6.

**Table 6: Mass Spectrometry Parameters for Intracellular Cofactor Concentration Analysis**

Compound	Primary Mass	Secondary Mass	Cone Voltage	Collison Energy
MNA <sup>+</sup> (IS)	137	94	20	20
NMN <sup>+</sup>	335	123	10	10
NAD <sup>+</sup>	664	135.9	20	40

IS: Internal Standard

## 2.3 Results

### 2.3.1 Engineering Bs GDH to utilize NMN<sup>+</sup>

NMN<sup>+</sup> is very similar to NAD(P)<sup>+</sup> in redox chemistry. With no modification on the nicotinamide, NMN<sup>+</sup> is suggested to have very similar redox potential to that of NAD(P)<sup>+</sup> <sup>20</sup> (Standard biochemical redox potential,  $E^{\circ}=-320$  mV <sup>21</sup>), which makes NMN<sup>+</sup> potentially compatible with all NAD(P)<sup>+</sup>-mediated chemistries in metabolism. More than 2,000 types of redox reactions directly use NAD(P)<sup>+</sup> as cofactors, which comprise one-fourth of all metabolic reaction types known to date (according to KEGG database).

On the other hand, NMN<sup>+</sup> is structurally distinct from NAD(P)<sup>+</sup> because it lacks the adenosine monophosphate (AMP) moiety (Figure 2A). With that in mind, our lab previously constructed two variants of the glucose dehydrogenase from *Bacillus subtilis*, Bs GDH, which were capable of the reduction of NMN<sup>+</sup> to NMNH<sup>+</sup> <sup>13</sup>. They achieved this by strengthening interactions between the terminal phosphate on NMN<sup>+</sup> with the protein, since the AMP “recognition handle” on NAD(P)<sup>+</sup> is not present in NMN<sup>+</sup>. The wild type protein exhibited near-zero activity with the NMN<sup>+</sup>. The first variant, Bs GDH Triple, contained mutations Y39Q-A93K-I195R, which enabled Bs GDH Triple to readily reduce NMN<sup>+</sup> ( $k_{\text{cat}} = 3.1 \text{ s}^{-1}$ ,  $K_{\text{M}} = 6.4 \text{ mM}$ ) <sup>13</sup>. The second variant, Bs GDH Ortho, added an additional mutation, S17E, on top of the previous mutations, which was designed to add steric hinderance with the native cofactors. This significantly decreased the enzyme’s activity with NAD<sup>+</sup> and NADP<sup>+</sup> ( $k_{\text{cat}} = 0.025$  and  $0.022 \text{ s}^{-1}$ , respectively;  $K_{\text{M}} = 6.5 \text{ mM}$  and  $2.0 \text{ mM}$ , respectively), with minimal decrease in activity towards NMN<sup>+</sup> ( $k_{\text{cat}} = 1.2 \text{ s}^{-1}$ ,  $K_{\text{M}} = 5.9 \text{ mM}$ ) <sup>13</sup>. Full steady state parameters are shown in Table 7. As discussed in Chapter 1, these two variants of Bs GDH have different applications due to their kinetic parameters with NMN<sup>+</sup> and NAD(P)<sup>+</sup>. GDH Triple is a strong candidate for *in vitro*, purified protein-based biotransformation based on its high  $k_{\text{cat}}$ . Whereas, Bs GDH Ortho is a strong candidate to *in vivo*, whole cell-based biotransformation based on its high  $K_{\text{M}}$  for the native cofactors relative to their intracellular concentrations.

**Table 7: Full Steady-State Kinetics Parameters**

Enzyme	Cofactor	$K_{ia}$ (mM)	$k_{cat}$ (s <sup>-1</sup> )	$K_A$ (mM)	$K_B$ (mM)	$k_1$ (mM <sup>-1</sup> s <sup>-1</sup> )	$k_2$ (s <sup>-1</sup> )	$k_3$ (mM <sup>-1</sup> s <sup>-1</sup> )	$(k_1k_3/k_2)$ (mM <sup>-2</sup> s <sup>-1</sup> )
Bs GDH WT	NAD <sup>+</sup>	$(6.8\pm 2.0) \times 10^{-2}$	$(3.7\pm 0.5) \times 10^1$	$(5.1\pm 0.2) \times 10^{-2}$	8.3±2.8	$(7.2\pm 1.3) \times 10^2$	$(5.0\pm 2.3) \times 10^1$	4.8±2.3	$(6.9\pm 1.3) \times 10^1$
	NADP <sup>+</sup>	$(8.5\pm 0.4) \times 10^{-3}$	$(3.0\pm 0.7) \times 10^1$	$(1.0\pm 0.1) \times 10^{-2}$	7.2±0.8	$(3.0\pm 0.4) \times 10^3$	$(2.5\pm 0.2) \times 10^1$	4.1±0.6	$(4.9\pm 0.9) \times 10^2$
	NMN <sup>+</sup>	n.d. <sup>†</sup>	n.d. <sup>†</sup>	n.d. <sup>†</sup>	n.d. <sup>†</sup>	$(8.6\pm 2.2) \times 10^{-2}$	n.d. <sup>†</sup>	n.d. <sup>†</sup>	$(2.5\pm 0.3) \times 10^{-4}$
Bs GDH Triple (I195R-A93K- Y39Q)	NAD <sup>+</sup>	n.d. <sup>‡</sup>	n.d. <sup>‡</sup>	n.d. <sup>‡</sup>	n.d. <sup>‡</sup>	n.d. <sup>‡</sup>	n.d. <sup>‡</sup>	$(2.6\pm 0.2) \times 10^{-4}$	$(6.6\pm 1.1) \times 10^{-5}$
	NADP <sup>+</sup>	4.6±0.6	$(3.7\pm 1.3) \times 10^{-1}$	$(4.7\pm 2.3) \times 10^1$	$(1.7\pm 0.6) \times 10^2$	$(8.8\pm 3.0) \times 10^{-2}$	$(4.2\pm 1.8) \times 10^{-1}$	$(2.2\pm 0.1) \times 10^{-3}$	$(4.8\pm 0.6) \times 10^{-4}$
	NMN <sup>+</sup>	$(3.4\pm 0.6) \times 10^{-1}$	$(4.1\pm 0.1) \times 10^{-1}$	$(1.9\pm 0.2) \times 10^{-1}$	$(9.0\pm 1.6) \times 10^1$	$(2.2\pm 0.2) \times 10^1$	$(7.5\pm 1.8) \times 10^{-1}$	$(4.7\pm 0.8) \times 10^{-3}$	$(1.4\pm 0.1) \times 10^{-2}$
Bs GDH Ortho (I195R-A93K- Y39Q-S17E)	NAD <sup>+</sup>	n.d. <sup>†</sup>	n.d. <sup>†</sup>	n.d. <sup>†</sup>	n.d. <sup>†</sup>	$(1.4\pm 0.7) \times 10^{-3}$	n.d. <sup>†</sup>	n.d. <sup>†</sup>	$(0.6\pm 0.2) \times 10^{-5}$
	NADP <sup>+</sup>	$(5.2\pm 0.5) \times 10^{-1}$	$(2.9\pm 0.3) \times 10^{-1}$	$(6.5\pm 1.4) \times 10^{-1}$	$(4.2\pm 0.7) \times 10^2$	$(4.6\pm 1.0) \times 10^{-1}$	$(2.4\pm 0.3) \times 10^{-1}$	$(7.1\pm 0.9) \times 10^{-4}$	$(1.4\pm 0.1) \times 10^{-3}$
	NMN <sup>+</sup>	4.6±2.7	$(2.7\pm 0.7) \times 10^{-1}$	4.9±4.1	$(3.9\pm 1.2) \times 10^1$	$(8.9\pm 6.4) \times 10^{-2}$	$(3.1\pm 2.2) \times 10^{-1}$	$(6.8\pm 0.3) \times 10^{-3}$	$(2.4\pm 2.1) \times 10^{-3}$

Reactions were performed in 35 mM Tris-HCl buffer (pH 8.0) at 25 °C.  $K_M$  is the apparent Michaelis constant for cofactor,  $k_{cat}$  is turnover number,  $K_A$  and  $K_B$  are full steady-state Michaelis constants for cofactor and substrate, respectively.  $k_{ia}$  is the dissociation constant for cofactor binding.  $k_1$  is the on-rate of cofactor,  $k_2$  is the off-rate of cofactor,  $k_3$  is the on-rate of glucose. The microscopic reaction rates were calculated from the relationships  $k_1 = k_{cat}/K_A$ ,  $k_2 = k_{cat} k_{ia} / K_A$ ,  $k_3 = k_{cat}/K_B$ . Detailed rate equations can be found in Methods. Errors shown are the standard deviation of three independent measurements.

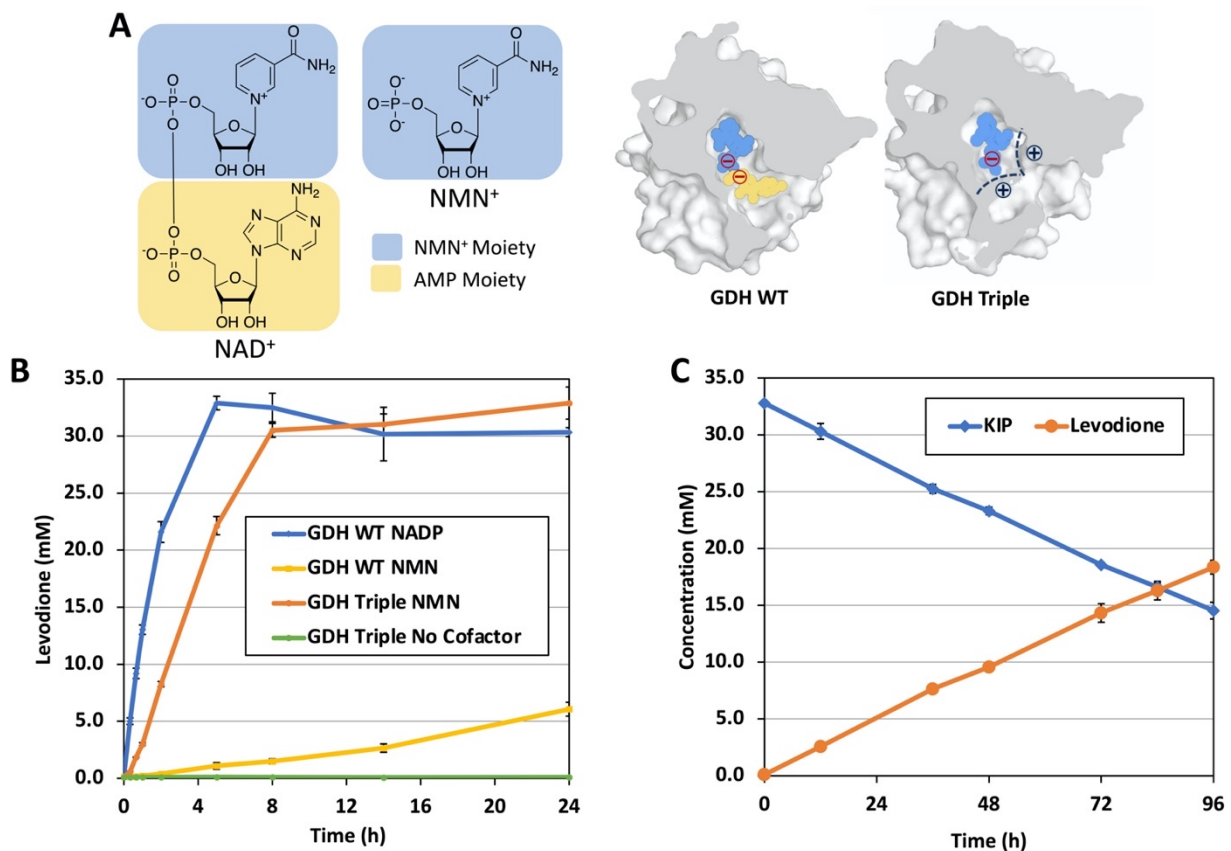
<sup>†</sup>Not determined. Enzyme could not be saturated with cofactor concentrations tested.

<sup>‡</sup>Not determined. Enzyme could not be saturated with glucose concentrations tested.

### 2.3.2 *in vitro* NMN(H) cycling supports efficient biocatalysis

First, we sought to determine whether NMN<sup>+</sup> and Bs GDH Triple could efficiently sustain enzymatic biotransformation *in vitro*. Previous studies using enoate reductases revealed true opportunities for industrial utilization of biomimetic cofactors at preparative scale <sup>22</sup>. The model reaction we chose was the asymmetric reduction of the activated C=C double bond in ketoisophorone (KIP) catalyzed by the enoate reductase XenA from *Pseudomonas putida* <sup>9</sup>, producing the chiral pharmaceutical intermediate, levodione <sup>23</sup>. XenA has been shown to be promiscuous for a range of biomimetic redox cofactors <sup>9</sup>, and it has been shown to accept NMNH with comparable activity to NADH and NADPH <sup>13</sup>.

Subsequently, KIP biotransformation was performed using Bs GDH variants to generate NMNH *in situ*. When using 6 mM NADP<sup>+</sup> as the cycling cofactor, the wild type Bs GDH supported an initial productivity of ~3.00 μM s<sup>-1</sup> (Figure 2B). However, when NMN<sup>+</sup> was used in place of NADP<sup>+</sup>, the initial productivity dropped to ~0.05 μM s<sup>-1</sup>. Importantly, the engineered Bs GDH Triple improved the NMN<sup>+</sup>-dependent productivity by 22-fold, reaching ~1.15 μM s<sup>-1</sup>. Given an enzyme loading of Bs GDH Triple at 11.7 μM, the initial turn over frequency of the triple mutant reached ~0.10 s<sup>-1</sup>, which is within the range of industrial catalysts (10<sup>-2</sup> - 10<sup>2</sup> s<sup>-1</sup>) <sup>14</sup>. With no redox cofactors added, the system showed virtually no conversion, which ruled out the possibility that the observed conversion in NMN(H) cycling reaction was conferred by the NAD(P)<sup>+</sup> contamination in recombinant proteins <sup>10</sup>.



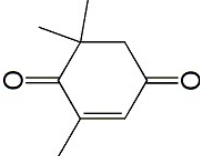
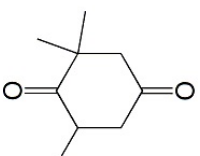
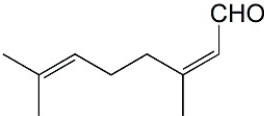
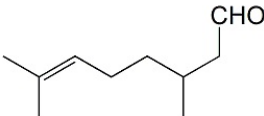
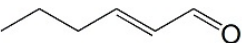

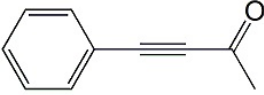
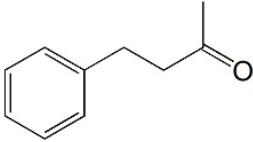
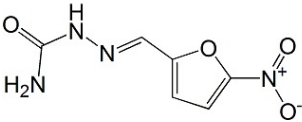
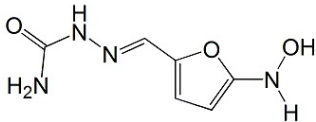
**Figure 2: GDH Triple efficiently recycles NMN<sup>+</sup> in *in vitro* biotransformation** (A) Structures of the natural redox cofactor NAD<sup>+</sup>, the noncanonical redox cofactor NMN<sup>+</sup>, and the sliced representation of the NAD<sup>+</sup>/NMN<sup>+</sup> binding pocket. Wild-type Bs GDH (GDH WT) interacts with both the NMN<sup>+</sup> moiety (blue) and the AMP moiety (yellow) of NAD<sup>+</sup>. GDH Triple was engineered with positively charged regions (black dashed lines) for the monophosphate of NMN<sup>+</sup> to anchor the ligand in a catalytically relevant conformation. (B) Bs GDH Triple (I195R-A93K-Y39Q), in combination with *Pseudomonas putida* XenaA, supported NMN(H)-dependent levodione generation from ketoisophorone (KIP) *in vitro*. (C) Bs GDH Triple was stable for at least 96 hours, as suggested by the steadily increasing of levodione and decreasing of KIP over 96 hours. Reactions were performed in 200 mM potassium phosphate buffer (pH 7.5), 1 M NaCl, 300 mM D-glucose, 6 mM NMN<sup>+</sup>, and 33 mM ketoisophorone at 30°C while mixing. Bs GDH variants were supplied at 0.33 mg mL<sup>-1</sup> (A) or 0.0132 mg mL<sup>-1</sup> (B). Values are an average of at least three biological replicates with error bars represent one standard deviation.

The stability of an enzymatic catalyst is critical for its practicality. Using a lower enzyme loading of 0.47 μM for Bs GDH Triple, longer-term KIP biotransformation was performed. The results showed robust conversion over 96 hours (Figure 2C). The TTN number of Bs GDH Triple was calculated to be ~39,000, which is substantially higher than those of previously reported

biomimetic cofactor recycling methods involving an artificial metalloenzyme (TTN ~2000) <sup>24</sup> or an engineered Ss GDH (TTN ~1183) <sup>10</sup>.

XenA is active towards a broad range of substrates containing activated C=C double bonds <sup>15</sup>. In addition to a >99 % conversion of 33 mM KIP to levodione in 24 hours (Table 8), the coupled XenA-Bs GDH Triple system also achieved ~76 % conversion of 10 mM citral, and ~49 % conversion of 50 mM trans-2-hexen-1-al in 24 hours, using NMN<sup>+</sup> as the cycling cofactor (Table 8).

**Table 8: Conversion of a range of substrates using NMN<sup>+</sup> as the cycling cofactor**

Substrate	Product	Enzyme	Substrate Concentration <sup>a</sup>	Conversion (%)
		XenA	33 mM	>99
		XenA	10 mM	76 ± 2
		XenA	50 mM	49 ± 3
		OYE3	5 mM	>99
		NfsB	2 mM	92 ± 1
<b>cytochrome <i>c</i> (oxidized)</b>	<b>cytochrome <i>c</i> (reduced)</b>	P450 BM3 W1046S	50 μM	>99

Reactions were performed in 200 mM potassium phosphate buffer (pH 7.5), 1 M NaCl, 300 mM D-glucose, 6 mM NMN<sup>+</sup>, and substrates at 30°C while mixing for 24 hours. Bs GDH was supplied at 0.33 mg mL<sup>-1</sup>. XenA, OYE3, NfsB, and P450 BM3 W1046S were supplied at 0.75 mg mL<sup>-1</sup>. Values are an average of at least three replicates with values after ± represent one standard deviation.

<sup>a</sup> Substrate concentration was limited by substrate solubility in the buffer.



### 2.3.3 *In vitro* NMN(H) cycling supports diverse chemistries

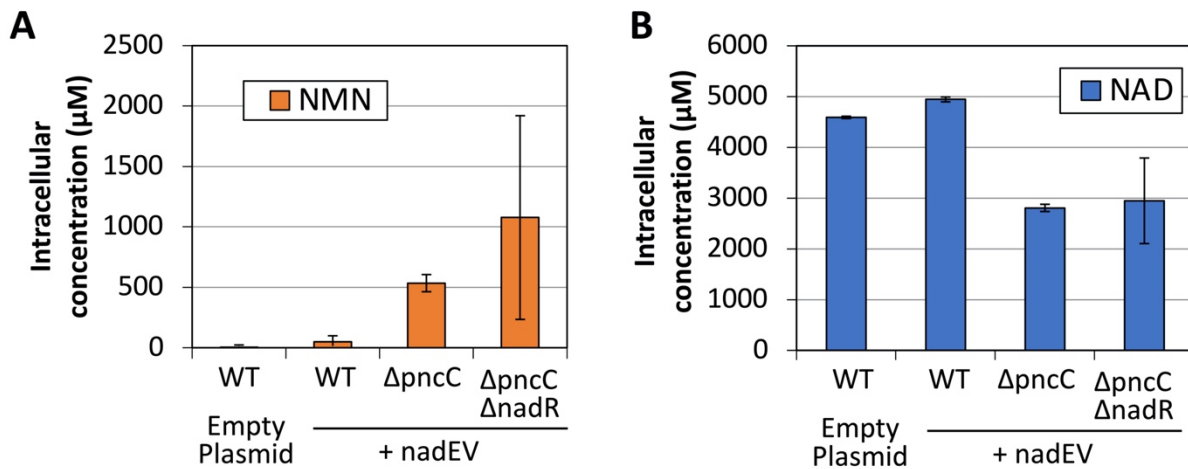
XenA's promiscuity for non-canonical redox cofactors may be attributed to its ping-pong mechanism of catalysis involving the flavin prosthetic groups. Specifically, the hydride transfer from cofactors to flavin might be less sensitive to the differences in binding modes of various cofactors<sup>9</sup>. Indeed, several other classes of flavoenzymes have been shown to accept biomimetic redox cofactors<sup>18,25,26</sup>. Given the versatility of flavoenzymes, there might be opportunities to extend the application of the NMN(H) cycling systems to other chemistries.

The NMN(H) cycling process was coupled with three enzymes other than XenA (Table 8). In the presence of Bs GDH Triple and NMN<sup>+</sup>, the enoate reductase OYE3 from *Saccharomyces cerevisiae*<sup>16</sup> reduced the activated C≡C triple bond in 4-phenyl-3-butyne-2-one with >99 % conversion, and the nitro reductase NfsB from *E. coli*<sup>17,26</sup> reduced the nitro group in nitrofurazone with ~92 % conversion (Table 8). Cytochrome P450 BM3 from *Bacillus megaterium* natively has low activity with NMNH. By mutating the highly conserved "shielding" tryptophan at the cofactor binding site to serine<sup>18</sup>, our lab previously demonstrated an improved NMNH-dependent activity of BM3 by ~46 fold<sup>13</sup>. Using the engineered BM3, we showed that Bs GDH Triple generated NMNH *in situ* to supply electrons to the engineered BM3 W1046S, allowing the latter to reduce cytochrome *c* with > 99% conversion (Table 8).

### 2.3.4 *In vivo* NMN(H) accumulation

After demonstrating efficient NMN(H) cycling *in vitro*, we looked to integrate the system in *E. coli* to support *in vivo* biotransformation. To achieve this, we first looked to accumulate NMN<sup>+</sup> in *E. coli* cells. Although NMN<sup>+</sup> is naturally produced by DNA ligases in *E. coli* in a small amount<sup>27</sup>, we hypothesized that this low level may not be sufficient to support effective redox cycling. Interestingly, other microorganisms possess NMN<sup>+</sup> biosynthetic pathways as part of the

salvage pathway of NAD<sup>+</sup><sup>27</sup>. To build up the intracellular NMN<sup>+</sup> pool in *E. coli*, we over-expressed the genes encoding nicotinamide phosphoribosyl transferase (*nadV*) and NMN synthetase (*nadE*) from *Francisella tularensis*<sup>28</sup>. Furthermore, we disrupted potential NMN<sup>+</sup>-degradation pathways in *E. coli* by knocking out genes *pncC* and *nadR*<sup>27</sup>. These manipulations together resulted in a ~1000-fold increase in intracellular NMN<sup>+</sup> concentration compared to that of wild type *E. coli* (from ~1 μM to ~1077 μM, Figure 3A). In the highest NMN<sup>+</sup>-producing strain, the level of the NMN<sup>+</sup> reached around 30% that of NAD<sup>+</sup> (Figure 3B).



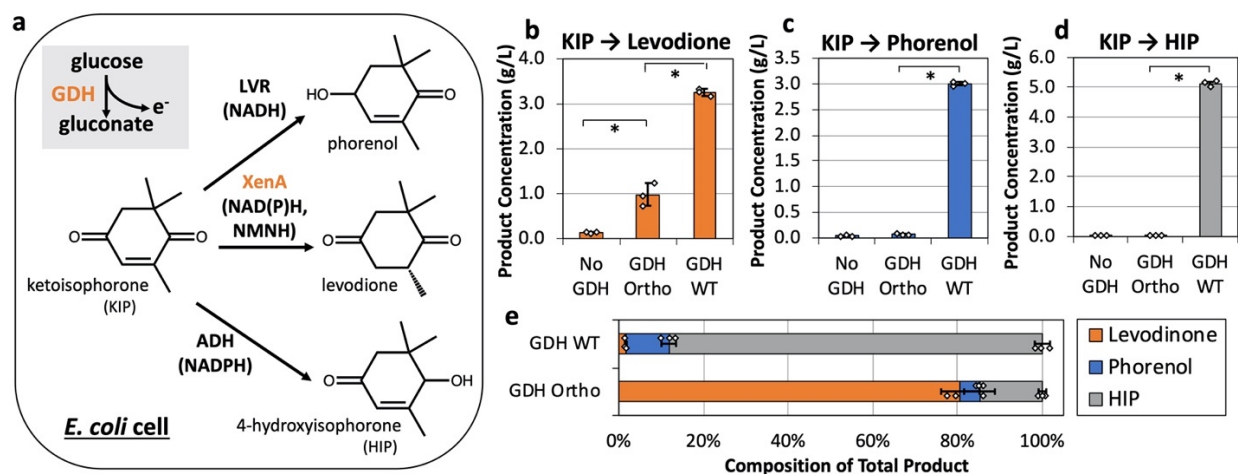
**Figure 3: *In vivo* NMN<sup>+</sup> cycling supports *E. coli* growth** (A) Disruption of NMN<sup>+</sup> degrading genes (*pncC* and *nadR*) and over-expression of NMN<sup>+</sup> producing genes (*Ft nadE* and *Ft nadV*) enabled elevated intracellular levels of NMN<sup>+</sup>. (B) Intracellular levels of NAD<sup>+</sup> were slightly lowered in the *ΔpncC* and *ΔnadR* cells. Values are an average of at least three biological replicates with error bars represent one standard deviation. XenA, enoate reductase from *Pseudomonas putida*. *Ft*, *Francisella tularensis*.

In other work from our lab, it was demonstrated that the built-in NMN<sup>+</sup> pool could support effective redox cycling, but it was shown that supplementing NMN<sup>+</sup> in the medium was beneficial. *E. coli* cells have been shown to both uptake and excrete NMN<sup>+</sup><sup>29,30</sup>. As NMN<sup>+</sup>-transporting systems continue to be discovered in various organisms<sup>31,32</sup>, genomics information may aid in the elucidation of transport mechanism of NMN<sup>+</sup> in *E. coli*.

### 2.3.5 NMN(H) enables specific electron delivery in *E. coli*

Compared to *in vitro* biotransformation, whole cell-based processes are considered more robust and inexpensive. However, one drawback is that the host's natural metabolism often interferes with the desired biotransformation reaction *in vivo*. For example, aldehydes are often reduced by the numerous, non-specific, C=O bond reducing-enzymes native to the hosts<sup>33-35</sup>. As such, a tool is needed to deliver reducing power only to the desired reaction *in vivo*. We sought to test if the Bs GDH Ortho-mediated NMN(H) cycling system can serve as such a tool.

We chose the levodione production reaction (Figure 2B, C) as the model system. In the substrate KIP, three sites are susceptible for enzymatic reduction (Figure 4A). While reduction of the C=C double bond by XenA yields the desired product levodione, reduction of the two C=O groups by the enzymes levodione reductase<sup>36</sup> (LVR from *Corynebacterium aquaticum*) and alcohol dehydrogenase<sup>37</sup> (ADH from *Ralstonia sp*) will result in the side products phorenol and 4-hydroxyisophorone (HIP), respectively.



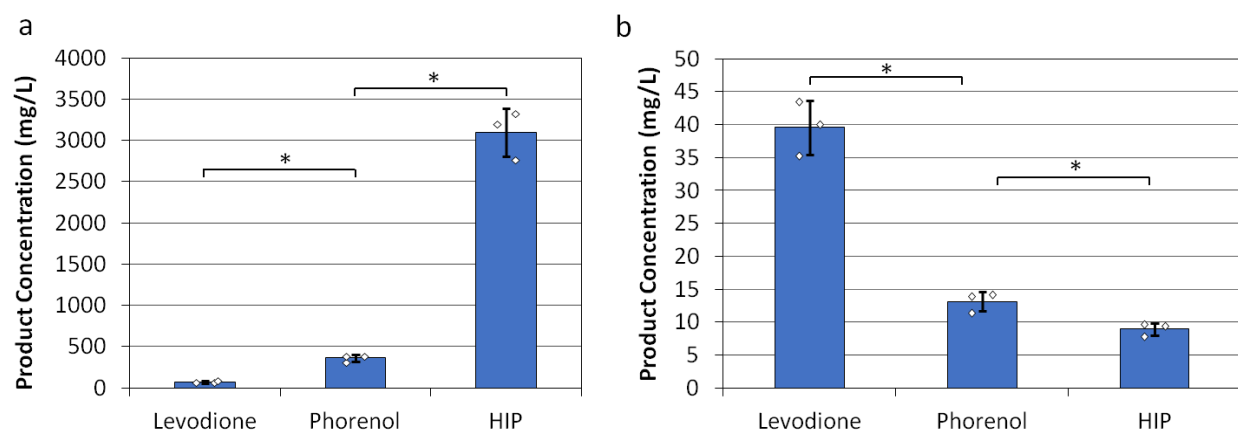
**Figure 4: Bs GDH Ortho selectively provides reducing power for levodione production in *E. coli* whole cells.** (a) Bs GDH derives reducing power from glucose, which can support the biotransformation enzymes LVR, XenA, and ADH to convert ketoisophorone (KIP) into phorenol, levodione, and 4-hydroxyisophorone (HIP), respectively. (b-d) KIP conversion using resting *E. coli* cells expressing Bs GDH variants and individual conversion enzymes (LVR, XenA, or ADH). Wild-type Bs GDH (GDH WT) supported all three conversion reactions, while Bs GDH Ortho

specifically facilitated the conversion of KIP to levodione, which is catalyzed by an NMNH-utilizing enzyme, XenA. (e) KIP conversion using resting *E. coli* cells expressing Bs GDH variants and all three conversion enzymes (LVR, XenA, and ADH) simultaneously. Total product composition switched towards levodione production when Bs GDH Ortho was expressed instead of Bs GDH WT. Whole-cell biotransformation was performed using resting *E. coli* cells of  $OD_{600nm} \sim 2$ , in buffer containing 100 mM potassium phosphate, 2 mM  $NMN^+$ , 200 mM glucose, and 5 g/L KIP, at 30°C for 48 hours. Values are an average of at least three biological replicates with error bars represent one standard deviation. Two-tailed t-tests were used to determine statistical significance ( $P < 0.05$ ), indicated by an asterisk. XenA, enoate reductase from *Pseudomonas putida*. LVR, levodione reductase from *Corynebacterium aquaticum*. ADH, alcohol dehydrogenase from *Ralstonia sp.*

We first built the whole-cell biotransformation chassis by disrupting the Embden–Meyerhof–Parnas (EMP pathway), pentose phosphate pathway (PPP), and Entner-Doudoroff pathways by disrupting *pgi*, *zwf*, and *gntk* genes in *E. coli*, leaving Bs GDH as the only enzyme that can generate reducing power from glucose. Next, we paired Bs GDH wild type or Bs GDH Ortho with XenA, LVR, or ADH, individually (Figure 4B, C, D). In resting cells with XenA and wild type Bs GDH, the whole cells produced  $\sim 3$  g/L levodione from 5 g/L KIP, using glucose as the co-substrate. Importantly, Bs GDH Ortho was also able to power the XenA-catalyzed reaction with  $NMN^+$  supplementation in the buffer ( $\sim 1$  g/L levodione was formed under the same conditions) (Figure 4B). By contrast, LVR and ADH-catalyzed reactions were only active when wild type Bs GDH was used (Figure 4C, D). When Bs GDH Ortho was used, minimal levels of phorenol or HIP was produced (Figure 4C, D), indicating that LVR and ADH, which catalyze the competing reactions in our model system, were not supplied with reducing power.

Lastly, we over-expressed XenA, LVR, and ADH simultaneously in resting cells, which resulted in a mixture of products being formed from KIP. Interestingly, by using different Bs GDH variants to generate reducing power, the composition of the mixtures can shift greatly (Figure 4E). When using wild type Bs GDH to generate NADH and NADPH, all three enzymes were active. However, XenA could not compete favorably with LVR and ADH for substrate conversion, which led to low product-to-byproduct ratio (levodione only constituted  $\sim 2$  % of total products by mass,

Figure 4E). On the other hand, when using Bs GDH Ortho, the fraction of levodione in the product mixture increased to ~80%. Analysis of the levodione, phorenol, and HIP concentrations suggested that the improved ratio was largely due to the substantially decreased byproduct formation (Figure 5).



**Figure 5: Product levels in whole-cell ketoisophorone (KIP) conversion with co-expression of XenA, LVR, and ADH.** With simultaneous expression of all three KIP converting enzymes, the principal product was determined by the cofactor specificity of GDH. (a) Production of 4-hydroxyisophorone (HIP) was dominant when the redox system was coupled with GDH WT (NAD(P)<sup>+</sup> preference). (b) Production of levodione was dominant when the redox system was coupled with GDH Ortho (NMN<sup>+</sup> preference). XenA, enoate reductase from *Pseudomonas putida*. LVR, levodione reductase from *Corynebacterium aquaticum*. ADH, alcohol dehydrogenase from *Ralstonia sp.* The error bars represent one standard deviation above the mean of triplicate experiments. Two-tailed t-tests were used to determine statistical significance (P < 0.05), indicated by an asterisk.

These results support that NMNH can be established as an alternative reducing power in *E. coli* to increase selectivity in whole-cell biotransformation. *E. coli*'s endogenous enoate reductase, NemA, might also contribute to levodione production. Based on previous report, this contribution may be minor due to the relatively low background activity of NemA without over-expression<sup>38</sup>.

## 2.4 Conclusion

In summary, we have developed a noncanonical redox cofactor system based on NMN<sup>+</sup>. We explored its applications in redox cycling *in vitro* and specific electron delivery *in vivo*. This

was enabled by a computationally designed Bs GDH that possesses the largest specificity switch toward a noncanonical nicotinamide cofactor achieved so far.

To increase the reaction rate of NMN<sup>+</sup>-dependent whole-cell biotransformation, future work may focus on further improving the catalytic efficiencies of the NMN<sup>+</sup>-dependent enzymes, potentially via directed evolution as mentioned above. Furthermore, recent efforts demonstrated pathways for efficient NMN<sup>+</sup> biosynthesis<sup>39</sup>, which could be used to further increase intracellular NMN<sup>+</sup> concentration toward ultimately eliminating the need for NMN<sup>+</sup> supplementation. We did not observe substantial growth deficiency in NMN<sup>+</sup>-accumulating cells. Future work is needed to characterize the physiological impacts of NMN<sup>+</sup> accumulation, such as potentially identifying host enzymes that are regulated by NMN(H) and studying transcriptomic changes caused by varying NMN(H) level.

## 2.5 References

- [1] Lee, S. Y.; Kim, H. U. Systems Strategies for Developing Industrial Microbial Strains. *Nature Biotechnology* **2015**, *33*, 1061–1072.
- [2] Mampel, J.; Buescher, J. M.; Meurer, G.; Eck, J. Coping with Complexity in Metabolic Engineering. *Trends in Biotechnology* **2013**, *31*, 52–60.
- [3] Paddon, C. J.; Keasling, J. D. Semi-Synthetic Artemisinin: A Model for the Use of Synthetic Biology in Pharmaceutical Development. *Nature Reviews Microbiology* **2014**, *12*, 355–367.
- [4] Pandit, A. V.; Srinivasan, S.; Mahadevan, R. Redesigning Metabolism Based on Orthogonality Principles. *Nature Communications* **2017**, *8*, 15188.
- [5] Wang, L.; Ji, D.; Liu, Y.; Wang, Q.; Wang, X.; Zhou, Y. J.; Zhang, Y.; Liu, W.; Zhao, Z. K. Synthetic Cofactor-Linked Metabolic Circuits for Selective Energy Transfer. *ACS Catal.* **2017**, *7*, 1977–1983.
- [6] De Wildeman, S. M. A.; Sonke, T.; Schoemaker, H. E.; May, O. Biocatalytic Reductions: From Lab Curiosity to “First Choice.” *Acc. Chem. Res.* **2007**, *40*, 1260–1266.

- [7] Martínez, A. T.; Ruiz-Dueñas, F. J.; Camarero, S.; Serrano, A.; Linde, D.; Lund, H.; Vind, J.; Tovborg, M.; Herold-Majumdar, O. M.; Hofrichter, M.; Liers, C.; Ullrich, R.; Scheibner, K.; Sannia, G.; Piscitelli, A.; Pezzella, C.; Sener, M. E.; Kılıç, S.; van Berkel, W. J. H.; Guallar, V.; Lucas, M. F.; Zuhse, R.; Ludwig, R.; Hollmann, F.; Fernández-Fueyo, E.; Record, E.; Faulds, C. B.; Tortajada, M.; Winckelmann, I.; Rasmussen, J.-A.; Gelo-Pujic, M.; Gutiérrez, A.; del Río, J. C.; Rencoret, J.; Alcalde, M. Oxidoreductases on Their Way to Industrial Biotransformations. *Biotechnology Advances* **2017**, *35*, 815–831.
- [8] Campbell, E.; Meredith, M.; Minteer, S. D.; Banta, S. Enzymatic Biofuel Cells Utilizing a Biomimetic Cofactor. *Chem. Commun.* **2012**, *48*, 1898–1900.
- [9] Knaus, T.; Paul, C. E.; Levy, C. W.; de Vries, S.; Mutti, F. G.; Hollmann, F.; Scrutton, N. S. Better than Nature: Nicotinamide Biomimetics That Outperform Natural Coenzymes. *J. Am. Chem. Soc.* **2016**, *138*, 1033–1039.
- [10] Nowak, C.; Pick, A.; Lommes, P.; Sieber, V. Enzymatic Reduction of Nicotinamide Biomimetic Cofactors Using an Engineered Glucose Dehydrogenase: Providing a Regeneration System for Artificial Cofactors. *ACS Catal.* **2017**, *7*, 5202–5208.
- [11] Flores, H.; Ellington, A. D. A Modified Consensus Approach to Mutagenesis Inverts the Cofactor Specificity of *Bacillus Stearotherophilus* Lactate Dehydrogenase. *Protein Eng Des Sel* **2005**, *18*, 369–377.
- [12] Lo, H. C.; Fish, R. H. Biomimetic NAD<sup>+</sup> Models for Tandem Cofactor Regeneration, Horse Liver Alcohol Dehydrogenase Recognition of 1,4-NADH Derivatives, and Chiral Synthesis. *Angewandte Chemie* **2002**, *114*, 496–499.
- [13] Black, W. B.; Zhang, L.; Mak, W. S.; Maxel, S.; Cui, Y.; King, E.; Fong, B.; Sanchez Martinez, A.; Siegel, J. B.; Li, H. Engineering a Nicotinamide Mononucleotide Redox Cofactor System for Biocatalysis. *Nature Chemical Biology* **2020**, *16*, 87–94.
- [14] Hagen, J. *Industrial Catalysis: A Practical Approach* 2nd edn, John Wiley & Sons, **2006**.
- [15] Chaparro-Riggers, J. F.; Rogers, T. A.; Vazquez-Figueroa, E.; Polizzi, K. M.; Bommaris, A. S. Comparison of Three Enoate Reductases and Their Potential Use for Biotransformations. *Advanced Synthesis & Catalysis* **2007**, *349*, 1521–1531.
- [16] Müller, A.; Stürmer, R.; Hauer, B.; Rosche, B. Stereospecific Alkyne Reduction: Novel Activity of Old Yellow Enzymes. *Angewandte Chemie International Edition* **2007**, *46*, 3316–3318.
- [17] Race, P. R.; Lovering, A. L.; Green, R. M.; Osson, A.; White, S. A.; Searle, P. F.; Wrighton, C. J.; Hyde, E. I. Structural and Mechanistic Studies of *Escherichia Coli* Nitroreductase with the Antibiotic Nitrofurazone. Reversed Binding Orientations in Different Redox States of the Enzyme. *J. Biol. Chem.* **2005**, *280*, 13256–13264.

- [18] Ryan, J. D.; Fish, R. H.; Clark, D. S. Engineering Cytochrome P450 Enzymes for Improved Activity towards Biomimetic 1,4-NADH Cofactors. *ChemBioChem* **2008**, *9*, 2579–2582.
- [19] Findik, B. T.; Randall, L. L. Determination of the Intracellular Concentration of the Export Chaperone SecB in Escherichia Coli. *PLOS ONE* **2017**, *12*, e0183231.
- [20] Everse, J.; Anderson, B.; You, K.-S. The Pyridine Dinucleotide Coenzymes. *Academic Press* **1982**.
- [21] Paul, C. E.; Arends, I. W. C. E.; Hollmann, F. Is Simpler Better? Synthetic Nicotinamide Cofactor Analogues for Redox Chemistry. *ACS Catal.* **2014**, *4*, 788–797.
- [22] Paul, C. E.; Gargiulo, S.; Opperman, D. J.; Lavandera, I.; Gotor-Fernández, V.; Gotor, V.; Taglieber, A.; Arends, I. W. C. E.; Hollmann, F. Mimicking Nature: Synthetic Nicotinamide Cofactors for C=C Bioreduction Using Enoate Reductases. *Org. Lett.* **2013**, *15*, 180–183.
- [23] Kataoka, M.; Kotaka, A.; Hasegawa, A.; Wada, M.; Yoshizumi, A.; Nakamori, S.; Shimizu, S. Old Yellow Enzyme from *Candida Macedoniensis* Catalyzes the Stereospecific Reduction of the C=C Bond of Ketoisophorone. *Bioscience, Biotechnology, and Biochemistry* **2002**, *66*, 2651–2657.
- [24] Okamoto, Y.; Köhler, V.; Paul, C. E.; Hollmann, F.; Ward, T. R. Efficient In Situ Regeneration of NADH Mimics by an Artificial Metalloenzyme. *ACS Catal.* **2016**, *6*, 3553–3557.
- [25] Paul, C. E.; Tischler, D.; Riedel, A.; Heine, T.; Itoh, N.; Hollmann, F. Nonenzymatic Regeneration of Styrene Monooxygenase for Catalysis. *ACS Catal.* **2015**, *5*, 2961–2965.
- [26] Knox, R. J.; Friedlos, F.; Jarman, M.; Davies, L. C.; Goddard, P.; Anlezark, G. M.; Melton, R. G.; Sherwood, R. F. Virtual Cofactors for an Escherichia Coli Nitroreductase Enzyme: Relevance to Reductively Activated Prodrugs in Antibody Directed Enzyme Prodrug Therapy (ADEPT). *Biochemical Pharmacology* **1995**, *49*, 1641–1647.
- [27] Gazzaniga, F.; Stebbins, R.; Chang, S. Z.; McPeck, M. A.; Brenner, C. Microbial NAD Metabolism: Lessons from Comparative Genomics. *Microbiol. Mol. Biol. Rev.* **2009**, *73*, 529–541.
- [28] Sorci, L.; Martynowski, D.; Rodionov, D. A.; Eyobo, Y.; Zogaj, X.; Klose, K. E.; Nikolaev, E. V.; Magni, G.; Zhang, H.; Osterman, A. L. Nicotinamide Mononucleotide Synthetase Is the Key Enzyme for an Alternative Route of NAD Biosynthesis in Francisella Tularensis. *PNAS* **2009**, *106*, 3083–3088.
- [29] Wang, X.; Zhou, Y. J.; Wang, L.; Liu, W.; Liu, Y.; Peng, C.; Zhao, Z. K. Engineering Escherichia Coli Nicotinic Acid Mononucleotide Adenylyltransferase for Fully Active Amidated NAD Biosynthesis. *Appl. Environ. Microbiol.* **2017**, *83*, e00692-17.



- [30] Witholt, B. Method for Isolating Mutants Overproducing Nicotinamide Adenine Dinucleotide and Its Precursors. *Journal of Bacteriology* **1972**, *109*, 350–364.
- [31] Grozio, A.; Mills, K. F.; Yoshino, J.; Bruzzone, S.; Sociali, G.; Tokizane, K.; Lei, H. C.; Cunningham, R.; Sasaki, Y.; Migaud, M. E.; Imai, S. Slc12a8 Is a Nicotinamide Mononucleotide Transporter. *Nature Metabolism* **2019**, *1*, 47–57.
- [32] Grose, J. H.; Bergthorsson, U.; Xu, Y.; Sternecker, J.; Khodaverdian, B.; Roth, J. R. Assimilation of Nicotinamide Mononucleotide Requires Periplasmic AphA Phosphatase in Salmonella Enterica. *Journal of Bacteriology* **2005**, *187*, 4521–4530.
- [33] Kunjapur, A. M.; Prather, K. L. J. Microbial Engineering for Aldehyde Synthesis. *Appl. Environ. Microbiol.* **2015**, *81*, 1892–1901.
- [34] Rodriguez, G. M.; Atsumi, S. Toward Aldehyde and Alkane Production by Removing Aldehyde Reductase Activity in Escherichia Coli. *Metabolic Engineering* **2014**, *25*, 227–237.
- [35] Hall, M.; Hauer, B.; Stuermer, R.; Kroutil, W.; Faber, K. Asymmetric Whole-Cell Bioreduction of an  $\alpha,\beta$ -Unsaturated Aldehyde (Citral): Competing Prim-Alcohol Dehydrogenase and C–C Lyase Activities. *Tetrahedron: Asymmetry* **2006**, *17*, 3058–3062.
- [36] Yoshisumi, A.; Wada, M.; Takagi, H.; Shimizu, S.; Nakamori, S. Cloning, Sequence Analysis, and Expression in Escherichia Coli of the Gene Encoding Monovalent Cation-Activated Levodione Reductase from Corynebacterium Aquaticum M-13. *Bioscience, Biotechnology, and Biochemistry* **2001**, *65*, 830–836.
- [37] Kulig, J.; Frese, A.; Kroutil, W.; Pohl, M.; Rother, D. Biochemical Characterization of an Alcohol Dehydrogenase from Ralstonia Sp. *Biotechnology and Bioengineering* **2013**, *110*, 1838–1848.
- [38] Oberleitner, N.; Peters, C.; Rudroff, F.; Bornscheuer, U. T.; Mihovilovic, M. D. *In Vitro* Characterization of an Enzymatic Redox Cascade Composed of an Alcohol Dehydrogenase, an Enoate Reductases and a Baeyer–Villiger Monooxygenase. *Journal of Biotechnology* **2014**, *192*, 393–399.
- [39] Marinescu, G. C.; Popescu, R.-G.; Stoian, G.; Dinischiotu, A.  $\beta$ -Nicotinamide Mononucleotide (NMN) Production in Escherichia Coli. *Scientific Reports* **2018**, *8*, 12278.
- [40] Hilt, W.; Pfeleiderer, G.; Fortnagel, P. Glucose Dehydrogenase from Bacillus Subtilis Expressed in *Escherichia Coli* I: Purification, Characterization and Comparison with Glucose Dehydrogenase from *Bacillus megaterium*. *Biochim. Biophys. Acta* **1991**, *1076*, 298–304.

- [41] Solanki, K.; Abdallah, W.; Banta, S. Engineering the Cofactor Specificity of an Alcohol Dehydrogenase via Single Mutations or Insertions Distal to the 2'-Phosphate Group of NADP(H). *Protein Eng. Des. Sel.* **2017**, *30*, 373–380.
- [42] Black, W. B.; Zhang, L.; Mak, W. S.; Maxel, S.; Cui, Y.; King, E.; Fong, B.; Sanchez Martinez, A.; Siegel, J. B.; Li, H. Engineering a Nicotinamide Mononucleotide Redox Cofactor System for Biocatalysis. *Nat. Chem. Biol.* **2020**, *16*, 87–94.

## **Chapter 3**

# **Aldehyde Production in Crude Lysate- and Whole Cell- Based Biotransformation Using a Noncanonical Redox Cofactor System**

The text, data, and figures in this chapter are adapted from a previously published manuscript. Reprinted with permission from Richardson, K. N., Black, W. B., Li, H., “Aldehyde Production in Crude Lysate- and Whole Cell-Based Biotransformation Using a Noncanonical Redox Cofactor System” *ACS Catalysis*, 10, 8898-8903, 2020. Copyright 2020 American Chemical Society.

The authors Richardson and Black contributed equally to this manuscript. All experiments, data analysis, and text were equally distributed, and both authors were involved in each area.

### 3.1 Introduction

Traditionally, biotransformation has been carried out either *in vivo* with engineered microbial whole cells or *in vitro* with purified enzymes. Recently, crude lysate-based biotransformation has emerged as an alternative which brings the benefits of both worlds: it contains a cell-like metabolism which includes glycolysis and TCA cycle that generate energy, cofactors, and key intermediates from inexpensive feedstocks<sup>1-4</sup>; it is easier to monitor, manipulate, and optimize because cell membrane barrier does not exist and operational parameters can be varied well outside what's tolerable by living cells<sup>5-7</sup>; it also eliminates the high cost of purifying proteins for *in vitro* biotransformation in large scale<sup>1</sup>.

However, just like in whole cells, crude lysate-based biotransformation faces the challenge of controlling side reactions, which are catalyzed by the numerous endogenous enzymes of the host<sup>1,2</sup>. A traditional method to tackle this challenge in whole cells involves identifying and genetically disrupting competing enzymes<sup>8,9</sup>, which, albeit effective, can often be time consuming and labor intensive. Instead of replicating the same approach in crude lysate-based process to eliminating competing enzymes, here we report an alternative method, which is based on an orthogonal redox cofactor system<sup>10</sup>.

We chose citronellal as the model product, which is a terpenoid aldehyde with wide usage in the flavor and fragrance industries, as the precursor of nonracemic menthol, and as an insect repellent<sup>11,12</sup>. Using enoate reductases (ERs), citronellal can be produced from citral (Figure 6), a low-cost substrate that can be readily obtained in large quantities. However, since both citral and citronellal are aldehydes, which are rapidly reduced to alcohols by a myriad of broad substrate-range alcohol dehydrogenases (ADHs) in the cell, this conversion is inefficient in microbial hosts *in vivo*<sup>11</sup> and with crude lysates *in vitro*<sup>13</sup>. Previously, Paul and coworkers employed a biomimetic

cofactor, 1-Benzyl-1,4-dihydronicotinamide, to increase the production of citronellal using poorly purified ER from *E. coli*<sup>13</sup>. This system operated based on the principle that only ER could utilize the biomimetic cofactor as reducing power, while the *E. coli* endogenous ADHs, which were also present in the crude ER-extract, could not. This method eliminated the cost of extensively purifying ER. However, because this system did not utilize a method of cofactor regeneration, a stoichiometric amount of biomimetic cofactor was required, which could add a formidable cost in large scale. In addition, application of this system *in vivo* was not examined.

As discussed in Chapter 2, we demonstrated the nicotinamide mononucleotide (NMN<sup>+</sup>)-dependent orthogonal redox cofactor system in *E. coli*, which features an engineered glucose dehydrogenase (GDH Ortho) from *Bacillus subtilis*, that can efficiently and specifically recycle NMN<sup>+</sup> using glucose as an inexpensive substrate<sup>10</sup>. In this work, we first demonstrate that the NMN<sup>+</sup>-based orthogonal redox cofactor system can enable efficient conversion of citral to citronellal in crude lysate-based, cell-free biotransformation without the need to identify or disrupt competing ADHs in *E. coli*. Next, we systematically optimized enzyme ratios, lysate preparation procedure, cofactor concentration, buffer composition, and pH to achieve citronellal production with 97-100% product purity with nominal levels alcohol byproducts, and ~60% conversion. Finally, the optimized crude lysate system was used to inform the design of whole-cell biotransformation in *E. coli* (Figure 6A), which produced 33 mg/L citronellal with 83% product purity. In contrast, biotransformation processes relying on the natural cofactors nicotinamide adenine dinucleotide (phosphate) (NAD(P)<sup>+</sup>) only yielded the alcohol byproducts, namely citronellol, nerol, and geraniol. We envision this approach may be adapted for different target products and different chassis hosts with relative ease.

## 3.2 Methods

### 3.2.1 Plasmids and Strains

All plasmids and strain MX102 were taken from previous work in our lab<sup>10</sup> (Table 9, Table 10). All plasmids were transformed by electroporation. When multiple plasmids were used in a strain, they were transformed simultaneously. When applicable, the following antibiotic concentrations were used, unless stated otherwise: 100 mg/L ampicillin, 50 mg/L kanamycin, 50 mg spectinomycin, or 20 mg/L chloramphenicol.

**Table 9: Strain and Plasmids Used in Chapter 3**

Strains	Description	Reference
MX102	<i>E. coli</i> $\Delta(\text{araD-araB})567$ , $\Delta\text{lacZ4787}>::\text{rrnB-3}$ , $\lambda$ -, <i>rph-1</i> , $\Delta(\text{rhaD-rhaB})568$ , <i>hsdR514</i> , $\Delta\text{pncC}$ , $\Delta\text{pgi}$ , $\Delta\text{zwf}$ , $\Delta\text{gntK}>::\text{kan}$	[10]
Plasmids	Description	Reference
pEK101	<i>P<sub>LlacO1</sub>::Bs gdh</i> , ColE1 <i>ori</i> , Amp <sup>R</sup>	[10]
pEK102	<i>P<sub>LlacO1</sub>::Pp xenA</i> , ColE1 <i>ori</i> , Amp <sup>R</sup>	[10]
pLZ216	<i>P<sub>LlacO1</sub>::Bs gdh</i> I195R-A93K-Y39Q-S17E, ColE1 <i>ori</i> , Amp <sup>R</sup>	[10]
pLZ217	<i>P<sub>BAD</sub>::Pp xenA</i> , RSF <i>ori</i> , Spec <sup>R</sup>	[10]
pSM106	<i>P<sub>BAD</sub>::Bs gdh</i> I195R-A93K-Y39Q-S17E, RSF <i>ori</i> , Spec <sup>R</sup>	[10]
pSM107	<i>P<sub>BAD</sub>::Bs gdh</i> , RSF <i>ori</i> , Spec <sup>R</sup>	[10]
pSM109	<i>P<sub>LlacO1</sub>::Zm glf</i> , p15A <i>ori</i> , Cm <sup>R</sup>	[10]

Abbreviations indicate source of genes: *Bs*, *Bacillus subtilis*; *Pp*, *Pseudomonas putida*; *Zm*, *Zymomonas mobilis*

**Table 10: Accession Numbers for Proteins Used in Chapter 3**

Protein Name	Full Name	Protein ID
<i>Pp</i> XenA	NADH: flavin oxidoreductase/NADH oxidase	Q9R9V9
<i>Bs</i> Gdh	Glucose 1-dehydrogenase	P12310
<i>Zm</i> Glf	Glucose facilitated diffusion porin	P21906

### 3.2.2 Crude Lysate Biotransformations

Cell-free reactions were performed with crude *E. coli* lysates in a modular system. In this system, each protein was overexpressed and processed separately. Then, different lysates were mixed at controlled ratios to complete the full system. *E. coli* strain MX102 was transformed with a plasmid expressing XenA (pEK102), GDH WT (pEK101), or GDH Ortho (pLZ216). 4 mL seed cultures containing 2xYT medium supplemented with 1% w/v mannitol and appropriate antibiotics were incubated at 30 °C while shaking at 250 r. p. m. for 16 hours. Next, 0.5% v/v seed cultures were used to inoculate 250 mL of 2xYT medium supplemented with 1% w/v mannitol and 200 mg/L ampicillin in a 500 mL baffled shake flask. Cultures were incubated at 30 °C while shaking at 250 r. p. m. for 4 hours. Protein expression was induced with 0.5 mM IPTG and 0.1% w/v arabinose. Cultures shook for an additional 10 hours under the same conditions. To harvest and process the cells, cultures were centrifuged at 4000 RCF for 20 minutes at 4 °C. The resulting cell pellets were washed 3 times in 250 mL of ice-cold wash buffer containing 120 mM potassium acetate, 28 mM magnesium acetate, and 20 mM tris base pH 8.2. After washing, cells were resuspended in 0.7 mL of wash buffer per 1 g wet-cell-weight of pelleted cells. The resuspended cells were then lysed by French press. The cell lysate was clarified by centrifugation twice at 20,000 RCF for 20 minutes at 4 °C. When stated in the text, an additional ultracentrifugation step was applied by centrifuging the supernatant from the preceding centrifugation step at 30,000 RCF for 30 minutes at 4 °C. The clarified lysate was aliquoted into 1.5 mL microcentrifuge tubes and stored at -80 °C until use. The total protein concentration in the lysate was quantified by Bradford Assay.

Cell-free reactions were performed at a 1 mL working volume in 2 mL glass vials sealed with a PTFE-lined cap at 37 °C without shaking. Clarified cell lysate was thawed on ice. The

XenA-enriched lysate was mixed with the GDH WT- or GDH Ortho-enriched lysate at various ratios to create a complete cycling system. The total lysate protein concentration was maintained constant at 4.5 mg/mL in the final reaction mixture. Lysate mixture was spiked into pre-warmed, concentrated assay buffer to start the reaction. Two different reaction mixtures were used depending on whether Buffer A or phosphate buffer was being investigated. The working concentration and composition of the Buffer A reaction mixture was 12 mM magnesium acetate, 10 mM ammonium acetate, 130 mM potassium acetate, 10 mM potassium phosphate, 200 mM D-glucose, 1 mM of oxidized cofactor (when optimizing, cofactor concentration was varied at 0, 0.1, 0.2, 0.5, 1, 2, 5, or 10 mM), and 500 mg/L citral. The working concentration and composition of the phosphate buffer reaction mixture was 200 mM potassium phosphate at pH 7.0, pH 7.5, or pH 8.0, 200 mM NaCl, 200 mM D-glucose, 0.1, 0.2, or 0.5 mM NMN<sup>+</sup>, and 500 mg/L citral. Samples were taken intermittently for analysis. Samples were extracted with an equal volume of chloroform containing 200 mg/L octanol as an internal standard. The organic fraction was used for GC-FID analysis, as detailed below.

### **3.2.3 Determination of Molar Concentrations of Recombinant Protein in Crude Lysates**

The molar concentration of XenA and GDH Ortho in crude lysates was determined by comparing the level of specific protein activity to a standard curve derived from purified proteins. To generate the purified proteins, *E. coli* strain BL21 (DE3) was transformed with a plasmid expressing XenA (pEK102) or GDH Ortho (pLZ216) with a 6x His-tag fusion at the N terminus. 4 mL seed cultures containing LB medium and appropriate antibiotics were incubated at 37 °C for ~16 hours while shaking at 250 r.p.m.. The seed cultures were used to inoculate 10 mL of LB medium with appropriate antibiotics in a 50 mL conical tube. Protein expression was induced with 0.5 mM IPTG. The tube cap was loosely affixed with tape. The cultures were then incubated at 30



°C for 24 hours while shaking at 250 r.p.m.. Proteins were purified using His-Spin Protein Purification Miniprep kit (Zymo Research Corporation). The purified protein concentrations were quantified by Bradford assay.

To generate the standard curves, purified protein was serially diluted with His-Elution Buffer (Zymo Research Corporation). The dilution series was spiked into assay buffer to start the reactions. For XenA, the assay buffer contained 200 mM potassium phosphate at pH 7.5, 0.2 mM NADPH, and 5 mM ketoisophorone at 37 °C. The initial reaction rate was determined by observing the decrease in light absorption at 340 nm, corresponding to the rate of NADPH consumption. Reactions containing no substrate were run to determine the non-specific XenA activity rate. Reaction rate was determined by subtracting the no substrate reaction rate from the reaction rate with substrate. For GDH Ortho, the assay buffer contained 50 mM Tris-Cl at pH 8, 140 mM D-glucose, 3 mM NMN<sup>+</sup> at 25 °C. The initial reaction rate was determined by observing the increase in light absorption at 340 nm, corresponding to NMNH production. The rate of cofactor consumption or formation was plotted against enzyme concentration, and a best-fit line was fit to the data. The equation of the best-fit line was used to determine molar concentrations of recombinant protein in crude lysate. To test XenA and GDH Ortho concentration in crude lysates, crude lysates were diluted with His-Elution Buffer (Zymo Research Corporation), and the diluted lysates were spiked into identical assay buffer as their respective purified proteins. Reaction rate was measured in the same way. The reaction rate in the crude lysates was compared to the standard curve to obtain the concentration of the respective recombinant protein in the lysates.

### **3.2.4 Resting Whole-Cell Biotransformation**

Three plasmids, one expressing XenA (selected from pEK102 or pLZ217), one expressing one of the GDH variants (selected from pLZ216, pSM106, or pSM107), and pSM109 expressing

a glucose transport facilitator were transformed into MX102. 4 mL seed cultures containing 2xYT medium supplemented with 1% w/v mannitol and appropriate antibiotics were incubated at 30 °C while shaking at 250 r.p.m. for 16 hours. Next, 0.5% v/v seed cultures were used to inoculate 100 mL of 2xYT medium supplemented with 1% w/v mannitol in a 250 mL baffled shake flask. Cultures were incubated at 30 °C while shaking at 250 r. p. m. for 4 hours. Protein expression was induced with 0.5 mM IPTG and 0.1% w/v arabinose. Cultures were shaken for an additional 10 hours under the same conditions. Cells were collected by centrifugation in 50 mL conical tubes for 15 minutes at 20 °C at 3,750 r.p.m.. The supernatant was discarded, and the cells were washed three times with 50 mL of room temperature 100 mM potassium phosphate (pH 7.4), followed by resuspension in room temperature 100 mM potassium phosphate at pH 7.4 to a standardized OD<sub>600</sub> = 50. 1 mL of washed cells were spiked into 4 mL of concentrated assay buffer in a 15 mL conical tube. The working concentration and composition of buffer contained 100 mM potassium phosphate (pH 7.4), 200 mM D-glucose, 2 mM NMN<sup>+</sup>, and 0.5 g/L citral. The tubes were sealed tight and mounted horizontally in an incubating shaker. The tubes were incubated at 30 °C while shaking at 250 r.p.m. for 3 hours. After incubation, 0.5 mL of cell suspension was pelleted, and 200 µL of supernatant was extracted with an equal volume of chloroform containing 200 mg/L octanol as an internal standard. The organic fraction was analyzed by GC-FID, as detailed below.

### **3.2.5 GC-FID Analysis**

All GC analysis was performed on an Agilent 6850 (Agilent Technologies) equipped with an FID. An Agilent DB-WAXetr capillary column (30 m x 0.56 mm x 1 µm) was used for separation. The inlet and detector were held at 250 and 260 °C, respectively. The GC was operated in constant flow mode with a flowrate of 3 mL/min. Helium was used as the carrier gas. Air and hydrogen were supplied to the FID at 350 and 40 mL/min, respectively. All gasses were purchased

from Airgas. 5  $\mu$ L of sample was injected with a 2:1 split ratio. The oven was held at 150 °C for 15 minutes, then ramped to 240 °C at a rate of 20 °C/minute before equilibration back to 150 °C. Elution times are as follows: citral, 7.26 and 8.42 minutes; citronellal, 4.08 minutes; citronellol, 8.72 minutes; nerol, 10.04 minutes; geraniol, 11.55 minutes; octanol, 4.59 minutes.

### 3.2.6 Determination of Relative Plasmid Expression Levels

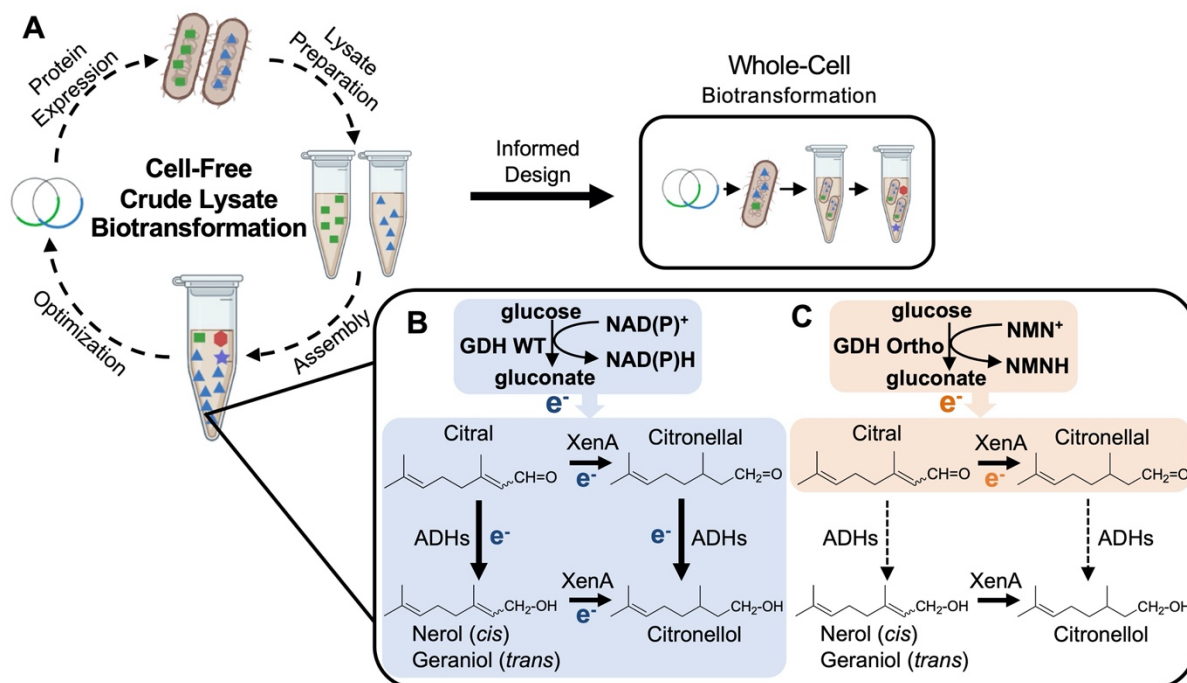
Strain MX102 was transformed with two sets of plasmids. The first set expressed XenA on a *P<sub>LlacO1</sub>* ColE1 *ori* vector (pEK102) and GDH Ortho on a *P<sub>BAD</sub>* RSF *ori* (pSM106). The second set expressed the same genes, but on the opposite vector (pLZ217 and pEK101 for XenA and GDH Ortho, respectively). Cells were cultured identically as resting whole-cell biotransformations detailed in the previous Methods section. 10 mL of culture was incubated on ice for 15 minutes, and then pelleted by centrifugation at 4 °C. The supernatant was discarded. The cell pellet was resuspended in 1 mL of ice-cold 35 mM Tris-Cl at pH 8.0. The resuspended cells were lysed by bead beating with glass beads. Lysates were quickly cooled in an ice water bath to remove any heat accumulated from bead beating. The lysate was clarified by centrifugation at 20,000 RCF for 20 minutes at 4 °C. The clarified lysate was transferred to a fresh 1.5 mL microcentrifuge tube on ice for immediate analysis. The protein concentration in the lysate was determined by Bradford Assay.

To measure the relative expression levels of the vector, GDH Ortho activity was measured by the change in light absorption at 340 nm, due to NMNH formation using a SpectraMax M3 at room temperature. No substrate was supplied to XenA, so change in light absorption is a measure of only GDH Ortho activity, not cycling activity. Lysate was spiked into concentrated assay buffer to start the reaction. The working concentration and composition of assay buffer was 35 mM Tris-Cl at pH 8.0, 140 mM glucose, 2 mM NMN<sup>+</sup>.

### 3.3 Results

#### 3.3.1 Citronellal production in crude lysate-based biotransformation

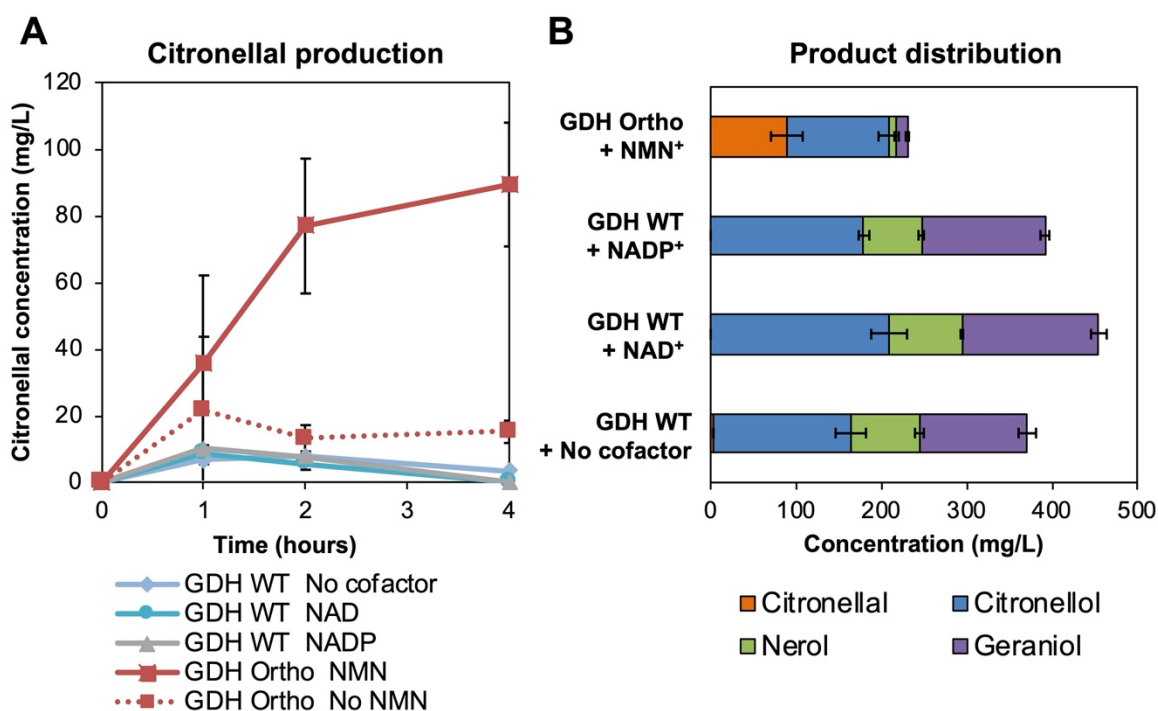
Using purified ER (*Pseudomonas putida* XenA) and GDH Ortho *in vitro*, we have demonstrated citronellal production from citral with NMN<sup>+</sup> as the cycling cofactor<sup>10</sup>. However, whether this redox cycle is well insulated from the numerous endogenous ADHs in *E. coli* crude lysates has not been tested. Based on previous studies, XenA can accept reducing power in the forms of both NADP(H) and reduced NMN<sup>+</sup> (NMNH)<sup>10</sup>, while endogenous ADHs greatly prefer NAD(P)H over NMNH, likely due to NMNH's truncated structure which lacks the adenosine moiety "handle" of NAD(P)H<sup>10,14-16</sup>. Thus, we hypothesized that when using GDH wild type (WT) to derive reducing power from glucose, both XenA and ADHs will receive electrons because NAD(P)<sup>+</sup> are the cycling cofactor (Figure 6B). On the other hand, when GDH Ortho is used with the supplementation of NMN<sup>+</sup>, only XenA will receive electrons because the stringent cofactor specificity of GDH Ortho allows it to only generate NMNH but not NAD(P)H<sup>10</sup> (Figure 6C).



**Figure 6: System design and reaction scheme for citronellal production.** (A) Crude *E. coli* lysates are used to form a two-part redox cofactor cycling system which facilitates the conversion of citral to citronellal through the action of *Pseudomonas putida* XenA. Redox cofactors are continuously regenerated by the glucose dehydrogenase, GDH, from *Bacillus subtilis*. Information gained from crude lysate-based biotransformation can be used to inform whole cell engineering. (B) When the wild type GDH is supplied, the native cofactors nicotinamide dinucleotide (phosphate), NAD(P)<sup>+</sup>, are reduced. This supplies the reducing power to both XenA and *E. coli*'s endogenous alcohol dehydrogenases (ADHs), resulting in the formation of alcohols (nerol, geraniol, citronellol) as the final products. (C) When a nicotinamide mononucleotide (NMN<sup>+</sup>)-specific GDH, GDH Ortho, is introduced, reducing power is only delivered to XenA, which can readily receive NMNH. Endogenous ADH activity is silenced since ADHs cannot receive NMNH. Therefore, citronellal, the target product, will accumulate.

To test this hypothesis, we performed the crude lysate-based biotransformation by pairing the XenA module with GDH WT or GDH Ortho module, respectively (Figure 7). GDH WT, GDH Ortho (on plasmids pEK101 or pLZ216, Table 9), and XenA (on plasmid pEK102) were individually overexpressed in *E. coli* strain MX102 (Table 9). The resulted cells were homogenized to yield three different lysates, which were subsequently mixed-and-matched (Figure 6A). The *E. coli* host, MX102 (Table 9), contains glycolysis knockouts ( $\Delta pgi$ ,  $\Delta zwf$ ,  $\Delta gntK$ ) to ensure that glucose is only metabolized by GDH, not the cell's central metabolism<sup>10</sup>.

When XenA and GDH WT lysates were mixed at a 1:1 mass ratio, and with the supplementation of no additional cofactor, 1 mM NAD<sup>+</sup>, or 1 mM NADP<sup>+</sup>, citronellal only transiently accumulated to a low level (<10 mg/L) before being rapidly consumed (Figure 7A). Importantly, when GDH Ortho was used in place of GDH WT, 89 mg/L of citronellal was produced in 4 hours with a 39% product purity (the percentage of citronellal in the sum of all products including citronellal, geraniol, nerol, and citronellol) when 1 mM of NMN<sup>+</sup> was supplemented (Figure 7A, B). When NMN<sup>+</sup> was omitted, citronellal production was not significant, demonstrating that aldehyde accumulation was indeed NMN<sup>+</sup>-dependent (Figure 7A). Remarkably, this was achieved without disrupting any aldehyde reductases or ADHs genes.



**Figure 7: NMN<sup>+</sup>-dependent orthogonal redox cofactor system enables citronellal accumulation.** Crude *Escherichia coli* lysates enriched with XenA and wild type *Bacillus subtilis* GDH (GDH WT) or engineered GDH (GDH Ortho) was used to convert citral to citronellal. (A) When GDH WT was used with XenA, citronellal only transiently accumulated to low levels. When GDH Ortho was used with XenA, citronellal was able to accumulate. (B) Product distribution of cycling reactions. The reactions were performed in Buffer A containing 4.5 mg/mL lysates, 1 mM of oxidized cofactor, and 500 mg/L citral. Reactions were incubated at 37 °C. Values are an average of at least three replicates, and the error bars represent one standard deviation.

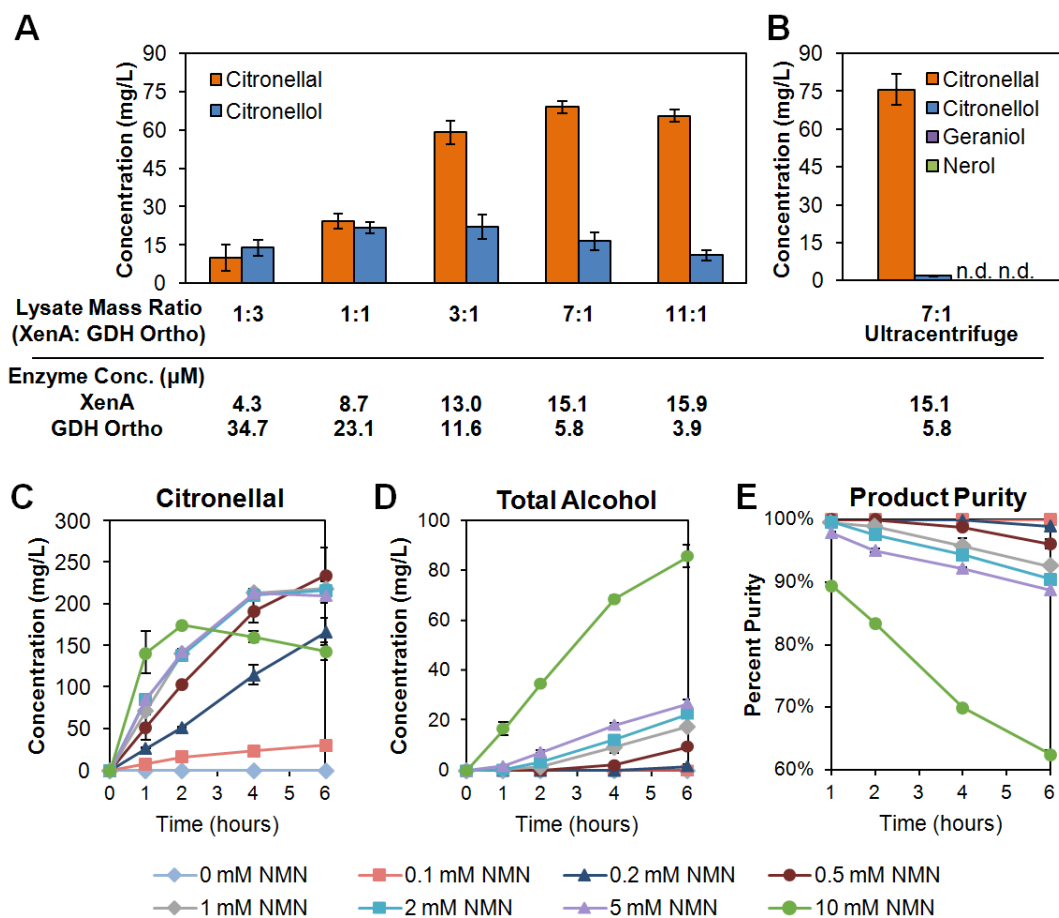
### 3.3.3 Optimizing the crude lysate-based biotransformation

Although the crude-lysate system was able to accumulate citronellal, key limitations existed (Figure 7B). First, the product purity was suboptimal (~60% of the products were still alcohols, with the major byproduct being citronellol). Second, the conversion was low (89 mg/L citronellal produced from 500 mg/L citral, a ~18% conversion).

We first focused on improving product purity. By running a short-term conversion for 1 hour, we used the crude lysate system as a tool to rapidly prototype various ratios of XenA:GDH Ortho lysates<sup>1,17,18</sup>, with the total amount of lysates held constant (Figure 8A). We quantified the active enzymes in crude lysates using specific activity assays and revealed that the 1:1 lysate mass ratio tested in the initial proof-of-concept (Figure 7) contained XenA at a much lower molar concentration than GDH Ortho (8.7  $\mu$ M XenA versus 23.1  $\mu$ M GDH Ortho in the reaction system), which led to the hypothesis that XenA might be limiting. Consistent with this hypothesis, increasing the proportion of XenA resulted in increased citronellal production and product purity. The best condition with 7:1 (XenA:GDH Ortho) lysate mass ratio (or 15.1  $\mu$ M XenA and 5.8  $\mu$ M GDH Ortho) produced 69 mg/L of citronellal with 16 mg/L citronellol and undetectable levels of geraniol and nerol (Figure 8A), which corresponds to a ~78% product purity, a two-fold improvement compared to the 39% product purity initially obtained using 1:1 ratio (Figure 7B). Citronellal production began to decline when XenA:GDH Ortho was further increased, likely because GDH Ortho became limiting (Figure 8A).

When we optimized the lysate preparation to include an ultracentrifugation step, the productivity and purity was further improved (Figure 8B), with 75 mg/L citronellal produced in 1 hour with a 98% product purity. Alcohol byproduct formation was minimized, with < 2 mg/L citronellol and undetectable levels of geraniol and nerol produced (Figure 8B). However, this high purity could

not be maintained as the conversion goes beyond 1 hour (Figure 8C, D, E, grey line with 1 mM NMN<sup>+</sup>), which motivated further optimization.



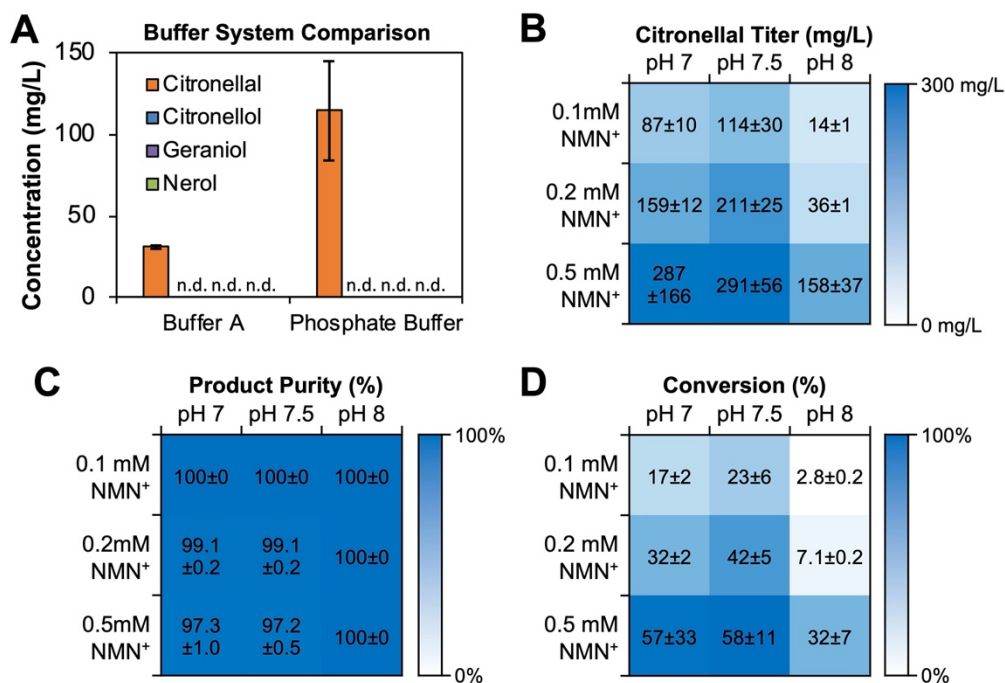
**Figure 8: Optimizing crude lysate conditions for citronellal production in Buffer A.** (A) Increasing the relative amount of XenA- to GDH Ortho-enriched *E. coli* crude lysate enabled increased citronellal production and specificity. The molar concentration of each enzyme in the final reaction was calculated for each mass ratio. (B) Further clarifying the lysate with an ultracentrifuge step further improved the performance, yielding a >98% pure production of citronellal. (C-E) Varying NMN<sup>+</sup> supplementation in reactions containing ultracentrifuged lysates at a 7:1 XenA:GDH Ortho mass ratio. Product purity was determined as a percentage of citronellal in the total amount of products formed (citronellal, citronellol, nerol, and geraniol). The reactions were performed in Buffer A containing 4.5 mg/mL lysates, 1 mM of NMN<sup>+</sup> (unless stated otherwise), and 500 mg/L citral. The reactions were incubated at 37 °C for 1 hour unless stated otherwise. Values are an average of at least three replicates, and the error bars represent one standard deviation. n.d., not detected.

Next, we examined the effect of NMN<sup>+</sup> concentration (Figure 8C, D, E). Increasing NMN<sup>+</sup> supplementation from 1 mM to 2, 5, or 10 mM did not improve final citronellal titer or product



purity because significant amount of alcohols (citronellol, nerol, and geraniol) were produced (Figure 8C, D, E). Further investigation is needed to identify the cause of increased alcohols, but one possible explanation could be that ADHs may be able to utilize NMNH only at a very high concentration. Although this NMNH-dependent ADH activity is much slower compared to the NMNH-dependent ER activity, at later time points, the former became significant. On the other hand, decreasing NMN<sup>+</sup> supplementation to 0.1, 0.2, and 0.5 mM enhanced the product purity (Figure 8E). Notably, a 0.1mM NMN<sup>+</sup> supplementation yielded a 100% product purity with non-detectable levels of alcohol byproducts throughout the entire conversion period. However, the productivity was slow which led to a low final titer of ~30 mg/L citronellal before the reaction plateaued at 6 hours (Figure 8C, D, E).

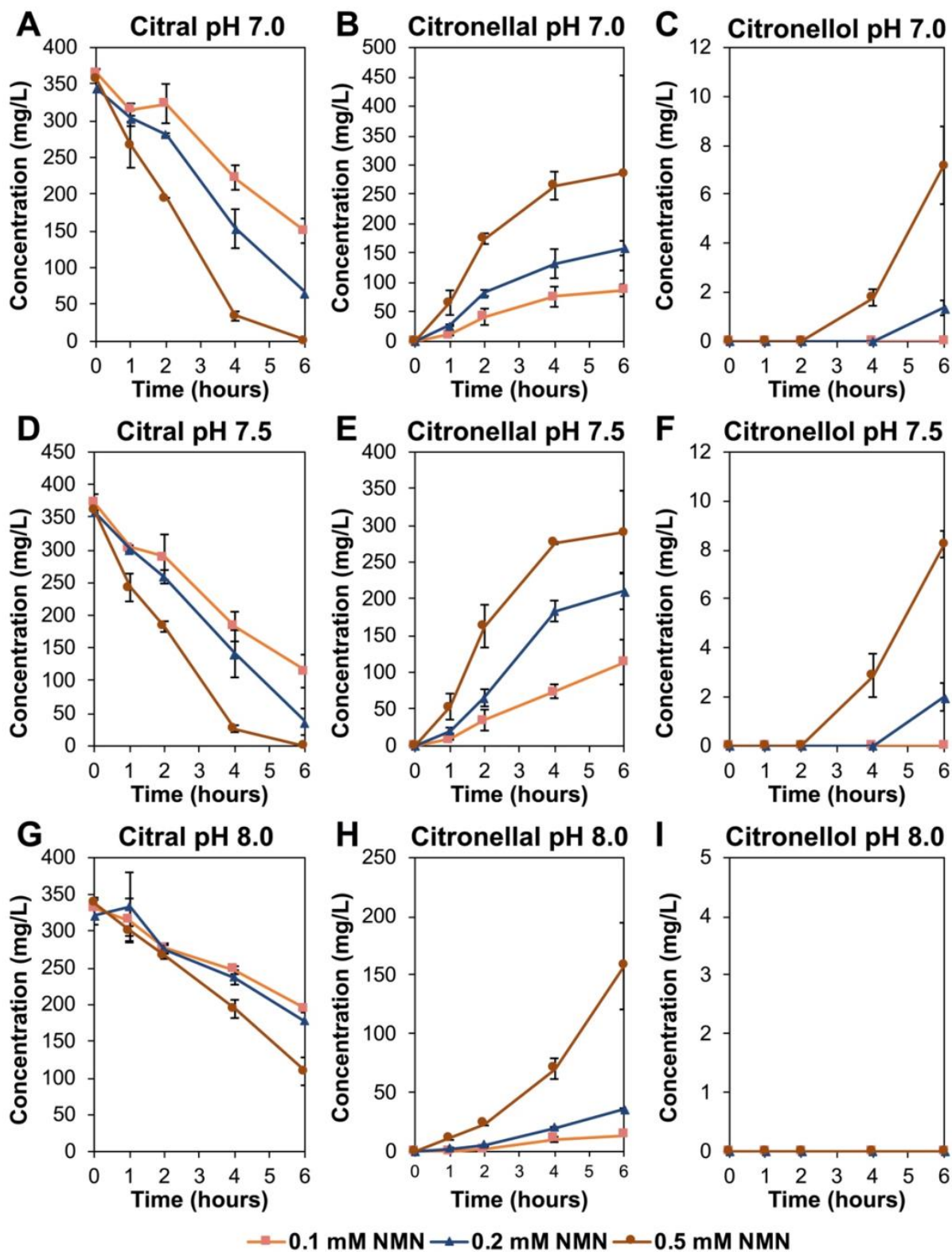
We next focused on improving the final citronellal titer and percent conversion (amount of citronellal produced over that of citral supplied), without sacrificing product purity. First, by switching the buffer system in the reaction from Buffer A to phosphate buffer, we increased the citronellal titer by roughly 4-fold, reaching ~114 mg/L, while still maintaining 100% product purity (Figure 9A). Second, we optimized the phosphate buffer conditions by varying both NMN<sup>+</sup> concentrations and pH simultaneously (Figure 9B, C, D). In light of the results mentioned above, NMN<sup>+</sup> titration focused on the lower concentration range.



**Figure 9: Crude lysate-based biotransformation in potassium phosphate buffer (A)** Performing the crude lysate-based biotransformations in phosphate buffer at pH 7.5 increased citronellal production over Buffer A without producing alcohol byproducts after 6 hours. Reactions were supplemented with 0.1 mM NMN<sup>+</sup>. (B-D) Optimizing pH and NMN<sup>+</sup> supplementation for citronellal production, product purity, and conversion. Product purity was determined as a percentage of citronellal in the total amount of products formed (citronellal, citronellol, nerol, and geraniol). Conversion was determined as a percentage of citronellal produced from the 500 mg/L of citral supplied. Phosphate buffered reactions contained 200 mM potassium phosphate, 200 mM sodium chloride, 200 mM D-glucose, 0.1-0.5 mM NMN<sup>+</sup>, and 500 mg/L citral. All reactions contained 4.5 mg/mL ultracentrifuged lysates at a 7:1 XenA:GDH Ortho mass ratio and were incubated at 37 °C for 6 hours. Values are an average of at least three replicates, and the error bars represent one standard deviation.

We identified the best condition at 0.5 mM NMN<sup>+</sup> and pH 7.5 in phosphate buffer (with ultracentrifuged lysates, and an enzyme loading of 15.1 μM XenA and 5.8 μM GDH Ortho, as previously mentioned). In this condition, ~292 mg/L citronellal was produced, resulting in ~60% conversion. Product purity was ~97%, with < 9 mg/L citronellol and undetectable levels of geraniol and nerol formed (Figure 10). In our previous work using purified GDH and XenA at a similar enzyme loading, we achieved ~75% conversion from citral to citronellal using NMN<sup>+</sup><sup>10</sup>. Alcohol byproducts were not produced in that process because ADHs were removed during protein

purification. Using crude lysates here, we were able to recapitulate the high purity and a comparable conversion, while bypassing the need to eliminate any ADHs or purify any proteins.

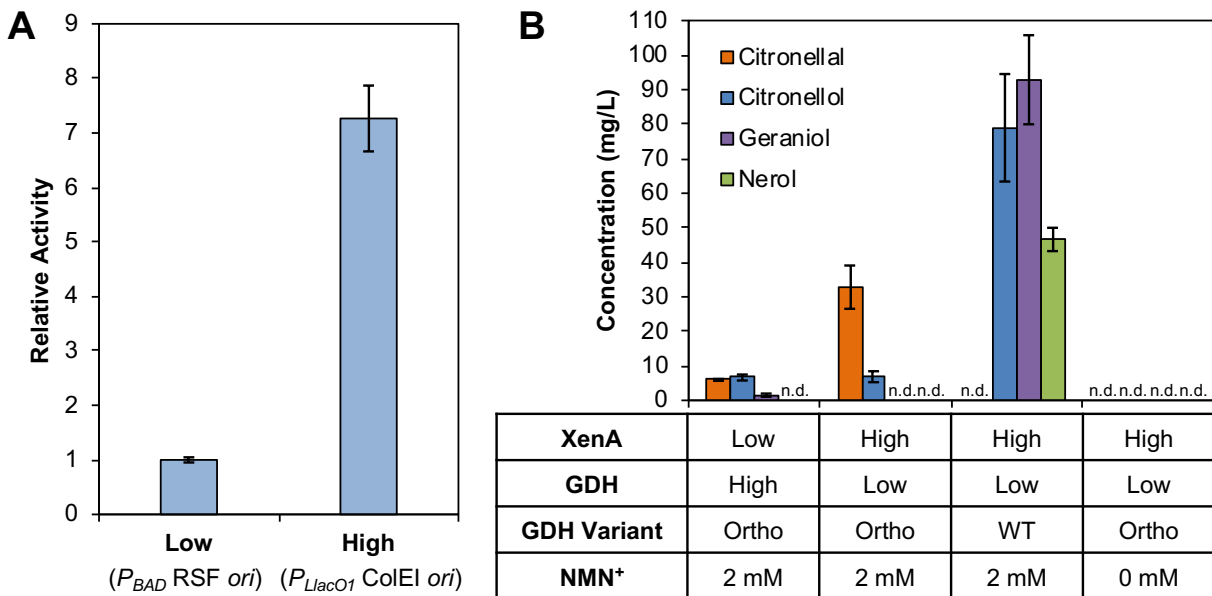


**Figure 10** Time-course of citral biotransformation and optimization in Phosphate Buffer (A-I) Citral consumption and product formation with varying NMN+ supplementation and buffer pH. Nerol and geraniol were not detected at any condition tested. Reactions were performed in assay

buffer containing 200 mM potassium phosphate at pH 7.0, 7.5, or 8.0, 200 mM NaCl, 200 mM D-glucose, 0.1-0.5 mM of oxidized cofactor, and 500 mg/L citral. Lysates were mixed at a 7:1 XenA:GDH Ortho mass ratio. Lysate was spiked into concentrated assay buffer to a final concentration of 4.5 mg/mL of protein in solution. Reactions were incubated at 37 °C without shaking. A detailed method can be found in the Methods section. Values are an average of at least three replicates, and error bars represent one standard deviation.

### 3.3.4 Citronellal production in *E. coli* whole cells

We next examined the ability of the orthogonal cofactor system to produce citronellal *in vivo* in *E. coli* whole cells. Previously, crude-lysate based biotransformation has been shown as a powerful tool to prototype and inform pathway design in whole-cells<sup>1,3,19</sup>. Here, we demonstrated the benefit of maintaining a high XenA:GDH Ortho ratio is translatable from *in vitro* to *in vivo*. To modulate the XenA:GDH ratio, XenA and GDH were expressed in strain MX102 on two, multicopy plasmids with different copy numbers and promoters ( $P_{BAD}$  RSF *ori* versus  $P_{LlacO1}$  Cole1 *ori*). The relative expression level of the two plasmids was determined by measuring GDH Ortho's NMN<sup>+</sup> reducing activity in crude lysate derived from the whole-cells (Figure 11A). When GDH Ortho was expressed on the  $P_{LlacO1}$  Cole1 *ori* vector (pLZ216), the activity was ~7-fold higher than on the  $P_{BAD}$  RSF *ori* vector (pSM106) (Figure 11A). Therefore, the  $P_{BAD}$  RSF *ori* or  $P_{LlacO1}$  Cole1 *ori* vectors were designated as the low and high expression vectors, respectively, for *in vivo* biotransformation.



**Figure 11: Orthogonal cofactor system enables specific aldehyde accumulation in *E. coli* whole cells**

(A) Relative expression levels of  $P_{BAD}$  RSF *ori* and  $P_{LlacO1}$  ColE1 *ori* vectors as measured by the levels of GDH Ortho activity in crude lysate derived from the co-expressed whole cells. The results indicate that  $P_{LlacO1}$  ColE1 *ori* and  $P_{BAD}$  RSF *ori* vectors can be treated as a high and low expression vectors, respectively. (B) With GDH Ortho, citronellal accumulation was achieved. High XenA expression relative to GDH Ortho resulted in higher citronellal productivity and product purity. With GDH WT, only alcohol byproducts were produced. When NMN<sup>+</sup> was not supplemented to cells expressing GDH Ortho, no product accumulation was observed. Whole-cell biotransformation was performed with resting *E. coli* cells at an OD600 of 10 in 100 mM potassium phosphate at pH 7.5, 200 mM D-glucose, 2 mM NMN<sup>+</sup>, and 500 mg/L citral, at 30 °C for 3 hours while shaking at 250 r.p.m. Values are an average of at least three replicates, and the error bars represent one standard deviation. n.d., not detected.

When resting *E. coli* whole cells were supplied with high XenA expression (on plasmid pEK102, Table 9), with low GDH Ortho expression (on plasmid pSM106), and a glucose facilitator, *Zymomonas mobilis* Glf (on plasmid pSM109) which transports glucose into the cell, 33 mg/L of citronellal was produced with a product purity of 83% (Figure 11B). Conversely, pairing high GDH Ortho expression with low XenA expression (on plasmids pLZ216 and pLZ217, respectively) caused a significant decrease in citronellal production (6 mg/L), and a poor product purity of 42%. In both conditions, the major byproduct citronellol was formed at 7 mg/L. When GDH Ortho was not supplied with NMN<sup>+</sup>, citronellal production was not observed (Figure 11B).

Expectedly, when GDH WT was supplied (on plasmid pSM107), endogenous ADH activity completely consumed citral and citronellal, resulting in the production of only geraniol, nerol, and citronellol (Figure 11B). Ongoing work in our lab is focused on further optimizing the whole-cell system.

### **3.4 Conclusions**

This work demonstrates the use of an NMN<sup>+</sup>-dependent redox cofactor system as a facile method to develop biocatalysts for aldehyde production. As a proof-of-concept, we achieved effective conversion of citral to citronellal (both are aldehydes) by silencing the highly active ADHs in both *E. coli* crude lysates and whole cells. Notably, we decreased the level of alcohol byproducts in crude lysate-based biotransformation from 60% to essentially zero by only optimizing the components in the NMN<sup>+</sup> redox loop and without relying on information about the host's metabolic background. The ease in optimization highlights the advantage of an insulated, orthogonal metabolic system, which may be particularly beneficial in engineering non-model organisms without well understood metabolisms. As more enzymes are engineered to efficiently utilize NMN(H), the methods established here may be readily adapted to produce various chemicals.

The orthogonal redox cofactor system is highly complementary to the commonly used host engineering methods. For example, while the orthogonal redox cofactor system bypassed the laborious process of knocking out the numerous, highly promiscuous ADHs and aldehyde reductases<sup>20,21</sup>, efforts to genetically eliminate the fewer, more substrate specific, and more easily identifiable competing enzymes that consume citral and citronellal (namely aldehyde dehydrogenases and citral lyase) may further improve biotransformation performance<sup>11,22</sup>.

### 3.5 References

- [1] Karim, A. S.; Dudley, Q. M.; Juminaga, A.; Yuan, Y.; Crowe, S.A.; Heggestad, J. T.; Garg, S.; Abdalla, T.; Grubbe, W. S.; Rasor, B. J.; Coar, D. N.; Torculas, M.; Krein, M.; Liew, F.; Quattlebaum, A.; Jensen, R. O.; Stuart, J. A.; Simpson, S. D.; Köpke, M.; Jewett, M. C. *In vitro* Prototyping and Rapid Optimization of Biosynthetic Enzymes for Cell Design. *Nat. Chem. Biol.* **2020**, *16*, 912-919.
- [2] Dudley, Q. M.; Nash, C. J.; Jewett, M. C. Cell-free Biosynthesis of Limonene Using Enzyme-Enriched *Escherichia coli* Lysates. *Synth. Biol.* **2019**, *4*, ysz003.
- [3] Karim, A. S.; Jewett, M. C. A Cell-Free Framework for Rapid Biosynthetic Pathway Prototyping and Enzyme Discovery. *Metab. Eng.* **2016**, *36*, 116-126.
- [4] Kay, J. E.; Jewett, M. C. Lysate of Engineered *Escherichia coli* Supports High-Level Conversion of Glucose to 2, 3-butanediol. *Metab. Eng.* **2015**, *32*, 133-142.
- [5] Kay, J. E.; Jewett, M. C. A Cell-Free System for Production of 2,3-Butanediol is Robust to Growth-Toxic Compounds. *Metab. Eng. Commun.* **2020**, *10*, e00114.
- [6] Honda, K.; Kimura, K.; Ninh, P. H.; Taniguchi, H.; Okano, K.; Ohtake, H. *In vitro* Bioconversion of Chitin to Pyruvate with Thermophilic Enzymes. *J. Biosci. Bioeng.* **2017**, *124*, 296-301.
- [7] Wang, W.; Liu, M.; You, C.; Li, Z.; Zhang, Y. H. P. ATP-Free Biosynthesis of a High-Energy Phosphate Metabolite Fructose 1,6-diphosphate by *in vitro* Metabolic Engineering. *Metab. Eng.* **2017**, *42*, 168-174.
- [8] Kunjapur, A. M.; Tarasova, Y.; Prather, K. L. J. Synthesis and Accumulation of Aromatic Aldehydes in an Engineered Strain of *Escherichia coli*. *J. Am. Chem. Soc.* **2014**, *136*, 11644-11654.
- [9] Rodriguez, G. M.; Atsumi, S. Toward Aldehyde and Alkane Production by Removing Aldehyde Reductase Activity in *Escherichia coli*. *Metab. Eng.* **2014**, *25*, 227-237.
- [10] Black, W. B.; Zhang, L.; Mak, W. S.; Maxel, S.; Cui, Y.; King, E.; Fong, B.; Sanchez Martinez, A.; Siegel, J. B.; Li, H. Engineering a Nicotinamide Mononucleotide Redox Cofactor System for Biocatalysis. *Nat. Chem. Biol.* **2020**, *16*, 87-94.
- [11] Hall, M.; Hauer, B.; Stuermer, R.; Kroutil, W.; Faber, K. Asymmetric Whole-Cell Bioreduction of an  $\alpha,\beta$ -Unsaturated Aldehyde (Citral): Competing prim-Alcohol Dehydrogenase and C-C Lyase Activities. *Tetrahedron: Asymmetry.* **2006**, *17*, 3058-3062.
- [12] Mahalwal, V. S.; Ali, M. Volatile Constituents of *Cymbopogon nardus* (Linn.) Rendle. *Flavour Fragrance J.* **2003**, *18*, 73-76.



- [13] Paul, C. E.; Gargiulo, S.; Opperman, D. J.; Lavandera, I.; Gotor-Fernández, V.; Gotor, V.; Taglieber, A.; Arends, I. W. C. E.; Hollmann, F. Mimicking Nature: Synthetic Nicotinamide Cofactors for C=C Bioreduction Using Enoate Reductases. *Org. Lett.* **2013**, *15*, 180-183.
- [14] Sicsic, S.; Durand, P.; Langrene, S.; le Goffic, F. A New Approach of Using Cofactor Dependent Enzymes: Example of Alcohol Dehydrogenase. *FEBS Lett.* **1984**, *6*, 321-324.
- [15] Campbell, E.; Meredith, M.; Minter, S. D.; Banta, S. Enzymatic Biofuel Cells Utilizing a Biomimetic Cofactor. *Chem. Commun.* **2012**, *48*, 1898-1900.
- [16] Josa-Culleré, L.; Kahdenperä, A. S. K.; Ribaucourt, A.; Höfler, G. T.; Gargiulo, S.; Liu, Y.; Xu, J.; Cassidy, J.; Paradisi, F.; Opperman, D. J.; Hollmann, F.; Paul, C. E. Synthetic Biomimetic Coenzymes and Alcohol Dehydrogenases for Asymmetric Catalysis. *Catalysis.* **2019**, *9*, No. 207.
- [17] Dudley, Q. M.; Anderson, K. C.; Jewett, M. C. Cell-Free Mixing of *Escherichia coli* Crude Extracts to Prototype and Rationally Engineer High-Titer Mevalonate Synthesis. *ACS Synth. Biol.* **2016**, *5*, 1578-1588.
- [18] Liu, Z.; Zhang, Y.; Jia, X.; Hu, M.; Deng, Z.; Xu, Y.; Liu, T. *In vitro* Reconstitution and Optimization of the Entire Pathway to Convert Glucose to Fatty Acid. *ACS Synth. Biol.* **2017**, *6*, 701-709.
- [19] Kelwick, R.; Ricci, L.; Chee, S. M.; Bell, D.; Webb, A. J.; Freemont, P. S. Cell-Free Prototyping Strategies for Enhancing the Sustainable Production of Polyhydroxyalkanoates Bioplastics. *Synth. Biol.* **2018**, *3*, ysy016.
- [20] Zhou, Y. J.; Buijs, N. A.; Zhu, Z.; Gomez, D. O.; Boonsombuti, A.; Siewers, V.; and Nielsen, J. Harnessing Yeast Peroxisomes for Biosynthesis of Fatty-Acid-Derived Biofuels and Chemicals with Relieved Side-Pathway Competition. *J. Am. Chem. Soc.* **2016**, *138*, 15368-15377.
- [21] Lau, Y. H.; Giessen, T. W.; Altenburg, W. J.; Silver, P. A. Prokaryotic Nanocompartments Form Synthetic Organelles in a Eukaryote. *Nat. Commun.* **2018**, *9*, No. 1311.
- [22] Esmaeili, A.; Rohany, S.; Safaiyan, S. Biotransformation of Citral by Free and Immobilized *Saccharomyces cerevisiae*. *Chem. Nat. Compd.* **2012**, *48*, 322-324.

## **Chapter 4**

# **Metabolic engineering of *Escherichia coli* for optimized biosynthesis of nicotinamide mononucleotide, a noncanonical redox cofactor**

The text, data, and figures in this chapter are adapted from a previously published manuscript. This work was published under Creative Commons license <http://creativecommons.org/licenses/by/4.0/>

Black, W. B., Aspacio, D., Bever, D.; King, E.; Zhang, L.; Li, H., “Metabolic Engineering of *Escherichia coli* for Optimized Biosynthesis of Nicotinamide Mononucleotide, a Noncanonical Redox Cofactor”, *Microbial Cell Factories*, 19, No. 150, 2020.

## 4.1 Introduction

As discussed in Chapter 3, cell free biosynthesis has emerged as a prominent tool in the production of renewable chemicals, fuels, and pharmaceuticals<sup>1-3</sup>. Cell-free systems, both purified enzyme-based and crude lysate-based, have unique advantages over whole-cell biotransformation systems. For example, environmental conditions can be varied within a wider range to favor product formation<sup>4</sup>; transportation issues across cell membranes are eliminated<sup>5</sup>; toxic compounds can be produced at much higher titers than the cell's tolerance limit<sup>6</sup>. Because components of the biosynthetic pathways can be readily mix-and-matched in a combinatorial fashion, cell-free biosynthesis has also been used as a high-throughput prototyping tool to inform pathway design in whole-cell biosynthesis<sup>7,8</sup>.

Cofactors such as nicotinamide adenine dinucleotide (phosphate) (NAD(P)<sup>+</sup>) are essential reagents in biosynthesis. In cell-free biosynthesis, cofactors are freed from the life-sustaining roles they play *in vivo*. Therefore, true opportunities exist to significantly expand the toolkit of cofactors beyond what is offered by Nature to achieve desirable goals in biocatalysis. For example, cheaper noncanonical cofactors, such as 3-carbamoyl-1-phenethylpyridin-1-ium chloride (P2NA<sup>+</sup>)<sup>9,10</sup>, have been used in purified enzyme-based redox catalysis to increase economic viability. Noncanonical cofactors with stronger electron-accepting capability, such as 3-acetylpyridine adenine dinucleotide<sup>11,12</sup>, have been used to drive the thermodynamically unfavorable reactions of alcohol oxidation.

As described in Chapter 2, we recently developed a cell-free biosynthesis platform surrounding the noncanonical redox cofactor nicotinamide mononucleotide (NMN<sup>+</sup>)<sup>13</sup>. NMN<sup>+</sup> was enzymatically cycled by pairing an engineered glucose dehydrogenase from *Bacillus subtilis* with a variety of enzymes to reduce activated C=C double bonds, activated C≡C triple bonds, nitro

groups, and to supply electrons to a cytochrome P450. This system demonstrated robust temporal stability over 96 hours and a total turnover number of ~39,000. Because of its smaller size, NMN<sup>+</sup> has also been shown to provide a faster mass transfer rate in enzymatic biofuel cells<sup>14</sup>.

Compared to other noncanonical cofactors which are made through chemical synthesis<sup>15-17</sup>, NMN<sup>+</sup> is particularly suited for fully renewable biomanufacturing processes because it is accessible through biosynthesis<sup>18-20</sup>. This feature is especially desirable in crude lysate-based cell-free biosynthesis and whole-cell biosynthesis, where NMN<sup>+</sup> produced in the cells does not need to be purified or exogenously supplied, and it can be directly used for downstream biocatalysis. Importantly, since we demonstrated its successful application in *E. coli* whole cells to enable orthogonal electron delivery<sup>13</sup>, NMN<sup>+</sup> can potentially be utilized in crude lysate-based biosynthesis to control the flow of reducing power and mitigate side reactions based on the same principles<sup>13,21</sup>.

Although NMN<sup>+</sup> has been biosynthesized previously in metabolically engineered *E. coli*<sup>13,19</sup>, further improving NMN<sup>+</sup> production requires more efficient pathways and a better understanding of its metabolism in the host. While previous efforts have primarily used the nicotinamide phosphoribosyltransferases, NadV, to convert nicotinamide to NMN<sup>+</sup>, only a few NadV homologs have been tested and many other NadV-independent pathways for NMN<sup>+</sup> biosynthesis remain unexplored. Furthermore, whether and how NMN<sup>+</sup> accumulation impacts cell physiology remains largely unknown. In this work, we developed a growth-based screening platform to identify pathways for efficient NMN<sup>+</sup> generation *in vivo*. This platform was designed by making NMN<sup>+</sup> an essential precursor in NAD<sup>+</sup> biosynthesis in engineered *E. coli*. We used this platform to demonstrate that NMN<sup>+</sup> synthetase, NadE\* from *Francisella tularensis*, effectively mediates an additional route for NMN<sup>+</sup> biosynthesis in *E. coli*. We also bioprospected for NadV

homologs based on comparative genomic data<sup>18</sup>, and we tested their ability to produce NMN<sup>+</sup> in combination with *F. tularensis* NadE\*. The best NMN<sup>+</sup> producing strain accumulated ~1.5 mM of intracellular NMN<sup>+</sup> while overexpressing *F. tularensis* NadE\* and *Ralstonia solanacearum* NadV simultaneously, as well as harboring a disruption in the gene encoding NMN<sup>+</sup> amidohydrolase, PncC. Although our current highest NMN<sup>+</sup> production titer did not cause growth inhibition, we observed inhibitory effect when very high concentrations of NMN<sup>+</sup> was fed to the cells through a heterologous NMN<sup>+</sup> transporter. Interestingly, we showed that this inhibitory effect can be alleviated when the transcriptional regulator of NAD<sup>+</sup> biosynthesis, NadR, was disrupted. Together, these results provide insight for future metabolic engineering efforts aiming to further improve NMN<sup>+</sup> biosynthesis. Compared to NAD(P)<sup>+</sup>, NMN<sup>+</sup> has been suggested to be less expensive<sup>22</sup>. The development of an efficient NMN<sup>+</sup> biosynthetic route from even cheaper precursors may further increase the economic viability of NMN<sup>+</sup>-dependent biotransformation processes.

## **4.2 Materials and methods**

### **4.2.1 Plasmid and Strain Construction**

All molecular cloning was performed in *E. coli* XL1-Blue cells (Stratagene). A summary of strains and plasmids used in this study can be found in Table 11. Plasmids were assembled by Gibson Isothermal DNA Assembly<sup>38</sup>. Polymerase chain reaction (PCR) fragments were generated using PrimeSTAR Max DNA Polymerase (TaKaRa). The method for plasmid construction is described below.

The *yqhD* gene was isolated from *E. coli* BL21 chromosomal DNA by PCR. The resulting PCR fragment was gel purified and assembled into a ColE1 *ori*, AmpR vector backbone by Gibson isothermal DNA assembly method. We used the *yqhD*-harboring plasmid (pWB301) as a control

vector in the growth rescue experiments, because it expresses a similar sized-protein to the NMN<sup>+</sup>-producing enzymes using the same promoter, and hence may cause similar growth burden. The gene product of *yqhD* has unrelated function to NMN<sup>+</sup> biosynthesis.

*E. coli pnuC*, *S. enterica nadR*, *S. cerevisiae NRK1*, *Synechocystis sp nadV*, and *S. elongatus nadV* were isolated by PCR from their respective chromosomal DNA. *F. tularensis nadE\**, *R. solanacearum nadV*, and *H. ducreyi nadV* genes were amplified from *E. coli* codon optimized synthesized DNA templates and assembled as described above.

*S. enterica PnuC\** is generated by site-directed mutagenesis based on the wild type *S. enterica pnuC* gene<sup>30</sup>. The *S. enterica pnuC* gene was isolated by PCR from chromosomal DNA and assembled as discussed above. To perform the KA insertion, which has been shown to enable NMN<sup>+</sup> transport<sup>30</sup>, a sequence of AAAGCA was inserted directly after the 321 base pair. This resulted in the insertion of a lysine and an alanine residue at the 108 and 109 residue positions. The insertion was introduced by PCR. The subsequent mutant PCR fragments were assembled as discussed above. To generate multi-gene plasmids, the genes were inserted sequentially with a ribosome binding site preceding each gene in the synthetic operon.

**Table 11: Strains and Plasmids Used in Chapter 4**

<b>Strains</b>	<b>Description</b>	<b>Reference</b>
XL-1 Blue	Cloning strain	Stratagene
BW25113	<i>E. coli</i> $\Delta(araD-araB)567$ , $\Delta lacZ4787(::rrnB-3)$ , $\lambda^-$ , <i>rph-1</i> ,	Invitrogen
JW2670-1	$\Delta(rhaD-rhaB)568$ , <i>hsdR514</i> BW25113 $\Delta pncC::kan$	Yale <i>E. coli</i> Genetic Stock Center
MX101	BW25113 $\Delta pncC$ $\Delta nadR::kan$	[13]
72c	<i>E. coli</i> F <sup>-</sup> , <i>lacZ4</i> , <i>nadD72(ts,Fs)</i> , $\lambda^-$ , <i>argG75</i>	[28]

<b>Plasmids</b>	<b>Descriptions</b>	<b>Reference</b>
pWB203	<i>P<sub>LlacOI</sub>::Ft nadE - Ft nadV</i> , <i>ColE1 ori</i> , <i>Amp<sup>R</sup></i>	[13]
pWB301	<i>P<sub>LlacOI</sub>::Ec yqhD</i> , <i>ColE1 ori</i> , <i>Amp<sup>R</sup></i>	This study
pWB302	<i>P<sub>LlacOI</sub>::Se pnuC* KA</i> , <i>ColE1 ori</i> , <i>Amp<sup>R</sup></i>	This study
pWB303	<i>P<sub>LlacOI</sub>::Ft nadE</i> , <i>ColE1 ori</i> , <i>Amp<sup>R</sup></i>	This study
pWB304	<i>P<sub>LlacOI</sub>::Ec pnuC - Se nadR</i> , <i>ColE1 ori</i> , <i>Amp<sup>R</sup></i>	This study
pWB305	<i>P<sub>LlacOI</sub>::Ec pnuC - Sc NRK1</i> , <i>ColE1 ori</i> , <i>Amp<sup>R</sup></i>	This study
pWB306	<i>P<sub>LlacOI</sub>::Hd nadV</i> , <i>ColE1 ori</i> , <i>Amp<sup>R</sup></i>	This study
pWB307	<i>P<sub>LlacOI</sub>::Rs nadV</i> , <i>ColE1 ori</i> , <i>Amp<sup>R</sup></i>	This study
pWB308	<i>P<sub>LlacOI</sub>::Ss nadV</i> , <i>ColE1 ori</i> , <i>Amp<sup>R</sup></i>	This study
pWB309	<i>P<sub>LlacOI</sub>::SynE nadV</i> , <i>ColE1 ori</i> , <i>Amp<sup>R</sup></i>	This study
pDB102	<i>P<sub>LlacOI</sub>::Ft nadE - Rs nadV</i> , <i>ColE1 ori</i> , <i>Amp<sup>R</sup></i>	This study
pDB103	<i>P<sub>LlacOI</sub>::Ft nadE - Ss nadV</i> , <i>ColE1 ori</i> , <i>Amp<sup>R</sup></i>	This study
pDB104	<i>P<sub>LlacOI</sub>::Ft nadE - SynE nadV</i> , <i>ColE1 ori</i> , <i>Amp<sup>R</sup></i>	This study
pLZ301	<i>P<sub>LlacOI</sub>::Ft nadE - Hd nadV</i> , <i>ColE1 ori</i> , <i>Amp<sup>R</sup></i>	This study

Abbreviations indicate source of genes: *Ec*, *Escherichia coli*; *Se*, *Salmonella enterica*; *Ft*, *Francisella tularensis*; *Sc*, *Saccharomyces cerevisiae*; *Rs*, *Ralstonia solanacearum*; *Ss*, *Synechocystis sp.* PCC 6803; *SynE*, *Synechococcus elongatus* PCC 7942; *Hd*, *Haemophilus ducreyi*. *Se pnuC\* KA* contains mutations compared to the wild type sequence (see section 4.2.1).

#### 4.2.2 Growth-based Screening Platform

Plasmids (selected from pWB301-305) were transformed into *E. coli* strains BW25113 and 72c<sup>28</sup> using the Mix & Go *E. coli* Transformation Kit (Zymo Research).

Overnight cultures were grown in LB medium supplemented with 2 g/L D-glucose, 0.1 mM IPTG, appropriate antibiotics in test tubes at 30 °C while shaking at 250 r.p.m. for 16 hours. For the growth assay, cells were cultured in 1 mL of LB medium supplemented with 2 g/L D-glucose, 0.1 mM isopropyl- $\beta$ -D-thiogalactopyranoside (IPTG), appropriate antibiotics, and 200  $\mu$ M of feeding compound, if applicable, in a 2 mL deep-well plate, with square wells, sealed with air permeable film. The medium was inoculated with 1% v/v overnight cultures. Cultures were grown at 42 °C while shaking at 250 r.p.m.. Cell growth was monitored by measuring optical density at 600 nm. When applicable, media contained 100 mg/L ampicillin to maintain the plasmids.

#### **4.2.3 Intracellular NMN<sup>+</sup> Generation and Quantification**

NMN<sup>+</sup> generation and quantification were performed as previously reported<sup>13</sup>. Briefly, plasmids (selected from pWB203, pDB102-104, and pLZ301) were transformed into *E. coli* strains BW25113 and JW2670-1 ( $\Delta pncC$ ) as described previously. Overnight cultures were grown in 2xYT medium containing 0.1 mM IPTG, 2 g/L D-glucose, and appropriate antibiotics for 12 hours at 30°C at 250 rotations per minute (r.p.m.). To cultivate cells for nucleotide analysis, cells were grown in a 50 mL conical tube containing 10 mL of 2xYT media supplemented with 0.5 mM IPTG, 1 mM nicotinamide, and appropriate antibiotics. Cultures were inoculated with 1% v/v overnight culture. Tubes were incubated at 30 °C with shaking at 250 r.p.m. for 4 hours. All media contained 100 mg/L ampicillin to maintain the plasmids.

Cells were processed as previously reported<sup>13</sup>. Briefly, 1 mL of cell culture was pelleted, washed with 1 mL of deionized water, and lysed by resuspension in 1 mL of 95 °C 1% formic acid containing 1  $\mu$ M of 1-methylnicotinamide as an internal standard. Lysates were quenched in an ice bath before pelleting cell debris. Supernatants were run on a Waters ACQUITY Ultra



Performance Liquid Chromatograph with a Waters ACQUITY UPLC CSH C18 column (1.7  $\mu$ M x 2.1 mm x 50mm). Mobile phases used for separation were (A) water with 2% acetonitrile and 0.2% acetic acid and (B) acetonitrile with 0.2% acetic acid. MS/MS detection was performed by a Waters Micromass Quattro Premier XE Mass Spectrometer. The detailed UPLC and MS parameters were reported previously<sup>13</sup>. Values from LC-MS/MS were correlated back to intracellular concentration using the number of cells per unit OD<sub>600nm</sub> in 1 mL of culture =  $1 \times 10^9$  and the intracellular volume of an *E. coli* cell as  $1 \times 10^{-15}$  L per cell<sup>39</sup>.

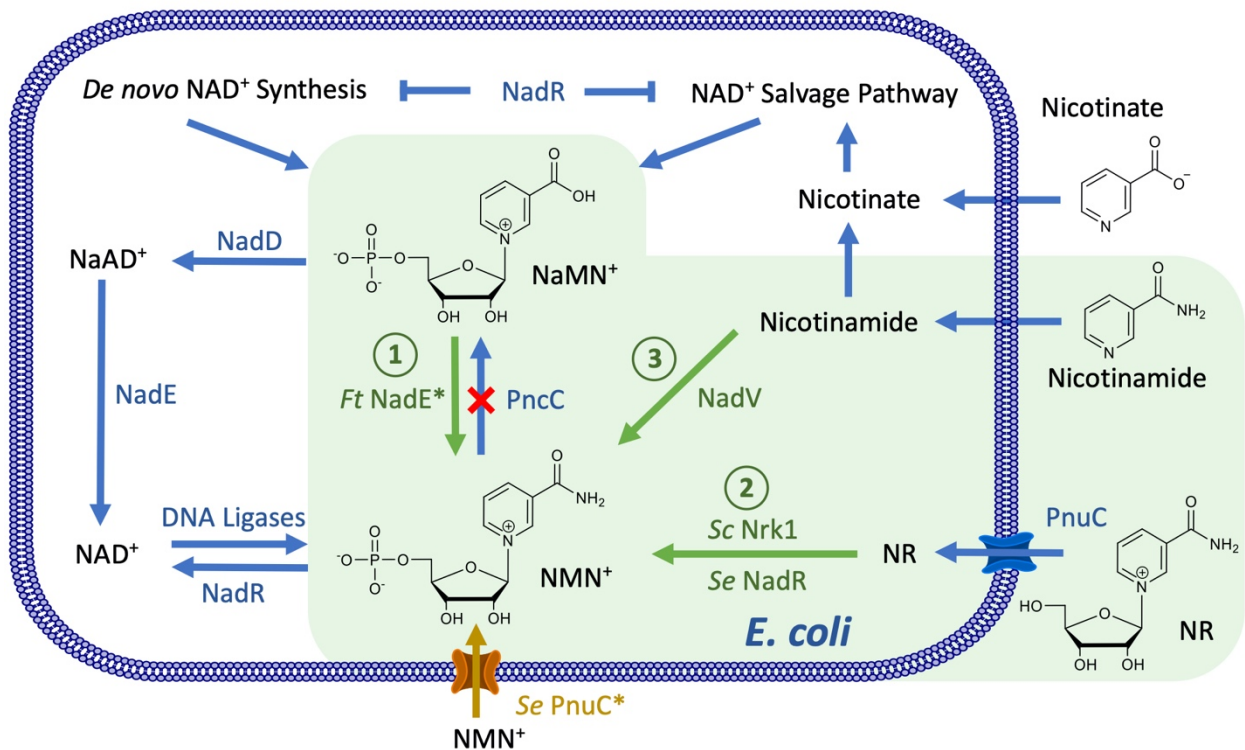
#### 4.2.4 Cell growth with high concentrations of NMN<sup>+</sup>

A plasmid containing the NMN<sup>+</sup> transporter *S. enterica* PnuC\* (pWB302) was transformed into *E. coli* strains JW2670-1 ( $\Delta pncC$ ) and MX101 ( $\Delta pncC \Delta nadR$ ). Overnight cultures were grown in 2xYT medium supplemented with 1 g/L D-glucose, 0.1 mM IPTG, and 100 mg/L ampicillin at 30 °C while shaking at 250 r.p.m. for ~14 hours. 1 mL of overnight culture was pelleted in a 1.5 mL microcentrifuge tube and washed twice with 1 mL of 1x M9 salts. The washed cells were resuspended in 1 mL of 1x M9 salts and used for inoculations. For the growth assay, cells were cultured in 1 mL of M9 minimal medium (1x M9 salts, 1 g/L glucose, 1 mM MgSO<sub>4</sub>, 0.1 mM CaCl<sub>2</sub>, 40 mg/L FeSO<sub>4</sub>, 1x A5 trace metals with cobalt) containing 0.5 mM IPTG in a 2 mL deep-well plate, with square wells, sealed with air permeable film. The medium was inoculated with 1% v/v of washed overnight cultures. Cultures were grown at 30 °C while shaking at 250 r.p.m.. Cell growth was monitored by measuring optical density at 600 nm. Media contained 100 mg/L ampicillin to maintain the plasmid.

## 4.3 Results

### 4.3.1 Identification of NMN<sup>+</sup> Biosynthetic Routes

In *E. coli* cells, NMN<sup>+</sup> is only present at a nominal level, ~11.5  $\mu\text{M}$  as previously reported<sup>13</sup>, as the product of the DNA ligase reaction<sup>18</sup>. On the other hand, NMN<sup>+</sup> accumulates to higher levels and serves as a main intermediate in NAD<sup>+</sup> biosynthesis in other organisms<sup>23,24</sup>. Here, we sought to systematically investigate the effectiveness of these heterologous NMN<sup>+</sup> biosynthetic routes in *E. coli* (Figure 12).



**Figure 12: Establishing NMN<sup>+</sup> Biosynthetic Routes in *Escherichia coli*.** NMN<sup>+</sup> is produced in a small amount through the DNA ligase reaction in the *E. coli* cell. Heterologous enzymes, shown in green, can introduce new routes to generate NMN<sup>+</sup>. *E. coli* endogenous genes and transport processes are shown in blue. Pathway 1 introduces an NMN<sup>+</sup> synthase from *Francisella tularensis* to produce NMN<sup>+</sup> from NaMN<sup>+</sup>. Pathway 2, NR salvage, produces NAD<sup>+</sup> from NR. Pathway 3, NA salvage, produces NMN<sup>+</sup> from NA. The NMN<sup>+</sup> transporter PnuC\* from *Salmonella enterica*, shown in orange, enabled transport of NMN<sup>+</sup> into the cell. The endogenous *pncC*, was targeted for

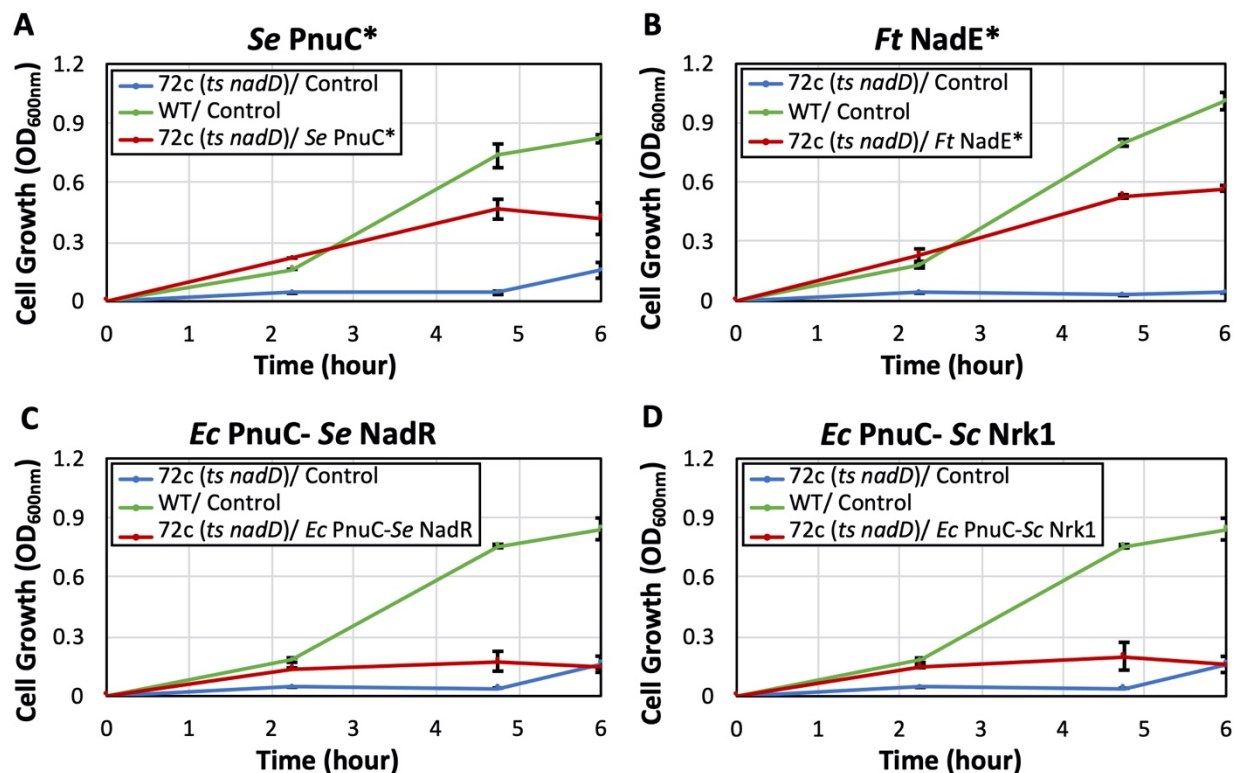
gene disruption to prevent NMN<sup>+</sup> degradation. In the presence of NAD<sup>+</sup>, NadR inhibits transcription of the genes involved in *de novo* NAD<sup>+</sup> biosynthesis, nicotinate salvage, and *E. coli* *pnuC*. NaMN<sup>+</sup>, nicotinic acid mononucleotide; NaAD<sup>+</sup>, nicotinic adenine dinucleotide; NAD<sup>+</sup>, nicotinamide adenine dinucleotide; NMN<sup>+</sup>, nicotinamide mononucleotide; NR, nicotinamide riboside; NadD, NaMN adenylyltransferase; NadR, NMN adenylyltransferase; NadE, NAD synthase; *Ft* NadE\*, NMN synthase from *Francisella tularensis*; PncC, NMN amidohydrolase; NadV, nicotinamide phosphoribosyltransferase; PnuC, nicotinamide riboside transporter; PnuC\*, a mutant PnuC enabling direct transport of NMN<sup>+</sup> across the cell membrane.

Three major NMN<sup>+</sup> biosynthetic pathways exist in Nature (Figure 12): Pathway 1 produces NMN<sup>+</sup> from nicotinic acid mononucleotide (NaMN<sup>+</sup>) using NMN<sup>+</sup> synthetase (NadE\*), and it was shown to be part of the *de novo* NAD<sup>+</sup> biosynthetic pathway in a small group of prokaryotes including *F. tularensis*<sup>24</sup>. Pathway 2 involves phosphorylation of nicotinamide riboside (NR) and functions to salvage NR to ultimately yield NAD<sup>+</sup>. To establish this pathway, we chose to overexpress the native NR transporter in *E. coli*, PnuC<sup>25</sup>, in conjunction with two different NR kinases, Nrk1 from *Saccharomyces cerevisiae*<sup>26</sup> and NadR from *Salmonella enterica*<sup>27</sup>. Pathway 3 uses nicotinamide phosphoribosyltransferase (NadV) to convert nicotinamide (NA) to NMN<sup>+</sup>; it plays a role in NA salvage in vertebrates and some bacteria. Marinescu and coworkers demonstrated NMN<sup>+</sup> accumulation in *E. coli* by heterologously expressing three NadV homologs from *Haemophilus ducreyi*, *Shewanella oneidensis*, and *Mus musculus* while feeding NA<sup>19</sup>, and they showed that *H. ducreyi* NadV performed the best<sup>19</sup>. We previously showed that NadV from *F. tularensis*, which belongs to a different clade in the NadV phylogenetic tree to *H. ducreyi* NadV<sup>18</sup>, can also effectively produce NMN<sup>+</sup> in *E. coli*<sup>13</sup>. Here, we sought to explore more bacterial NadVs in the same family of *F. tularensis* NadV and compare them with *H. ducreyi* and *F. tularensis* NadV. Namely, we chose NadV homologs from *R. solanacearum*, *Synechocystis* sp., and *Synechococcus elongatus*<sup>18</sup>.

All three pathways have unique advantages. While Pathway 3 requires a much cheaper substrate than Pathway 2 (NA versus NR), the latter incorporates ATP hydrolysis as a robust driving force. Since NaMN<sup>+</sup> is an intermediate in *E. coli*'s *de novo* NAD<sup>+</sup> biosynthesis and can be efficiently produced from central metabolites (Figure 12), Pathway 1 has the potential to achieve complete *de novo* NMN<sup>+</sup> biosynthesis from simple feed stocks such as glucose.

#### **4.3.2 Evaluating the NMN<sup>+</sup> biosynthetic pathways *in vivo***

We evaluated the three above-mentioned pathways in *E. coli* using a growth-based screening platform (Figure 12, Figure 13). To link NMN<sup>+</sup> production to cell survival, we employed *E. coli* strain 72c, which contains a temperature sensitive allele of *nadD*, an essential gene in NAD<sup>+</sup> biosynthesis. As a result, the cells cannot grow at 42 °C<sup>28</sup> unless NMN<sup>+</sup> can accumulate inside the cells and be converted to NAD<sup>+</sup> by *E. coli* NadR (Figure 12, Figure 13). Previous work has also established NMN<sup>+</sup>-dependent NAD<sup>+</sup> biosynthesis to rescue NAD<sup>+</sup> auxotrophy in *E. coli*<sup>29</sup>.

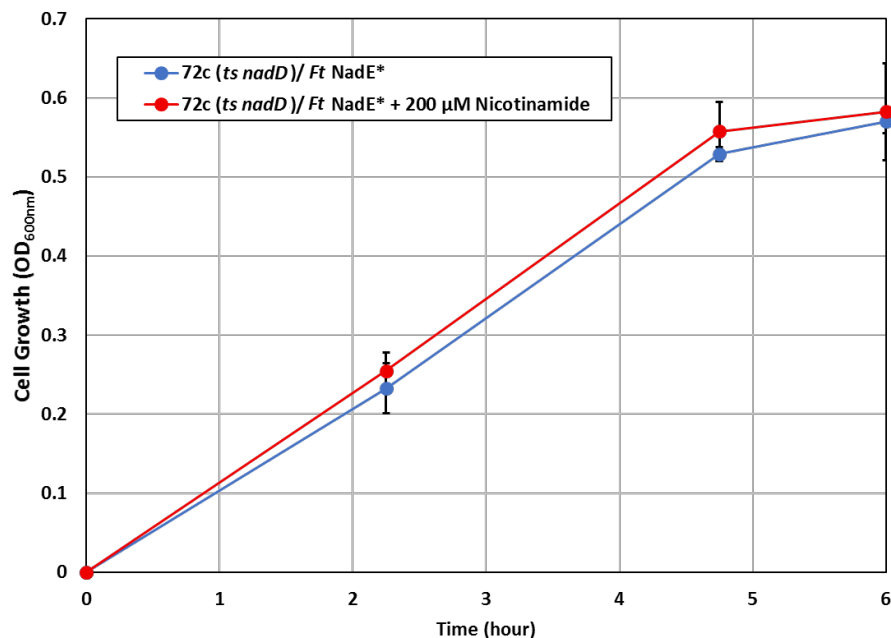


**Figure 13: Identification of efficient NMN<sup>+</sup> production pathways *in vivo* using a growth-based screening platform.** A growth-base screening platform was used to identify pathways which efficiently generated NMN<sup>+</sup> *in vivo*. *E. coli* strain 72c, which contains a temperature sensitive allele of *nadD* (*ts nadD*), which exhibits a conditionally lethal phenotype when cultured at 42 °C because the native NAD<sup>+</sup> biosynthesis is disrupted. Therefore, the cell must rely on intracellular NMN<sup>+</sup> to restore NAD<sup>+</sup> formation and growth. (A) Direct feeding of NMN<sup>+</sup> into the growth medium with the overexpression of an NMN<sup>+</sup> transporter, PnuC\* from *S. enterica*, restored growth to levels near the wild type control, indicating the platform is effective for NMN<sup>+</sup> production screening. (B) Introducing *F. tularensis* NadE\* also restored growth with the supplementation of nicotinamide. (C, D) Overexpression of *E. coli*'s native nicotinamide riboside (NR) transporter PnuC, paired with *S. enterica* NadR (C) or *S. cerevisiae* Nrk1 (D) while feeding NR failed to efficiently restore growth. Screening was performed in a deep-well 96-well plate containing 1 mL of LB medium supplemented with 2 g/L D-glucose and 200 μM of NMN<sup>+</sup> precursors, if applicable.

When 200 μM NMN<sup>+</sup> was directly fed to the cells expressing an NMN<sup>+</sup> transporter from *S. enterica* PnuC\*<sup>30</sup> (on a multiple-copy plasmid pWB302), growth was restored to levels comparable to wild type cells after 6 hours (Figure 13A). In contrast, cells carrying a control plasmid (pWB301) could not grow, suggesting the basal level of NMN<sup>+</sup> in *E. coli* cells does not

cause background issues in this growth-based screening, possibly because *E. coli* NadR has low affinity towards NMN<sup>+</sup> <sup>31</sup>. These results demonstrate that the screening platform is functioning properly, and cell growth is serving as a readout for intracellular NMN<sup>+</sup> level. We and others have previously shown that NMN<sup>+</sup> can enter *E. coli* cells without expressing a heterologous transporter <sup>13,29</sup>. In this work, the amount of NMN<sup>+</sup> supplementation can be substantially reduced, suggesting that *S. enterica* PnuC\* improves the efficiency of NMN<sup>+</sup> transportation into *E. coli* cells.

Overexpression of *F. tularensis* NadE\* (Figure 12, Pathway 1, on the plasmid pWB303) with 200 μM nicotinamide supplementation restored growth to a similar level as directly feeding NMN<sup>+</sup> (Figure 13B). Nicotinamide can yield the substrate of NadE\*, namely NaMN<sup>+</sup>, through *E. coli*'s native salvage pathway. Interestingly, growth restoration by *F. tularensis* NadE\* does not depend on nicotinamide feeding (Figure 14). NMN<sup>+</sup> production using *S. cerevisiae* Nrkl or *S. enterica* NadR (Figure 13, Pathway 2, on the plasmids pWB304 and pWB305) with 200 μM NR supplementation was not efficient enough to restore growth (Figure 13C, D). This may be due to the poor expression of these heterologous kinases in *E. coli* and their relatively high  $K_M$  for NR and ATP <sup>30</sup>. Therefore, we did not proceed with Pathway 2.



**Figure 14: *Francisella tularensis* NadE\*-based Growth Restoration is Not Nicotinamide Feeding Dependent.** A growth restoration platform was used to screen pathways for the efficient generation of nicotinamide mononucleotide (NMN<sup>+</sup>). The *Escherichia coli* strain 72c contains a temperature sensitive allele of *nadD* (*ts nadD*). As a result, this strain cannot grow at 42 °C. By overexpressing *Francisella tularensis nadE\**, cells are able to produce NMN<sup>+</sup>, which can then be converted to NAD<sup>+</sup>, and thus restoring growth. We observed no dependence of growth restoration with feeding 200 μM nicotinamide (NA). This indicates either efficient NMN<sup>+</sup> generation can be achieved through channeling the intermediate nicotinic acid mononucleotide (NaMN<sup>+</sup>) from *E. coli*'s native de novo NAD<sup>+</sup> biosynthesis pathway, or LB medium used in this experiment already contains sufficient precursors for this pathway. Screening was performed in a deep-well 96-well plate containing 1 mL of LB medium supplemented with 2 g/L D-glucose and 200 μM of NA if applicable. Detailed conditions are described in the Methods section.

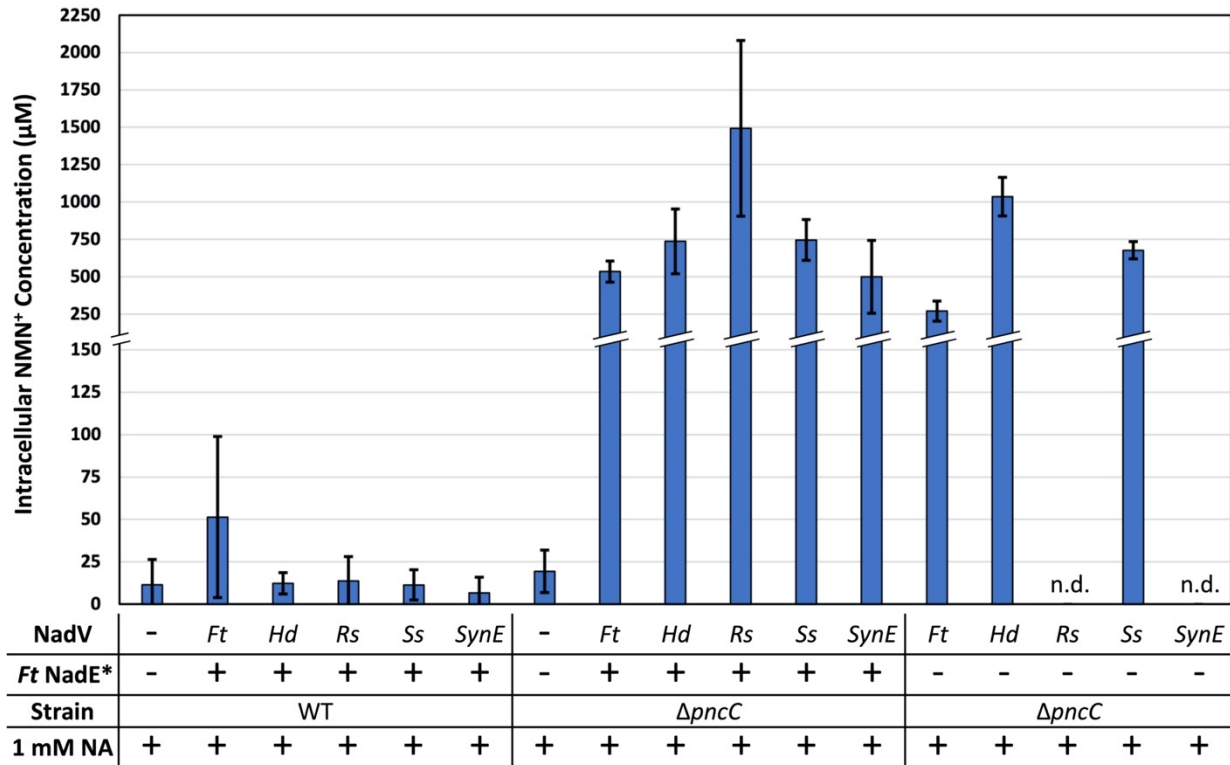
Taken together, these results suggest that besides the well-established NadV route (Figure 12, Pathway 3)<sup>19</sup>, the *F. tularensis* NadE\*-dependent pathway (Pathway 1) is also effective in *E. coli* for NMN<sup>+</sup> biosynthesis.

#### 4.3.3 Bioprospecting NadV homologs and optimizing NMN<sup>+</sup> biosynthesis

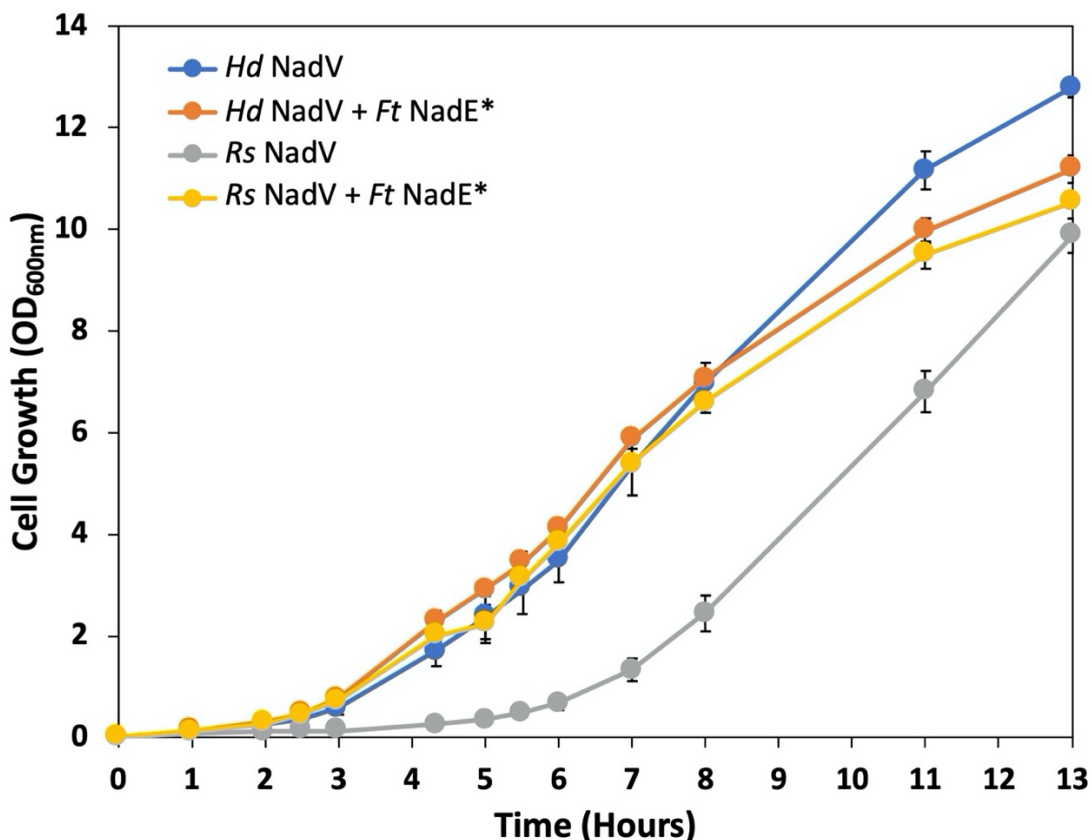
After demonstrating NMN<sup>+</sup> can be effectively generated by overexpressing *F. tularensis* NadE\*, we examined the effects of pairing it with different NadV homologs. *F. tularensis* NadE\* was overexpressed in a synthetic operon on a multiple-copy plasmid with each of the five NadV

candidates as described above (pWB203, pDB101, pDB102, pDB103, pDB104). Cells were fed 1 mM of NA and grown for four hours before processing and quantification of intracellular NMN<sup>+</sup> and NAD<sup>+</sup> levels *via* LC-MS analysis as previously described<sup>13</sup>. When using the wild type BW25113 cells as the host, ~12 to 51 μM of NMN<sup>+</sup> was produced through these pathways (Figure 15). We previously found that low levels of intracellular NMN<sup>+</sup> could be attributed to NMN<sup>+</sup> degradation by the NMN<sup>+</sup> amidohydrolase, PncC<sup>13</sup>. Expression of the NadE\*/NadV pathways in a  $\Delta pncC$  strain, JW2670-1 significantly increased the intracellular NMN<sup>+</sup> levels. When the NadV candidates were expressed without *F. tularensis* NadE\* in JW2670-1 (on plasmids pWB303, pWB306, pWB307, pWB308, pWB309), intracellular NMN<sup>+</sup> levels were lower for all NadVs except *H. ducreyi* (Figure 15). Notably, expressing *R. solanacerum* and *S. elongatus* NadVs alone resulted in a significant growth challenge (Figure 16) and the concomitant diminishing of NMN<sup>+</sup> production (Figure 15). However, this growth challenge could be overcome by expressing the NadV with *F. tularensis* NadE\* (Figure 16), indicating that *Ft* NadE\* may provide a synergistic benefit to the stability, activity, or expression for some NadV candidates. Future work is needed to pinpoint the molecular mechanism behind this synergy.





**Figure 15: Pathway combination and strain modification improved NMN<sup>+</sup> production.** NadV homologs were co-overexpressed with and without *F. tularensis* NadE\* in wild type and  $\Delta pncC$  cells. In wild type cells, introducing *F. tularensis* NadE\* and NadV homologs only resulted in low levels of NMN<sup>+</sup> accumulation. Disrupting the NMN<sup>+</sup> degrading-enzyme PncC greatly increased intracellular NMN<sup>+</sup> levels. When the NadV homologs were expressed without *F. tularensis* NadE\*, intracellular NMN<sup>+</sup> levels decreased for all candidates except *H. ducreyi*. In some cases, only expressing NadV caused a significant growth detriment (shown as n.d.). Of the NadV homologs tested, *R. solanacearum* NadV demonstrated the highest intracellular NMN<sup>+</sup> production of ~1.5 mM in  $\Delta pncC$  cells, a 130-fold increase over the cell's basal level when expressed with *F. tularensis* NadE\*. Cells were grown in 2xYT medium supplemented with 1 mM nicotinamide at 30 °C for 4 hours. NMN<sup>+</sup> concentration was determined by LC-MS. *Ft*, *Francisella tularensis*; *Hd*, *Haemophilus ducreyi*; *Rs*, *Ralstonia solanacearum*; *Ss*, *Synechocystis sp.*; *SynE*, *Synechococcus elongatus*. n.d., not determined due to poor growth.

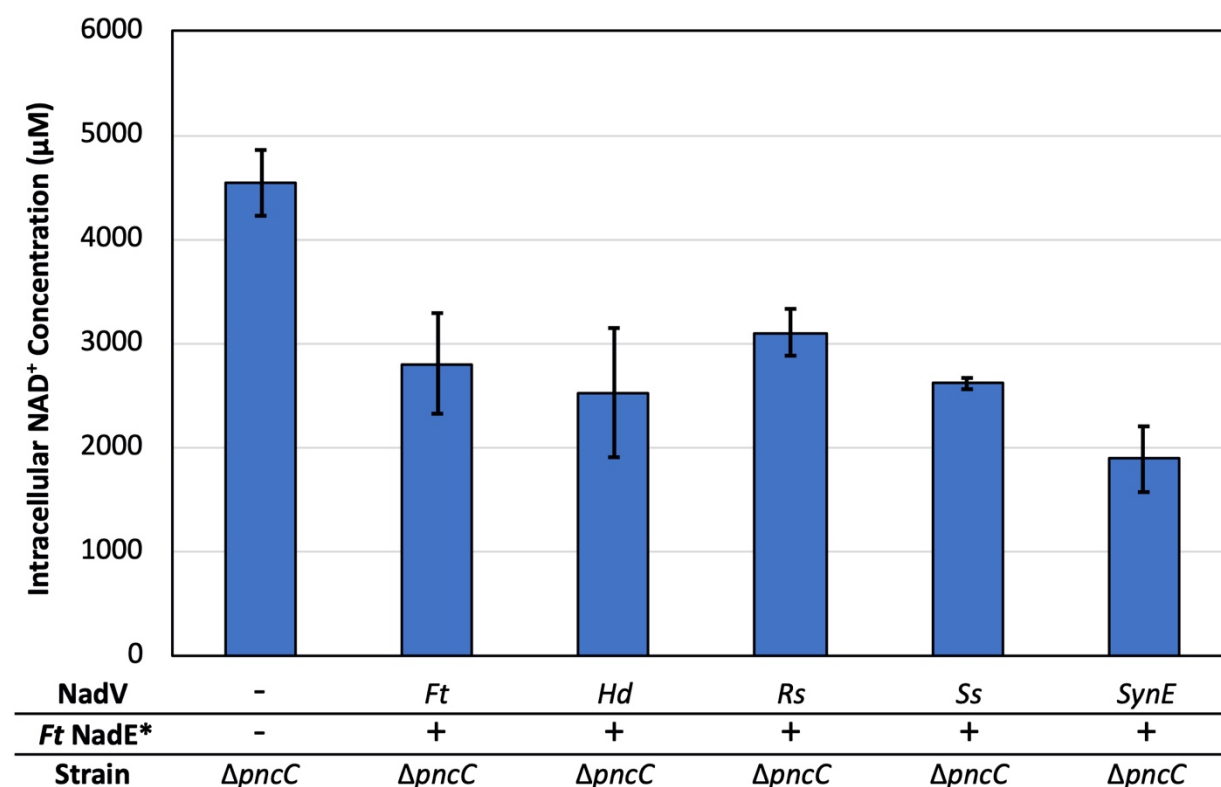


**Figure 16: *Francisella tularensis* NadE\* Expression Alleviates *R. solanacearum* NadV Growth Challenge.** BW25113  $\Delta$ pnc cells expressing *R. solanacearum* NadV demonstrate a growth challenge. However, when paired with *F. tularensis* NadE\*, the growth challenge is alleviated. Interestingly, this challenge is not seen when *H. ducreyi* NadV is expressed. Therefore, *F. tularensis* NadE\* may play a synergistic role in stability, activity, or expression of some NadV candidates. Cells were cultured identically to the intracellular NMN<sup>+</sup> generation cultures described in the Methods section. Cell growth was monitored by measuring optical density at 600 nm. Abbreviations indicate source of genes: *Ft*, *Francisella tularensis*, *Hd*, *Haemophilus ducreyi*; *Rs*, *Ralstonia solanacearum*.

Cells expressing *F. tularensis* NadE\* and *R. solanacearum* NadV in  $\Delta$ pnc strain reached the highest intracellular NMN<sup>+</sup> level of ~1.5 mM, a 130-fold increase over the cell's basal NMN<sup>+</sup> level<sup>13</sup>, when tested under the same conditions (Figure 15). Furthermore, the *R. solanacearum* NadV strain performed better than *F. tularensis* NadV, the NadV we used in our previous work<sup>13</sup>, exhibiting a 2.8-fold increase in intracellular NMN<sup>+</sup> concentration. *R. solanacearum* NadV also performed better than *H. ducreyi* NadV<sup>19</sup> when paired with *F. tularensis* NadE\*.

#### 4.3.4 Investigating the physiological response to NMN<sup>+</sup> accumulation

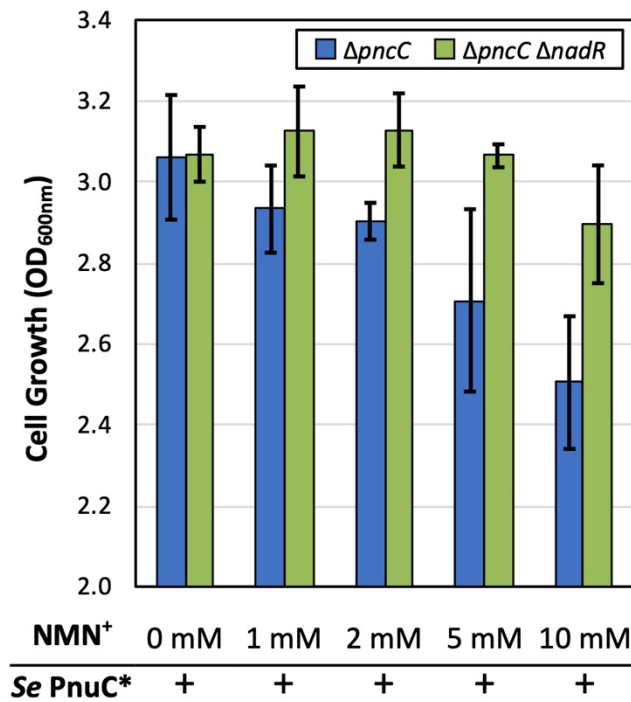
Even though the *de novo* NAD<sup>+</sup> biosynthesis pathway was unmodified, the  $\Delta pncC$  cells overexpressing *F. tularensis* NadE\* and NadV homologs had lower intracellular NAD<sup>+</sup> levels compared to the control strain in which no proteins were overexpressed and intracellular NMN<sup>+</sup> level was low (Figure 15, Figure 17). This suggests that maintaining intracellular NMN<sup>+</sup> at millimolar-range concentrations may be detrimental to cellular fitness. Although we observed no growth defects in our current best NMN<sup>+</sup> producing strain, the potential physiological effects of NMN<sup>+</sup> accumulation may become a bottleneck for future strain optimization.



**Figure 17: Intracellular NAD<sup>+</sup> Decreases in NMN<sup>+</sup> Accumulating Strains** From Figure 15, co-overexpression of NMN<sup>+</sup> generating *Francisella tularensis* NadE\* and NadVs increases intracellular NMN<sup>+</sup> when the NMN<sup>+</sup> degrading PncC is disrupted. However, as shown here, NAD<sup>+</sup> levels decreased in cells expressing *F. tularensis* NadE\* and NadV compared to cells without overexpression. This potentially indicates NMN<sup>+</sup> plays a regulatory role in NAD<sup>+</sup> biosynthesis. Cells were cultured in 2xYT medium supplemented with 1 mM nicotinamide at 30 °C for four

hours. Intracellular NAD<sup>+</sup> concentrations were determined by UPLC-MS/MS. Detailed conditions and analytical techniques are described in the Methods section.

Since the effects of NMN<sup>+</sup> accumulation on *E. coli* are not well understood, we sought to stress the cells by drastically increasing the intracellular NMN<sup>+</sup> levels in the  $\Delta pncC$  strain and observe cellular growth. NMN<sup>+</sup> concentration was titrated in the medium while expressing the exogenous NMN<sup>+</sup> transporter *S. enterica* PnuC\*. We found that cell growth was inhibited at high NMN<sup>+</sup> concentrations (> 5 mM) (Figure 18), which suggests that elevated NMN<sup>+</sup> level may interfere with physiological processes in *E. coli*. Although intracellular NMN<sup>+</sup> levels were not measured in this application, PnuC\*-mediated NMN<sup>+</sup> transport was shown to be active with as low as 200  $\mu$ M of NMN<sup>+</sup> supplementation to support growth restoration (Figure 13A). Given the decrease in intracellular NAD<sup>+</sup> level upon NMN<sup>+</sup> accumulation (Figure 17), we hypothesized that NMN<sup>+</sup> may regulate NAD<sup>+</sup> biosynthesis, and we sought to examine whether this regulation was mediated by the transcriptional regulator of NAD<sup>+</sup> biosynthesis, NadR<sup>32</sup>. Interestingly, when NadR was disrupted, the growth inhibition effect of NMN<sup>+</sup> was significantly alleviated (Figure 18). These results suggest that NadR may indeed play a role in the physiological response to NMN<sup>+</sup> accumulation in *E. coli*. NAD<sup>+</sup> has been suggested to allosterically modulate NadR's function<sup>33</sup>. Given NadR's capability to also recognize NMN<sup>+</sup><sup>31</sup>, further studies are needed to investigate whether NMN<sup>+</sup> binding induces conformational change in the DNA-binding domain of NadR and modulates its function as a transcriptional regulator.



**Figure 18 NMN<sup>+</sup> accumulation affects cell physiology possibly via NadR.** To determine if NMN<sup>+</sup> accumulation impacts cell fitness, NMN<sup>+</sup> was titrated in the growth medium of cells expressing the NMN<sup>+</sup> transporter *S. enterica* PnuC\*. The  $\Delta pncC$  strain exhibited decreased growth at high NMN<sup>+</sup> concentrations. Disruption of *nadR* significantly alleviated the growth inhibition. This suggests the NadR may mediate the physiological response to NMN<sup>+</sup> accumulation in *E. coli*. Cells were grown at 30 °C for 6.5 hours in a deep-well 96-well plate containing 1 mL of medium per well.

#### 4.4 Discussion

This work represents the initial steps towards filling some of the fundamental knowledge gaps that remained open in previous work on NMN<sup>+</sup> biosynthesis in *E. coli*. The important work by Marinescu and coworkers<sup>19</sup> focused on the NadV pathway, but it left many other naturally occurring NMN<sup>+</sup> biosynthetic routes unexplored. Our previous work<sup>13</sup> sought to simply recapitulate the NMN<sup>+</sup> metabolism of *F. tularensis*<sup>24</sup> by overexpressing both NadE\* and NadV from this organism, without dissecting the role of each pathway. Moreover, both efforts did not study the physiological response in *E. coli* to NMN<sup>+</sup> accumulation. Beside functioning as a cofactor, NAD<sup>+</sup> is also a universal signaling compound that allosterically controls key enzymes

and transcriptional regulators in response to the fluctuating cellular redox state<sup>31, 34-37</sup>. Since NMN<sup>+</sup> is an analog of NAD<sup>+</sup>, it is an open question whether NMN<sup>+</sup>, when it accumulates to a high level, can also interact with the numerous proteins that are modulated by NAD<sup>+</sup>.

The rich information provided by comparative genomic analysis can greatly aid metabolic engineering efforts. By bioprospecting NadV homologs from evolutionarily diverse organisms, we identified *R. solanacearum* NadV, which outperformed the two NadVs that have been previously reported as efficient NMN<sup>+</sup>-producing enzymes in *E. coli*<sup>13,19</sup>, when they are compared in the same condition at a bench scale (Figure 15). Since *F. tularensis* NadE\* also showed promise to produce NMN<sup>+</sup> efficiently, a similar approach may be taken in the future to bioprospect NadE\* homologs.

To gain fundamental understanding of nicotinamide cofactor biosynthesis, the mass spectrometry method reported in this work needs to be further expanded to quantify the biosynthetic intermediates of NMN<sup>+</sup>, such as NR and NaMN<sup>+</sup>. While we only produced NMN<sup>+</sup> in oxidized form, quantification of intracellular NMNH is also important when enzymes that can cycle NMN<sup>+</sup> are introduced. Our future work will focus on investigating the reduction potential of NMN(H) redox pair *in vivo*, as well as its interplay with NAD(P)/H redox pairs.

An intracellular NMN<sup>+</sup> level of 1.5 mM is comparable to the levels of native cofactors found *E. coli*, and similar concentrations have been shown to enable NMN-dependent biotransformation in whole cells<sup>13</sup>. In the future, additional work will be performed to determine the optimal NMN<sup>+</sup> production levels to pair with cell-free applications. Moving forward, culture medium and growth conditions can be optimized to potentially yield increased intracellular NMN<sup>+</sup> levels. In this work, all NMN<sup>+</sup> production was performed with laboratory standard medium and without optimization. Marinescu and coworkers demonstrated a 32.7-fold increase from 0.72 mM

to 23.57 mM of intracellular NMN<sup>+</sup> upon scale-up to a 500 mL bioreactor while optimizing pH, NA feeding concentration, and dissolved oxygen while culturing in PYA8 medium<sup>19</sup>. Therefore, performing a similar scale-up with our NMN<sup>+</sup> producing strain may yield significant increases in NMN<sup>+</sup> production.

In addition, host selection may play a significant role in efficient NMN<sup>+</sup> biosynthesis. While most industrial model hosts including *E. coli* and *S. cerevisiae* utilize a nicotinic acid adenine dinucleotide (NaAD)-mediated route for *de novo* NAD<sup>+</sup> biosynthesis, a small group of prokaryotes use NMN<sup>+</sup> as the primary precursor to NAD<sup>+</sup><sup>18,24</sup>. Since NMN<sup>+</sup> adopts a distinct role and is naturally maintained at a higher level in these organisms<sup>23,24</sup>, the physiological responses to intracellular NMN<sup>+</sup> accumulation may be different. Thus, organisms which utilize NMN<sup>+</sup>-mediated NAD<sup>+</sup> biosynthesis may be interesting targets for metabolic engineering.

Ultimately, efficient and cost-effective production and purification of NMN<sup>+</sup> is key for the long-term viability of NMN<sup>+</sup>-based cell-free biotransformation. Once upstream pathways for the renewable production of NMN<sup>+</sup> are further established, NMN<sup>+</sup> will need to be extracted and purified before use in cell-free systems. Cells can be isolated through centrifugation, washed, and lysed through homogenization to isolate NMN<sup>+</sup> from cellular debris. Alternatively, cells can also be permeabilized to release NMN<sup>+</sup> across the cell membrane, allowing for fewer steps of isolating NMN<sup>+</sup> from cell mass. Finally, a major advantage of producing NMN<sup>+</sup> *in vivo* is the direct compatibility with crude lysate-based cell-free and whole-cell biosynthesis. By using cells that are capable of both producing intracellular NMN<sup>+</sup> and expressing enzymes of interest, crude lysates or whole cells can be directly used for NMN<sup>+</sup>-dependent biosynthesis without the exogenous supply of redox cofactors.

## 4.5 Conclusions

In this work, we explored routes to efficiently produce NMN<sup>+</sup> in *E. coli*. After surveying the routes for NMN<sup>+</sup> production *in vivo*, bioprospecting NadVs enabled the production of 1.5 mM of NMN<sup>+</sup> using the NadV from *R. solanacearum*. Under the conditions tested, *R. solanacearum* outperformed the previous best NadV's shown to accumulate NMN<sup>+</sup> efficiently<sup>13,19</sup>. In addition, this work began to elucidate the physiological effects of NMN<sup>+</sup> accumulation in *E. coli*. However, further investigation is necessary to maintain productivity as NMN<sup>+</sup> levels are further increased. Ultimately, advancing noncanonical redox cofactor biosynthesis in microorganisms may enable the application of self-sustained, fully renewable cell-free and whole-cell biocatalysis.

## 4.6 References

- [1] Bowie, J. U.; Sherkhonov, S.; Korman, T. P.; Valliere, M. A.; Opgenorth, P. H.; Liu, H. Synthetic Biochemistry: The Bio-Inspired Cell-Free Approach to Commodity Chemical Production. *Trends Biotechnol.* **2020**, *38*, 766–778.
- [2] Dudley, Q. M.; Karim, A. S.; Jewett, M. C. Cell-Free Metabolic Engineering: Biomanufacturing beyond the Cell. *Biotechnol. J.* **2015**, *10*, 69–82.
- [3] Wilding, K. M.; Schinn, S.-M.; Long, E. A.; Bundy, B. C. The Emerging Impact of Cell-Free Chemical Biosynthesis. *Curr. Opin. Biotechnol.* **2018**, *53*, 115–121.
- [4] Honda, K.; Kimura, K.; Ninh, P. H.; Taniguchi, H.; Okano, K.; Ohtake, H. *In Vitro* Bioconversion of Chitin to Pyruvate with Thermophilic Enzymes. *J. Biosci. Bioeng.* **2017**, *124* (3), 296–301.
- [5] Wang, W.; Liu, M.; You, C.; Li, Z.; Zhang, Y.-H. P. ATP-Free Biosynthesis of a High-Energy Phosphate Metabolite Fructose 1,6-Diphosphate by *in vitro* Metabolic Engineering. *Metab. Eng.* **2017**, *42*, 168–174.
- [6] Kay, J. E.; Jewett, M. C. A Cell-Free System for Production of 2,3-Butanediol Is Robust to Growth-Toxic Compounds. *Metab. Eng. Commun.* **2020**, *10*, e00114.
- [7] Karim, A. S.; Jewett, M. C. A Cell-Free Framework for Rapid Biosynthetic Pathway Prototyping and Enzyme Discovery. *Metab. Eng.* **2016**, *36*, 116–126.



- [8] Kelwick, R.; Ricci, L.; Chee, S. M.; Bell, D.; Webb, A. J.; Freemont, P. S. Cell-Free Prototyping Strategies for Enhancing the Sustainable Production of Polyhydroxyalkanoates Bioplastics. *Synth. Biol.* **2018**, *3*, ysy016.
- [9] Nowak, C.; Pick, A.; Csepei, L.-I.; Sieber, V. Characterization of Biomimetic Cofactors According to Stability, Redox Potentials, and Enzymatic Conversion by NADH Oxidase from *Lactobacillus Pentosus*. *ChemBioChem* **2017**, *18*, 1944–1949.
- [10] Nowak, C.; Pick, A.; Lommès, P.; Sieber, V. Enzymatic Reduction of Nicotinamide Biomimetic Cofactors Using an Engineered Glucose Dehydrogenase: Providing a Regeneration System for Artificial Cofactors. *ACS Catal.* **2017**, *7*, 5202–5208.
- [11] Kaplan, N. O.; Ciotti, M. M.; Stolzenbach, F. E. Reaction of Pyridine Nucleotide Analogues with Dehydrogenases. *J. Biol. Chem.* **1956**, *225*, 833–844.
- [12] Kaufman RA. Use of Nicotinamide Adenine Dinucleotide (NAD) Analogs to Measure Ethanol. European Patent Specification Patent No. EP 1 242 440 B1, filed December 27, 2000, and published September 16, **2015**.
- [13] Black, W. B.; Zhang, L.; Mak, W. S.; Maxel, S.; Cui, Y.; King, E.; Fong, B.; Sanchez Martinez, A.; Siegel, J. B.; Li, H. Engineering a Nicotinamide Mononucleotide Redox Cofactor System for Biocatalysis. *Nat. Chem. Biol.* **2020**, *16*, 87–94.
- [14] Campbell, E.; Meredith, M.; D. Minter, S.; Banta, S. Enzymatic Biofuel Cells Utilizing a Biomimetic Cofactor. *Chem. Commun.* **2012**, *48*, 1898–1900.
- [15] Ji, D.; Wang, L.; Liu, W.; Hou, S.; Zhao, K. Z. Synthesis of NAD Analogs to Develop Bioorthogonal Redox System. *Sci. China Chem.* **2013**, *56*, 296–300.
- [16] Paul, C. E.; Arends, I. W. C. E.; Hollmann, F. Is Simpler Better? Synthetic Nicotinamide Cofactor Analogues for Redox Chemistry. *ACS Catal.* **2014**, *4*, 788–797.
- [17] Makarov, M. V.; Migaud, M. E. Syntheses and Chemical Properties of  $\beta$ -Nicotinamide Riboside and Its Analogues and Derivatives. *Beilstein J. Org. Chem.* **2019**, *15*, 401–430.
- [18] Gazzaniga, F.; Stebbins, R.; Chang, S. Z.; McPeck, M. A.; Brenner, C. Microbial NAD Metabolism: Lessons from Comparative Genomics. *Microbiol. Mol. Biol. Rev.* **2009**, *73*, 529–541.
- [19] Marinescu, G. C.; Popescu, R.-G.; Stoian, G.; Dinischiotu, A.  $\beta$ -Nicotinamide Mononucleotide (NMN) Production in *Escherichia Coli*. *Sci. Rep.* **2018**, *8*, 12278.
- [20] Sinclair, D. A.; EAR, P. H. Biological Production of Nad Precursors and Analogs. WO2015069860A1, May 14, 2015.

- [21] Paul, C. E.; Gargiulo, S.; Opperman, D. J.; Lavandera, I.; Gotor-Fernández, V.; Gotor, V.; Taglieber, A.; Arends, I. W. C. E.; Hollmann, F. Mimicking Nature: Synthetic Nicotinamide Cofactors for C=C Bioreduction Using Enoate Reductases. *Org. Lett.* **2013**, *15*, 180–183.
- [22] Rollin, J.; Kin Tam, T.; Percival Zhang, Y.-H. New Biotechnology Paradigm: Cell-Free Biosystems for Biomanufacturing. *Green Chem.* **2013**, *15*, 1708–1719.
- [23] Evans, C.; Bogan, K. L.; Song, P.; Burant, C. F.; Kennedy, R. T.; Brenner, C. NAD<sup>+</sup> Metabolite Levels as a Function of Vitamins and Calorie Restriction: Evidence for Different Mechanisms of Longevity. *BMC Chem. Biol.* **2010**, *10*, 2.
- [24] Sorci, L.; Martynowski, D.; Rodionov, D. A.; Eyobo, Y.; Zogaj, X.; Klose, K. E.; Nikolaev, E. V.; Magni, G.; Zhang, H.; Osterman, A. L. Nicotinamide Mononucleotide Synthetase Is the Key Enzyme for an Alternative Route of NAD Biosynthesis in *Francisella Tularensis*. *PNAS* **2009**, *106*, 3083–3088.
- [25] Sauer, E.; Merdanovic, M.; Mortimer, A. P.; Bringmann, G.; Reidl, J. PnuC and the Utilization of the Nicotinamide Riboside Analog 3-Aminopyridine in *Haemophilus Influenzae*. *Antimicrob. Agents Chemother.* **2004**, *48*, 4532–4541.
- [26] Belenky, P.; Christensen, K. C.; Gazzaniga, F.; Pletnev, A. A.; Brenner, C. Nicotinamide Riboside and Nicotinic Acid Riboside Salvage in Fungi and Mammals. *J. Biol. Chem.* **2009**, *284*, 158–164.
- [27] Kurnasov, O. V.; Polanuyer, B. M.; Ananta, S.; Sloutsky, R.; Tam, A.; Gerdes, S. Y.; Osterman, A. L. Ribosylnicotinamide Kinase Domain of NadR Protein: Identification and Implications in NAD Biosynthesis. *J. Bacteriol.* **2002**, *184*, 6906–6917.
- [28] Stancek, M.; Isaksson, L. A.; Rydén-Aulin, M. FusB Is an Allele of NadD, Encoding Nicotinate Mononucleotide Adenylyltransferase in *Escherichia Coli*. *Microbiology*, **2003**, *149*, 2427–2433.
- [29] Wang, X.; Zhou, Y. J.; Wang, L.; Liu, W.; Liu, Y.; Peng, C.; Zhao, Z. K. Engineering *Escherichia coli* Nicotinic Acid Mononucleotide Adenylyltransferase for Fully Active Amidated NAD Biosynthesis. *Appl. Environ. Microbiol.* **2017**, *83*, e00692-17.
- [30] Grose, J. H.; Bergthorsson, U.; Xu, Y.; Sternecker, J.; Khodaverdian, B.; Roth, J. R. Assimilation of Nicotinamide Mononucleotide Requires Periplasmic AphA Phosphatase in *Salmonella Enterica*. *J. Bacteriol.* **2005**, *187*, 4521–4530.
- [31] Raffaelli, N.; Lorenzi, T.; Mariani, P. L.; Emanuelli, M.; Amici, A.; Ruggieri, S.; Magni, G. The *Escherichia coli* NadR Regulator Is Endowed with Nicotinamide Mononucleotide Adenylyltransferase Activity. *J. Bacteriol.* **1999**, *181*, 5509–5511.
- [32] Tritz, G. J.; Chandler, J. L. Recognition of a Gene Involved in the Regulation of Nicotinamide Adenine Dinucleotide Biosynthesis. *J. Bacteriol.* **1973**, *114*, 128–136.

- [33] Zhu, N.; Olivera, B. M.; Roth, J. R. Activity of the Nicotinamide Mononucleotide Transport System Is Regulated in *Salmonella Typhimurium*. *J. Bacteriol.* **1991**, *173*, 1311–1320.
- [34] Euro, L.; Belevich, G.; Bloch, D. A.; Verkhovsky, M. I.; Wikström, M.; Verkhovskaya, M. The Role of the Invariant Glutamate 95 in the Catalytic Site of Complex I from *Escherichia coli*. *Biochim. Biophys. Acta, Bioenerg.* **2009**, *1787*, 68–73.
- [35] Leonardo, M. R.; Dailly, Y.; Clark, D. P. Role of NAD in Regulating the AdhE Gene of *Escherichia coli*. *J. Bacteriol.* **1996**, *178*, 6013–6018.
- [36] Rodionov, D. A.; De Ingeniis, J.; Mancini, C.; Cimadamore, F.; Zhang, H.; Osterman, A. L.; Raffaelli, N. Transcriptional Regulation of NAD Metabolism in Bacteria: NrtR Family of Nudix-Related Regulators. *Nucleic Acids Res* **2008**, *36*, 2047–2059.
- [37] Shone, C. C.; Fromm, H. J. Steady-State and Pre-Steady-State Kinetics of Coenzyme A-Linked Aldehyde Dehydrogenase from *Escherichia coli*. *Biochemistry* **1981**, *20*, 7494–7501.
- [38] Gibson, D. G.; Young, L.; Chuang, R.-Y.; Venter, J. C.; Hutchison, C. A.; Smith, H. O. Enzymatic Assembly of DNA Molecules up to Several Hundred Kilobases. *Nat. Methods* **2009**, *6*, 343–345.
- [39] Findik, B. T.; Randall, L. L. Determination of the Intracellular Concentration of the Export Chaperone SecB in *Escherichia coli*. *PLoS ONE* **2017**, *12*, e0183231.

## **Chapter 5**

### **Construction of a Noncanonical Redox Cofactor System in *Saccharomyces cerevisiae***

## 5.1 Introduction

As discussed in Chapters 3 and 4, we have successfully demonstrated the construction and application of an NMN(H)-dependent orthogonal redox cofactor system in *E. coli*. However, *E. coli*, and prokaryotic hosts in general, are not always ideal microbial hosts for biotransformation and renewable product generation. *Saccharomyces cerevisiae*, baker's yeast, has been used for millennia for fermentation and more recently as a model eukaryotic host for metabolic engineering. In biotransformation, *S. cerevisiae* has been engineered to produce a wide array of products including biofuels<sup>1-3</sup>, polyketides<sup>4,5</sup>, and therapeutics<sup>6-10</sup>. Interestingly, *S. cerevisiae* natively maintains higher levels of intracellular NMN<sup>+</sup> than *E. coli*, in some conditions as high as 20% of the native NAD<sup>+</sup> pool<sup>11</sup>. Therefore, *S. cerevisiae* may serve as a strong host to engineer, maintain, and utilize an intracellular NMN<sup>+</sup> pool for a bio-orthogonal redox cofactor system.

An advantage of the NMN(H)-cycling system is that it can be integrated into a microbial host by simply expressing the NMN(H) reducing (Bs GDH Ortho) and oxidizing proteins (XenA) and delivering intracellular NMN<sup>+</sup>. Then, to deliver specific reducing power, native consumption of glucose needs to be disrupted, which is highly conserved and understood in many organisms. In this chapter, we translate our NMN(H)-cycling system into *S. cerevisiae*, and we demonstrate its ability to deliver specific reducing power to XenA for the production of citronellal, 12 mg/L, while minimizing endogenous alcohol dehydrogenase activity without the need to disrupt the genes encoding the ADHs. Furthermore, we investigate pathways to increase the intracellular NMN<sup>+</sup> pool to 188  $\mu$ M by feeding nicotinamide riboside and introducing the NMN<sup>+</sup> synthetase, NadE\*, and phosphoribosyltransferase, NadV, from *Francisella tularensis* into the genome. Pairing of the NMN(H)-cycling system with the NMN<sup>+</sup>-overproducing strain may enable NMN-

dependent biotransformation without the need for exogenous NMN<sup>+</sup> supplementation into the assay buffer.

## 5.2 Methods

### 5.2.1 Plasmid and Strain Construction

All molecular cloning was performed in *E. coli* XL1-Blue cells (Stratagene). The strains and plasmids used in this study are summarized in Table 12. Plasmids were assembled by restriction enzyme digestion and ligation. Gene fragments used for digestion and ligation were generated by polymerase chain reaction (PCR) using PrimeSTAR Max DNA Polymerase (TaKaRa). The method of plasmid construction is described below.

**Table 12: Strains and Plasmids Used in Chapter 5**

<b>Strain</b>	<b>Description</b>	<b>Reference</b>
BY4741	<i>MATa his3Δ1; leu2Δ0; met15Δ0; ura3Δ0</i>	[12]
WB601	BY4741 <i>ZWF1Δ PGI1::URA3</i>	This work
WB602	BY4741 <i>ZWF1Δ PGI1::URA3 ho::P<sub>PGK1</sub>-Ft nadV-T<sub>ADHI</sub>-P<sub>TEF2</sub>-Ft nadE*-T<sub>ENO1</sub>-natMX6</i>	This work
<b>Plasmid</b>	<b>Description</b>	<b>Reference</b>
pWB601	CEN/ARS, KanMX, <i>P<sub>TEF1</sub>-NRT1-T<sub>CYCI</sub>, P<sub>TEF1</sub>-NRK1-T<sub>CYCI</sub></i>	This work
pWB602	CEN/ARS, KanMX, <i>P<sub>TEF1</sub>-Ft nadE*-T<sub>CYCI</sub>, P<sub>TEF1</sub>-Ft nadV-T<sub>CYCI</sub></i>	This work
pWB603	CEN/ARS, KanMX, <i>P<sub>TEF1</sub>-Pp xenA-T<sub>CYCI</sub>, P<sub>TEF1</sub>-Bs gdh-T<sub>CYCI</sub></i>	This work
pWB604	CEN/ARS, KanMX, <i>P<sub>TEF1</sub>- Pp xenA-T<sub>CYCI</sub>, P<sub>TEF1</sub>- Bs gdh (I195R-A93K-Y39Q-S17E)-T<sub>CYCI</sub></i>	This work
pWB605	CEN/ARS, KanMX, <i>P<sub>TEF1</sub>-Pp xenA-T<sub>CYCI</sub>, P<sub>TEF1</sub>-Empty-T<sub>CYCI</sub></i>	This work

Abbreviations indicate source of genes: *Ft*, *Francisella tularensis*; *Pp*, *Pseudomonas putida*; *Bs*, *Bacillus subtilis*. Empty: no gene encoded.

The *xenA* gene was amplified from a plasmid which was previously generated in our lab<sup>13</sup>. Primers for PCR contained an overhang region on the 5' side to add multiple cloning digestion sites on either side of the gene. The resulting DNA fragment was digested with appropriate restriction digestion enzymes. A vector containing a CEN/ARS replication origin, a KanMX cassette, and two gene expression cassettes with a TEF1 promoter and CYC1 terminator with

multiple cloning sites was digested with identical restriction digest enzymes at one of the multiple cloning sites for ligation with *xenA* using T4 DNA Ligase (Roche). The resulting plasmid was used for the subsequent ligation of *B. subtilis gdh* into the second expression cassette by the same method to generate the resulting plasmid pWB603.

The additional plasmids were constructed in the same manner. *B. subtilis gdh*, *B. subtilis gdh* S17E-Y39Q-A93K-I195R, *F. tularensis nadE\**, and *F. tularensis nadV* were isolated from plasmids which were previously generated in our lab. *S. cerevisiae NRT1* and *NRK1* were isolated from *S. cerevisiae* BY4741 genomic DNA.

The *ZWF1* and *PGII* knockout strain was generated with two genome editing methods. First, *ZWF1* was disrupted in *S. cerevisiae* BY4741 using CRISPR/Cas9. The CRISPR/Cas9 system was introduced on plasmid pRCC-K (Addgene #81191) using the gRNA target sequence CGGGTCTAAGCCCGCCTACG. The donor DNA used to fix the double strand break contained two 40 base pair regions directly before or after the start and stop codon of *ZWF1*, respectively. The plasmid and donor DNA were transformed into BY4741 using the Zymo Research Frozen-EZ Yeast Transformation II Kit and plated on YPD plates containing 2% D-glucose and 50 mg/L G418. After disruption, the plasmid was lost through sequential growth on non-selective YPD media containing 2% D-glucose. The disruption was confirmed by sequencing. To disrupt *PGII*, homologous recombination with PCR generated donor DNA was used as described by Akada et al. with slight modification<sup>14</sup>. Briefly, a PCR fragment containing a *URA3* expression cassette with short homologous flanking regions as described by Akada et al.<sup>14</sup> was constructed. In addition, two 1000 base pair homologous arms directly upstream and downstream of the *PGII* start and stop codon, respectively, were isolated by PCR from *S. cerevisiae* genomic DNA. The three fragments were spliced together by splicing-overlap-extension PCR. The resultant fragment

was transformed into the aforementioned BY4741 *ZWF1*Δ cells using the Zymo Research Frozen-EZ Yeast Transformation II Kit, and the cells were plated on selective synthetic media containing 6.7 g/L yeast nitrogen base without amino acids, 5 g/L casamino acids, 40 mg/L adenine, 0.1 g/L glucose, 5 g/L fructose, and 15 g/L agarose. The resulting strain, WB601, was confirmed by sequencing.

To integrate *F. tularensis nadE* and *nadV* into the genomic DNA of WB601 to generate strain WB602, homologous recombination at the *ho* locus was used. The  $P_{PGK1}$ -*Ft nadV*- $T_{ADHI}$ - $P_{TEF2}$ -*Ft nadE*\*- $T_{ENO1}$  fragment was prepared by isolating each component from previously constructed or obtained plasmids by PCR. *Ft nadV* and *Ft nadE*\* were isolated from pWB602. The promoters, terminators, and connector were isolated from plasmids from the Yeast Toolkit<sup>15</sup>. The PCR fragments were spliced together using splicing-overlap-extension PCR. The subsequent PCR fragment was integrated by Gibson Isothermal DNA Assembly<sup>16</sup> into a high copy plasmid containing two 500 base pair homology arms which were split by a *natMX6* cassette. The  $P_{PGK1}$ -*Ft nadV*- $T_{ADHI}$ - $P_{TEF2}$ -*Ft nadE*\*- $T_{ENO1}$  was placed between the *natMX6* cassette and the upstream homology arm. The resultant plasmid was digested with *EcoRI*-*HF* on either side of the homology arms, linearizing the complete homologous fragment. The digestion was directly transformed into strain WB601 and plated on selective synthetic media containing 6.7 g/L yeast nitrogen base without amino acids, 5 g/L casamino acids, 5 g/L ammonium acetate, 40 mg/L adenine, 0.1 g/L glucose, 20 g/L fructose, 15 g/L agarose, and 100 mg/L nourseothricin. Integration was confirmed by sequencing.



### 5.2.2 Resting Cell Biotransformations

*S. cerevisiae* strain WB601 was transformed with a plasmid containing XenA and Bs GDH variant (selected from pWB603, pWB604, and pWB605) using the Zymo Research Frozen-EZ Yeast Transformation II Kit. Then, 4 mL seed cultures with synthetic media containing 6.7 g/L yeast nitrogen base without amino acids, 5 g/L casamino acids, 5 g/L ammonium acetate, 40 mg/L adenine, 0.1 g/L glucose, 20 g/L fructose, and 100 mg/L G418 were cultured at 30 °C while shaking at 250 r.p.m. for 48 hours. Next, 0.5% v/v seed cultures were used to inoculate 100 mL of identical media in a 250 mL baffled shake flask and cultured at 30 °C while shaking at 250 r.p.m. for 36 hours. Cells were collected by centrifugation for 5 minutes at 20 °C at 3750 r.p.m.. The supernatant was discarded, and the cell pellet was washed three times by resuspending in 50 mL of 100 mM potassium phosphate buffer at pH 7.4. The pellets of both the non-permeabilized and permeabilized cells were then resuspended to an  $OD_{600} = 400$ . The cells were then spiked into assay buffer at a 10x dilution, resulting in a final cell density of  $OD_{600} = 40$ . The working assay buffer concentration was 100 mM potassium phosphate at pH 7.4, 200 mM D-glucose, and 500 mg/L citral. 2 mM NMN<sup>+</sup> was also added unless otherwise stated. Reactions were performed in 2 mL glass vials sealed with a PTFE-lined cap. Vials were incubated at 30 °C while shaking at 250 r.p.m. for 24 hours. After 24 hours, the cell suspension was pelleted, and the supernatant was used for analysis. 200  $\mu$ L of supernatant was extracted with an equal volume of chloroform containing 200 mg/L octanol as an internal standard, and the organic fraction was analyzed by GC (see detailed method below).

If cells were permeabilized, the 3x washed pellet was resuspended in 10 mL of 0.4% wt/v Triton X-100 in water per 1 g wet cell weight, and the cell suspension was shook at 350 r.p.m on a shake table at 20 °C for 15 minutes. Then, the cells were immediately pelleted by centrifugation

for 5 minutes at 20 °C and 3,750 r.p.m.. The pellet was then washed twice in 5 mL of 100 mM potassium phosphate buffer at pH 7.4.. Then, the cell pellet was resuspended to an OD<sub>600</sub> = 400 and used as stated above.

### 5.2.3 GC-FID Analytical Method

All GC analysis was performed on an Agilent Technologies 6850 equipped with an FID as described previously<sup>17</sup>. Briefly, an Agilent Technologies DB-WAXetr capillary column (30 m × 0.56 mm × 1 μm) was used for separation. 5 μL of samples was injected at a 2:1 split ratio. The oven was held at 150 °C for 15 minutes, then ramped to 240 °C at a rate of 20 °C/min before equilibration back to 150 °C. Compound elution times are as follows: citral, 7.26 and 8.42 minutes; citronellal, 4.08 minutes; citronellol, 8.72 minutes; nerol, 10.04 minutes; geraniol, 11.55 minutes; octanol, 4.59 minutes.

### 5.2.4 Intracellular NMN<sup>+</sup> Generation

*S. cerevisiae* strain WB601 was transformed with either plasmid pWB601 or pWB602, which encoded candidate NMN<sup>+</sup> generating proteins. When genomic expression of *F. tularensis* NadE\* and NadV was investigated, pWB604 was transformed to enable growth in media containing G418. Then, 4 mL seed cultures of synthetic media containing 6.7 g/L yeast nitrogen base without amino acids, 5 g/L casamino acids, 5 g/L ammonium acetate, 40 mg/L adenine, 0.1 g/L glucose, 20 g/L fructose, and 100 mg/L G418 were cultured at 30 °C while shaking at 250 r.p.m. for 48 hours. Next, 0.5% v/v seed cultures were used to inoculate 10 mL of identical media containing varying nicotinamide riboside in a 50 mL conical tube and cultured at 30 °C while shaking at 250 r.p.m. for 48 hours, unless otherwise specified. Tube caps were loosely placed on the tube and secured with tape. After the specified growth time, 1.4 mL of culture was pelleted for 30 seconds at 20 °C and 20,000 RCF. The supernatant was discarded, and the pellet was washed

once with 1 mL of deionized water and repelleted. The washed pellet was resuspended in 100  $\mu$ L of deionized water, and the resuspended pellet was spiked into 2 mL screw-cap tube containing 0.5 mL of 0.5 mm zirconium beads (Cole-Parmer) and 1 mL 1% formic acid with 1  $\mu$ M 1-methylnicotinamide. The tube and its contents were preheated at 95  $^{\circ}$ C for 10 minutes prior to spiking the cells. After spiking the cells, the tube was closed and incubated for 2 minutes at 95  $^{\circ}$ C with intermittent vortexing to ensure the solution was well mixed. Then, the samples were homogenized by bead beating at 6 m/s for 2 minutes using a FastPrep-24 (MP Biomedicals). Then, the samples were immediately quenched in an ice water bath. To remove the cell debris, the samples were pelleted for 20 minutes at 4  $^{\circ}$ C and 20,000 RCF. The supernatant was removed and used for UPLC-MS/MS analysis. UPLC-MS/MS was performed as previously described<sup>13</sup>. Briefly, UPLC-MS/MS was performed on a Waters ACQUITY UPLC using a Waters ACQUITY UPLC CSH C18 column (1.7  $\mu$ m  $\times$  2.1 mm  $\times$  50 mm) for separation. Mobile phases consisted of (A) water with 2% acetonitrile and 0.2% acetic acid and (B) acetonitrile with 0.2% acetic acid. The instrument was equipped with a Waters Micromass Quattro Premier XE Mass Spectrometer. Detailed method parameters were listed previously. Values from UPLC-MS/MS were used to determine intracellular metabolite concentration using  $4.2 \times 10^{-14}$  L as the intracellular volume<sup>18</sup> and  $3 \times 10^7$  cells per unit OD<sub>600</sub> per mL<sup>19</sup>.

## 5.3 Results and Discussion

### 5.3.1 System and Stain Construction

Next, we sought to translate our *in vivo* NMN(H) cycling system to *S. cerevisiae*. A plasmid-based expression system was designed to express XenA and the Bs GDH candidates. Three plasmids were generated (pWB603, pWB604, and pWB605). Each plasmid contained two expression cassettes for XenA and the Bs GDH variants, a CEN/ARS origin of replication, and a

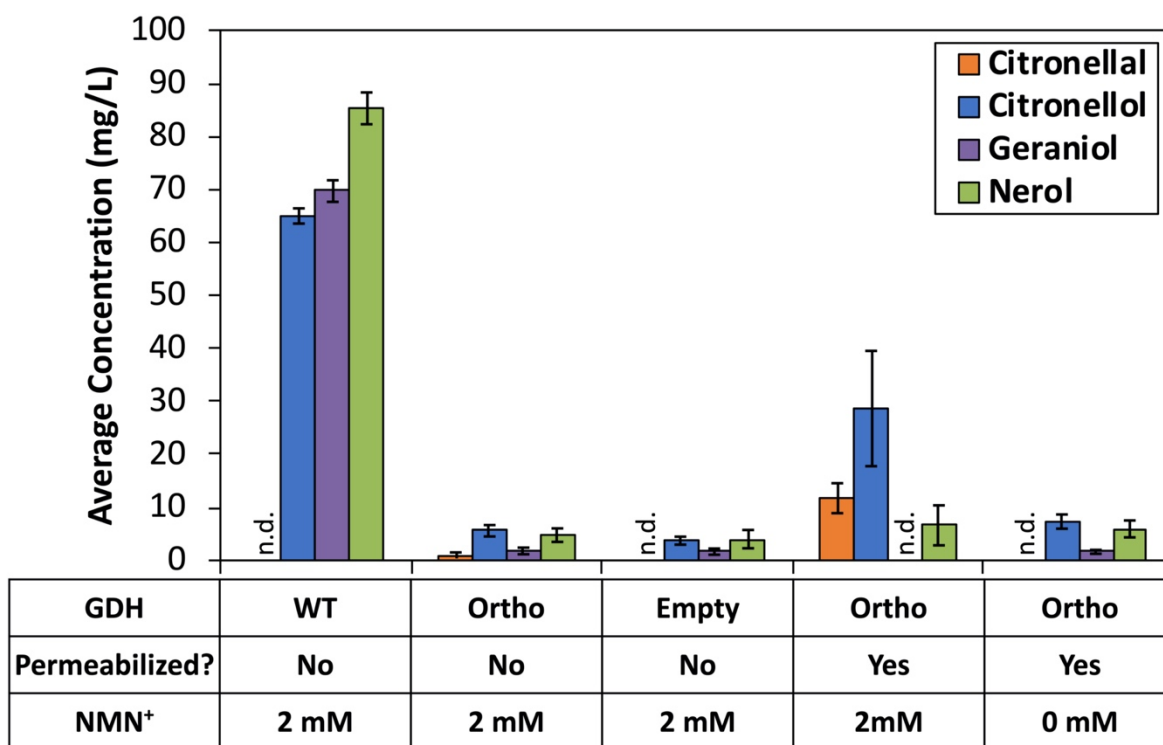
KanMX marker. Both XenA and the Bs GDH variants were expressed under the control of a TEF1 promoter and CYC1 terminator. As a negative control, an empty expression cassette (pTEF1-tCYC1) was used.

Next, similarly to *E. coli*, in order for specific reducing power to be delivered to NMN<sup>+</sup> *in vivo*, the ability of the cell to consume glucose through the central metabolism was removed. To achieve this, the genes encoding the phosphoglucoisomerase, PGI1, and glucose-6-phosphate dehydrogenase, ZWF1, were disrupted in *S. cerevisiae* strain BY4741. The resultant strain (WB601) was unable to grow on glucose as the sole carbon source, and fructose was used as the primary carbon source for cell growth (2% w/v). Consistent with literature reports, this strain still required trace amounts of glucose to grow (0.01% w/v)<sup>20</sup>. However, growth was curtailed with glucose concentrations above 0.01% w/v.

### 5.3.2 Resting Whole Cell Biotransformation in *S. cerevisiae*

To examine the ability to orthogonally deliver reducing power in *S. cerevisiae* through NMN(H), we chose the production of citronellal from citral, as previously discussed<sup>17</sup>, as a model system. Briefly, the activated C=C double bond in citral can be reduced by XenA to produce citronellal, both compounds are aldehydes. However, these aldehydes are highly reactive in the cellular matrix. The multitude of alcohol dehydrogenases expressed by *S. cerevisiae* can readily reduce citral and citronellal to their respective alcohols, nerol and geraniol or citronellol, respectively<sup>17</sup>. Since alcohol dehydrogenases have demonstrated low activity with NMNH, GDH Ortho generation of NMNH should enable XenA activity while keeping alcohol dehydrogenase activity low. The plasmids containing XenA and the GDH variants (pWB603, pWB604, and pWB605) were transformed into *S. cerevisiae* strain WB601 to express the system. In resting cells with XenA and Bs GDH wild type (pWB603), citral was rapidly consumed and only alcohol

products were formed (Figure 19). However, when cells expressed Bs GDH Ortho (pWB604), citronellal accumulated at 0.8 mg/L, and alcohol production was significantly decreased, resulting in a citronellal product purity of 6% (Figure 19). When no Bs GDH was supplied to the cells (pWB605), citronellal was not detected (Figure 19).



**Figure 19: Citral Biotransformation with resting *S. cerevisiae* cells.** When wild type glucose dehydrogenase is supplied, native cofactors were recycled, delivering reducing power to XenA and endogenous ADHs, and only citronellol, nerol, and geraniol accumulated. When GDH Ortho is supplied, citronellal only accumulates to a low level. When no GDH is supplied, no citronellal was detected, and alcohol accumulation remained low. When cells with GDH Ortho are permeabilized, citronellal production increased in an NMN<sup>+</sup>-dependent manner. Resting cell assays are performed at OD<sub>600</sub> = 40. NMN<sup>+</sup> is supplemented to the assay buffer when stated. Assay buffer contained 100 mM potassium phosphate at pH 7.4, 200 mM D-glucose, and 500 mg/L citral. Reactions were incubated at 30 °C for 24 hours with shaking at 250 r.p.m.. Values are an average of three replicates, and the error bars represent one standard deviation of the mean. n.d., not detected.

While these data indicate that GDH Ortho was able to selectively deliver reducing power to the cell through NMNH, citronellal production levels were low. We hypothesized that this was due to low intracellular NMN<sup>+</sup> levels. Although 2 mM NMN<sup>+</sup> was exogenously supplied to the

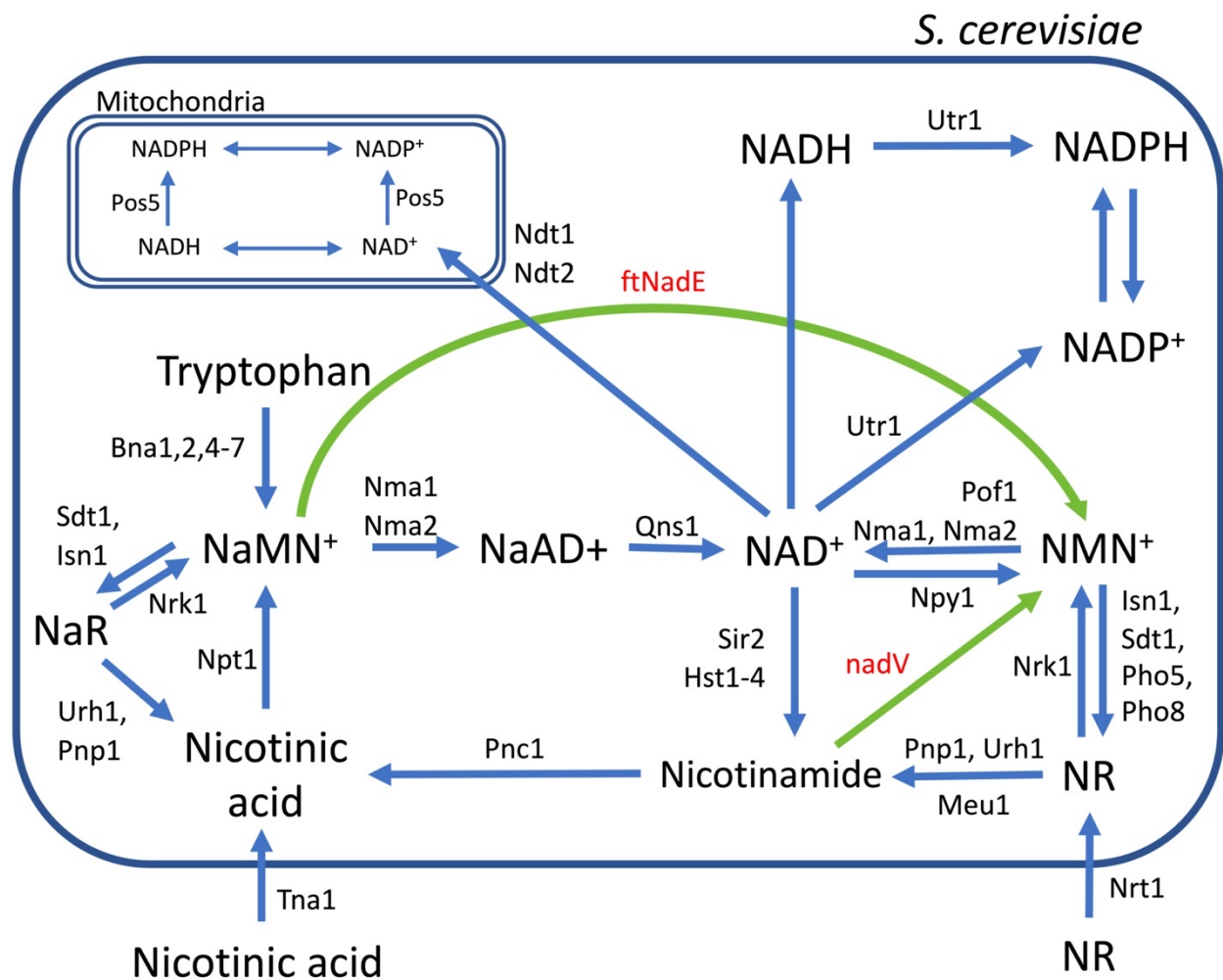
assay buffer, an NMN<sup>+</sup> transporter has not been demonstrated in *S. cerevisiae*. Therefore, to enable NMN<sup>+</sup> to enter the cell, we added a permeabilization step with 0.4% w/v Triton X-100 to the resting cell preparation protocol. When permeabilized cells expressing GDH Ortho were supplemented to 2 mM NMN<sup>+</sup>, citronellal accumulated to 12 mg/L at a product purity of 25%, indicating NMN<sup>+</sup> levels were indeed limiting citronellal production (Figure 19). However, this increase also resulted in increased accumulation of citronellol, 28 mg/L. Previously, we demonstrated that increasing the relative level of XenA to GDH Ortho in *E. coli* whole cells enables significantly increased product purity<sup>17</sup>. Further tuning of the expression ratio and total level of the two proteins may enable a similar improvement in both yield and purity in *S. cerevisiae*. Furthermore, when NMN<sup>+</sup> was not supplied to the permeabilized resting cells, no citronellal was produced, indicating the citronellal accumulation was indeed NMN-dependent (Figure 19).

### 5.3.3 Intracellular NMN<sup>+</sup> Generation in *S. cerevisiae*

Interestingly, the inability for NMN<sup>+</sup> to freely cross the cell wall may be able to be used as an advantage for biotransformation. To date, *in vivo* orthogonal redox cofactor systems have relied on exogenous cofactor supply to accumulate high intracellular cofactor levels<sup>13,17,21,22</sup>. Using the cell wall as a barrier, engineering cells to accumulate increased levels of NMN<sup>+</sup> may enable NMN-based *in vivo* biotransformation without the need to supply exogenous NMN<sup>+</sup> to the assay buffer.

To examine the accumulation of NMN<sup>+</sup> *in vivo*, we expressed two candidate pathways to produce NMN<sup>+</sup> from nicotinamide riboside, NR (Figure 20). The first pathway we investigated was the NR salvage pathway for NAD<sup>+</sup> biosynthesis, which uses NMN<sup>+</sup> as an intermediate<sup>23,24</sup>. In NR salvage, NR is natively transported into the cell by a nicotinamide riboside transporter, Nrt1<sup>25</sup>. Then, NR is converted to NMN<sup>+</sup> by the nicotinamide riboside kinase, Nrk1<sup>23</sup>. After, NMN<sup>+</sup>

can be converted to  $\text{NAD}^+$  by multiple enzymes. However, in some conditions,  $\text{NMN}^+$  has been shown to accumulate to levels  $\sim 20\%$  of  $\text{NAD}^+$ <sup>11</sup>, indicating  $\text{NMN}^+$  consuming enzymes may not need to be disrupted for high levels of  $\text{NMN}^+$  accumulation. The second pathway we investigated was the previously demonstrated pairing of *F. tularensis*  $\text{NMN}^+$  synthetase,  $\text{NadE}^*$ , and phosphoribosyl transferase,  $\text{NadV}$ <sup>13,26</sup> (Figure 20). *F. tularensis*  $\text{NadE}^*$  produces  $\text{NMN}^+$  from nicotinic acid mononucleotide, and *F. tularensis*  $\text{NadV}$  produces  $\text{NMN}^+$  from nicotinamide,  $\text{NA}$ <sup>27</sup>. While both of these genes do not use  $\text{NR}$  directly,  $\text{NA}$  can be produced from  $\text{NR}$  using nucleosidases<sup>28</sup>, and  $\text{NaMN}^+$  is an intermediate in *de novo*  $\text{NAD}^+$  biosynthesis<sup>29,30</sup> (Figure 20).

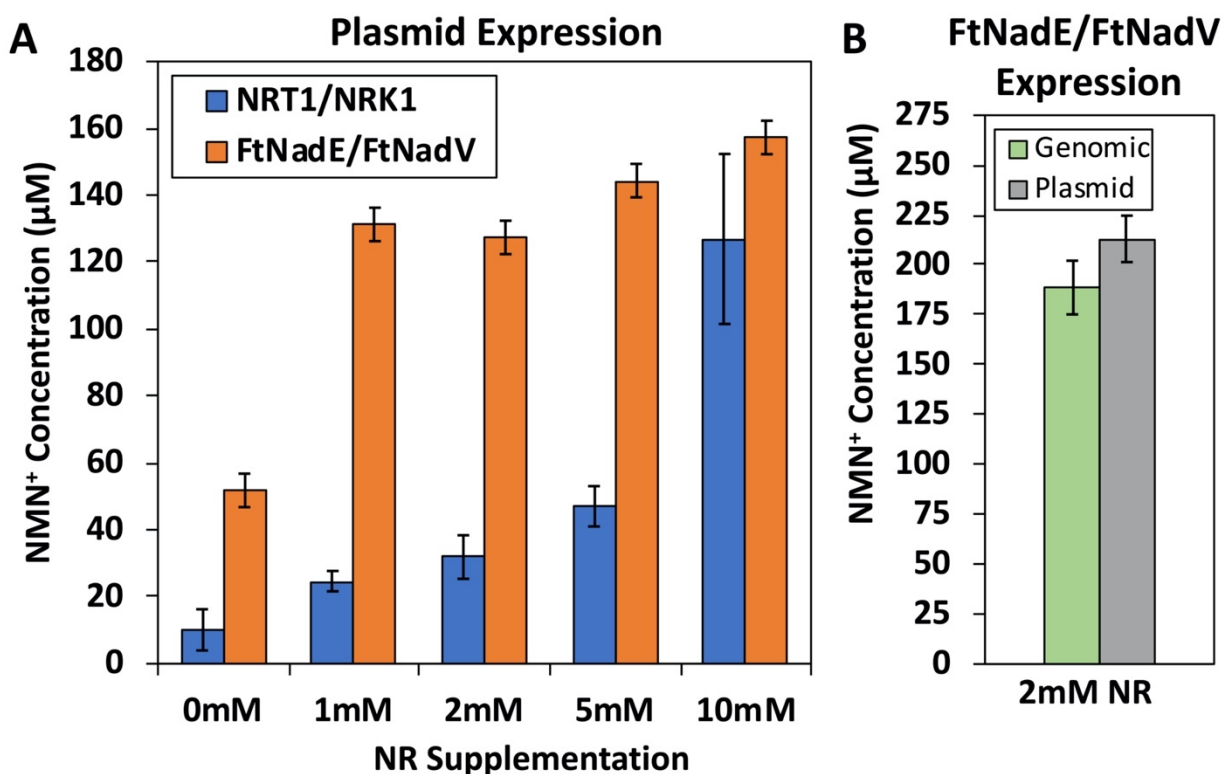


**Figure 20: Establishing  $\text{NMN}^+$  biosynthetic routes in *Saccharomyces cerevisiae*.**  $\text{NMN}^+$  is produced *in vivo* as an intermediate in  $\text{NAD}^+$  salvage pathways. Endogenous enzymes are shown

with blue arrows. Heterologous enzymes used for NMN<sup>+</sup> synthesis in this study are shown with green arrows. NMN<sup>+</sup> is predominantly produced endogenously as an intermediate in nicotinamide riboside (NR) salvage. A route for NMN<sup>+</sup> production can be established from nicotinamide by introducing a phosphoribosyltransferase (NadV). An additional route for NMN<sup>+</sup> production can be established from nicotinic acid mononucleotide, NaMN<sup>+</sup>, by introducing the NMN<sup>+</sup> synthase from *Francisella tularensis*, FtNadE\*. NaAD<sup>+</sup>, nicotinic acid adenine dinucleotide; NAD<sup>+</sup>, nicotinamide adenine dinucleotide (oxidized); NADH, nicotinamide adenine dinucleotide (reduced); NMN<sup>+</sup>, nicotinamide mononucleotide; NR, nicotinamide riboside; NaR, nicotinic acid riboside; NaMN<sup>+</sup>, nicotinic acid mononucleotide; NADPH, nicotinamide adenine dinucleotide phosphate (reduced); NADP<sup>+</sup>, nicotinamide adenine dinucleotide phosphate (oxidized).

To test the ability of these two pathways to produce NMN<sup>+</sup>, cells expressing the endogenous NR salvage pathway (Nrt1/Nrk1, pWB601) or the heterologous enzymes (*F. tularensis* NadE\*/NadV, pWB602) were fed varying concentrations of NR, and their intracellular NMN<sup>+</sup> levels were measured after 48 hours of growth (Figure 21A). Cells expressing the *F. tularensis* genes accumulated 52  $\mu$ M of NMN<sup>+</sup> without feeding NR, while the cells overexpressing the native NR pathway only accumulated 10  $\mu$ M (Figure 21A). When 1 mM of NR was supplemented into the growth media, cells expressing the *F. tularensis* genes produced 131  $\mu$ M NMN<sup>+</sup>, while the native NR pathway overexpression cells only produced 25  $\mu$ M (Figure 21A). Interestingly, as NR supplementation was further increased, NMN<sup>+</sup> levels only increased slowly in the cells expressing the *F. tularensis* genes, while the native NR salvage pathway expressing cells eventually reached 127  $\mu$ M NMN<sup>+</sup> when 10 mM NR was supplemented (Figure 21A). The slow increase of NMN<sup>+</sup> production in the NR salvage overexpression cells may be caused by regulatory effects at the protein level which are not active towards the heterologous *F. tularensis* genes. Next, *F. tularensis* *nadE\** and *nadV* were integrated into the genomic DNA at the *ho* locus (strain WB602). Genomic integration of the genes performed comparably to the plasmid-based expression, achieving 188  $\mu$ M of intracellular NMN<sup>+</sup> accumulation after 36 hours with 2 mM NR supplementation (Figure 21B).





**Figure 21: Intracellular NMN<sup>+</sup> levels increase with heterologous pathway introduction.** (A) NMN producing pathways were overexpressed in *S. cerevisiae* strain WB601. When the native pathway to produce NMN is overexpressed, NMN<sup>+</sup> concentration increases slowly. When the heterologous NMN<sup>+</sup> pathway is introduced, NMN<sup>+</sup> levels quickly rose with only 1 mM of NR supplementation. (B) When the genes encoding *F. tularensis* NadE\* and NadV were integrated in the genome, intracellular NMN<sup>+</sup> levels were comparable to a plasmid-based expression system. Cells were cultured in synthetic media containing 2% fructose and 0.01% D-glucose. Cultures were grown at 30 °C for 48 (A) or 36 hours (B). Values represent an average of three replicates. Error bars represent on standard deviation of the average.

Although the intracellular NMN<sup>+</sup> levels achieved here, 188 µM, is lower than the 2 mM fed to the permeabilized cells, we have previously demonstrated that levels as low as 100 µM in *E. coli* crude lysate were capable of supporting efficient biotransformation with our NMN-cycling system (Figure 8) <sup>17</sup>. If additional intracellular NMN<sup>+</sup> is necessary to support biotransformation, further investigation of NadV candidate and disruption of genes encoding NMN<sup>+</sup>-consuming enzymes may further increase the ability to maintain higher intracellular NMN<sup>+</sup>.

## 5.4 Conclusion

In conclusion, the work in this chapter demonstrates the use of an orthogonal redox cofactor cycling system in *S. cerevisiae*. By selectively recycling the noncanonical redox cofactor NMN<sup>+</sup> using an engineering glucose dehydrogenase, specific reducing power was used to reduce the terpenoid aldehyde citral to citronellal, producing 12 mg/L. Interestingly, this was achieved without the need to disrupt any endogenous alcohol dehydrogenases. In addition, *S. cerevisiae* was engineered to accumulate NMN<sup>+</sup> *in vivo* by introducing new pathways with the NMN<sup>+</sup> synthetase and phosphoribosyltransferase from *F. tularensis*. Pairing the NMN<sup>+</sup> accumulating strain with the NMN(H)-cycling system may enable NMN-mediated biotransformation without the need to exogenously supply cofactor to the cells.

## 5.5 References

- [1] Fernandez-Moya, R.; Da Silva, N. A. Engineering *Saccharomyces cerevisiae* for High-Level Synthesis of Fatty Acids and Derived Products. *FEMS Yeast Res* **2017**, *17*, fox071.
- [2] Avalos, J. L.; Fink, G. R.; Stephanopoulos, G. Compartmentalization of Metabolic Pathways in Yeast Mitochondria Improves the Production of Branched-Chain Alcohols. *Nat. Biotechnol.* **2013**, *31*, 335–341.
- [3] Favaro, L.; Jansen, T.; Zyl, W. H. van. Exploring Industrial and Natural *Saccharomyces cerevisiae* Strains for the Bio-Based Economy from Biomass: The Case of Bioethanol. *Crit. Rev. Biotechnol.* **2019**, *39*, 800–816.
- [4] Cardenas, J.; Da Silva, N. A. Engineering Cofactor and Transport Mechanisms in *Saccharomyces cerevisiae* for Enhanced Acetyl-CoA and Polyketide Biosynthesis. *Metab. Eng.* **2016**, *36*, 80–89.
- [5] Palmer, C. M.; Alper, H. S. Expanding the Chemical Palette of Industrial Microbes: Metabolic Engineering for Type III PKS-Derived Polyketides. *Biotechnol. J.* **2019**, *14*, 1700463.
- [6] Luo, X.; Reiter, M. A.; d’Espaux, L.; Wong, J.; Denby, C. M.; Lechner, A.; Zhang, Y.; Grzybowski, A. T.; Harth, S.; Lin, W.; Lee, H.; Yu, C.; Shin, J.; Deng, K.; Benites, V. T.; Wang, G.; Baidoo, E. E. K.; Chen, Y.; Dev, I.; Petzold, C. J.; Keasling, J. D. Complete

- Biosynthesis of Cannabinoids and Their Unnatural Analogues in Yeast. *Nature* **2019**, *567*, 123–126.
- [7] Paddon, C. J.; Westfall, P. J.; Pitera, D. J.; Benjamin, K.; Fisher, K.; McPhee, D.; Leavell, M. D.; Tai, A.; Main, A.; Eng, D.; Polichuk, D. R.; Teoh, K. H.; Reed, D. W.; Treynor, T.; Lenihan, J.; Jiang, H.; Fleck, M.; Bajad, S.; Dang, G.; Dengrove, D.; Diola, D.; Dorin, G.; Ellens, K. W.; Fickes, S.; Galazzo, J.; Gaucher, S. P.; Geistlinger, T.; Henry, R.; Hepp, M.; Horning, T.; Iqbal, T.; Kizer, L.; Lieu, B.; Melis, D.; Moss, N.; Regentin, R.; Secrest, S.; Tsuruta, H.; Vazquez, R.; Westblade, L. F.; Xu, L.; Yu, M.; Zhang, Y.; Zhao, L.; Lievens, J.; Covello, P. S.; Keasling, J. D.; Reiling, K. K.; Renninger, N. S.; Newman, J. D. High-Level Semi-Synthetic Production of the Potent Antimalarial Artemisinin. *Nature* **2013**, *496*, 528–532.
- [8] Chen, R.; Yang, S.; Zhang, L.; Zhou, Y. J. Advanced Strategies for Production of Natural Products in Yeast. *iScience* **2020**, *23*, 100879.
- [9] Li, M.; Kildegaard, K. R.; Chen, Y.; Rodriguez, A.; Borodina, I.; Nielsen, J. De Novo Production of Resveratrol from Glucose or Ethanol by Engineered *Saccharomyces cerevisiae*. *Metab. Eng.* **2015**, *32*, 1–11.
- [10] Ro, D.-K.; Paradise, E. M.; Ouellet, M.; Fisher, K. J.; Newman, K. L.; Ndungu, J. M.; Ho, K. A.; Eachus, R. A.; Ham, T. S.; Kirby, J.; Chang, M. C. Y.; Withers, S. T.; Shiba, Y.; Sarpong, R.; Keasling, J. D. Production of the Antimalarial Drug Precursor Artemisinic Acid in Engineered Yeast. *Nature* **2006**, *440*, 940–943.
- [11] Evans, C.; Bogan, K. L.; Song, P.; Burant, C. F.; Kennedy, R. T.; Brenner, C. NAD<sup>+</sup> Metabolite Levels as a Function of Vitamins and Calorie Restriction: Evidence for Different Mechanisms of Longevity. *BMC Chem. Biol.* **2010**, *10*, 2.
- [12] Brachmann, C. B.; Davies, A.; Cost, G. J.; Caputo, E.; Li, J.; Hieter, P.; Boeke, J. D. Designer Deletion Strains Derived from *Saccharomyces Cerevisiae* S288C: A Useful Set of Strains and Plasmids for PCR-Mediated Gene Disruption and Other Applications. *Yeast* **1998**, *14*, 115–132.
- [13] Black, W. B.; Zhang, L.; Mak, W. S.; Maxel, S.; Cui, Y.; King, E.; Fong, B.; Sanchez Martinez, A.; Siegel, J. B.; Li, H. Engineering a Nicotinamide Mononucleotide Redox Cofactor System for Biocatalysis. *Nat. Chem. Biol.* **2020**, *16*, 87–94.
- [14] Akada, R.; Kitagawa, T.; Kaneko, S.; Toyonaga, D.; Ito, S.; Kakihara, Y.; Hoshida, H.; Morimura, S.; Kondo, A.; Kida, K. PCR-Mediated Seamless Gene Deletion and Marker Recycling in *Saccharomyces cerevisiae*. *Yeast* **2006**, *23*, 399–405.
- [15] Lee, M. E.; DeLoache, W. C.; Cervantes, B.; Dueber, J. E. A Highly Characterized Yeast Toolkit for Modular, Multipart Assembly. *ACS Synth. Biol.* **2015**, *4*, 975–986.

- [16] Gibson, D. G.; Young, L.; Chuang, R.-Y.; Venter, J. C.; Hutchison, C. A.; Smith, H. O. Enzymatic Assembly of DNA Molecules up to Several Hundred Kilobases. *Nat. Methods* **2009**, *6*, 343–345.
- [17] Richardson, K. N.; Black, W. B.; Li, H. Aldehyde Production in Crude Lysate- and Whole Cell-Based Biotransformation Using a Noncanonical Redox Cofactor System. *ACS Catal.* **2020**, *10*, 8898–8903.
- [18] Jorgensen, P.; Nishikawa, J. L.; Breitkreutz, B.-J.; Tyers, M. Systematic Identification of Pathways That Couple Cell Growth and Division in Yeast. *Science* **2002**, *297*, 395–400.
- [19] Day, A.; Schneider, C.; Schneider, B. L. Yeast Cell Synchronization. In *Cell Cycle Checkpoint Control Protocols*; Lieberman, H. B., Ed.; Methods in Molecular Biology<sup>TM</sup>; Humana Press: Totowa, NJ, **2004**; pp 55–76.
- [20] Boles, E.; Lehnert, W.; Zimmermann, F. K. The Role of the NAD-Dependent Glutamate Dehydrogenase in Restoring Growth on Glucose of a *Saccharomyces cerevisiae* Phosphoglucose Isomerase Mutant. *Eur. J. Biochem.* **1993**, *217*, 469–477.
- [21] Wang, L.; Ji, D.; Liu, Y.; Wang, Q.; Wang, X.; Zhou, Y. J.; Zhang, Y.; Liu, W.; Zhao, Z. K. Synthetic Cofactor-Linked Metabolic Circuits for Selective Energy Transfer. *ACS Catal.* **2017**, *7*, 1977–1983.
- [22] Guo, X.; Liu, Y.; Wang, Q.; Wang, X.; Li, Q.; Liu, W.; Zhao, Z. K. Non-Natural Cofactor and Formate-Driven Reductive Carboxylation of Pyruvate. *Angew. Chem. Int. Ed.* **2020**, *59*, 3143–3146.
- [23] Bieganowski, P.; Brenner, C. Discoveries of Nicotinamide Riboside as a Nutrient and Conserved NRK Genes Establish a Preiss-Handler Independent Route to NAD<sup>+</sup> in Fungi and Humans. *Cell* **2004**, *117*, 495–502.
- [24] Croft, T.; Venkatakrishnan, P.; Lin, S.-J. NAD<sup>+</sup> Metabolism and Regulation: Lessons From Yeast. *Biomolecules* **2020**, *10*, 330.
- [25] Belenky, P. A.; Moga, T. G.; Brenner, C. *Saccharomyces Cerevisiae* YOR071C Encodes the High Affinity Nicotinamide Riboside Transporter Nrt1. *J. Biol. Chem.* **2008**, *283*, 8075–8079.
- [26] Black, W. B.; Aspacio, D.; Bever, D.; King, E.; Zhang, L.; Li, H. Metabolic Engineering of *Escherichia coli* for Optimized Biosynthesis of Nicotinamide Mononucleotide, a Noncanonical Redox Cofactor. *Microb. Cell Fact.* **2020**, *19*, 150.
- [27] Sorci, L.; Martynowski, D.; Rodionov, D. A.; Eyobo, Y.; Zogaj, X.; Klose, K. E.; Nikolaev, E. V.; Magni, G.; Zhang, H.; Osterman, A. L. Nicotinamide Mononucleotide Synthetase Is the Key Enzyme for an Alternative Route of NAD Biosynthesis in *Francisella tularensis*. *PNAS* **2009**, *106*, 3083–3088.

- [28] Belenky, P.; Christensen, K. C.; Gazzaniga, F.; Pletnev, A. A.; Brenner, C. Nicotinamide Riboside and Nicotinic Acid Riboside Salvage in Fungi and Mammals. *J. Biol. Chem.* **2009**, *284*, 158–164.
- [29] Preiss, J.; Handler, P. Biosynthesis of Diphosphopyridine Nucleotide I. Identification of Intermediates. *J. Biol. Chem.* **1958**, *233*, 488–492.
- [30] Preiss, J.; Handler, P. Biosynthesis of Diphosphopyridine Nucleotide II. Enzymatic Aspects. *J. Biol. Chem.* **1958**, *233*, 493–500.